LEVEL II

12

9 TECHNICAL REPORT. 1 Jul 75-30 Sep 80

on

6 COMPLEX DIELECTRIC PROPERTIES OF SEVERAL IGNEOUS AND METAMORPHIC ROCKS .

12 171

Institution: Department of Earth and Planetary Sciences
Massachusetts Institute of Technology
Cambridge, Massachusetts 02139

Principal Investigator: 10 Gene Simmons

Scientific Collaborators: Lou Caruso and Frank Miller

Contract Title: Physical Properties of Deep Crustal Rocks

Contract Number: 15 N00014-76-C-0478

Period: 1 July 1975 through 30 September 1980

Submitted: 11 1 October 1980

404784

COMPLEX DIELECTRIC PROPERTIES OF SEVERAL IGNEOUS AND METAMORPHIC ROCKS

by

Gene Simmons,

Lou Caruso,

and

Frank Miller

Department of Earth and Planetary Sciences
Massachusetts Institute of Technology
Cambridge, Massachusetts 02139

1 October 1980

TABLE OF CONTENTS

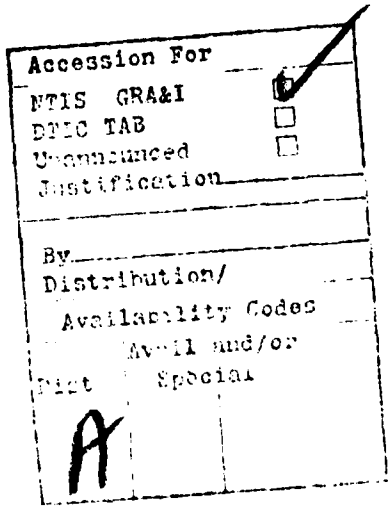

INTRODUCTION

The complex dielectric properties of rocks are interesting scientifically and important practically. The scientific interest derives from a desire to understand the properties of materials, the electrical structure of the earth's crust, and the (electrical) loss mechanisms in the crust. The practical significance stems from potential applications in borehole logging, geothermal prospecting, mineral prospecting, and in lithospheric radiowave communications.

The dielectric properties of rocks and minerals have been reported previously by several investigators; for examples, see Parkhomenko (1967 and references cited by her), Iglesias and Westphal (1967), Saint-Amant and Strangway (1970), and Olhoeft (1979). Methods of measurement have been described by von Hippel (1954), Alvarez (1973), and General Radio (1974, undated). The real part of the permittivity (ε') of a rock is an average of the permittivity of the individual minerals; the volume fraction of each mineral appears to be a suitable weighting function for most purposes. The loss factor (ε'') obviously depends on the various loss mechanisms present and on the frequency. In rocks, the value and behavior with temperature and frequency are dominated by the water (and dissolved ions) present in microcracks. In this study, we have removed the water from the microcracks in order to obtain data suitable for use in inferring the properties of rocks at depths where the microcracks are not present. Such depths may be as shallow as 1 km - see Feves et al. (1977) for examples and further discussion of the effect of pressure on microcracks.

NOTATION AND TERMINOLOGY

We follow the notation and terminology of von Hippel (1954). The dielectric properties of a material may be described by the complex permittivity

$$\varepsilon^* = \varepsilon' - j\varepsilon''$$

where ε' is the permittivity and ε'' is the loss factor. The complex relative permittivity

$$K^* = \varepsilon^*/\varepsilon_o = K' - jK''$$

where ε_o is the permittivity of vacuum, K' is the relative permittivity (also usually termed relative dielectric constant), and K" is the relative loss factor. The loss tangent ($\tan \delta$) is given by

$$\tan \delta = \frac{\varepsilon''}{\varepsilon'} = \frac{K''}{K'}$$

The dielectric conductivity, which includes all dissipative effects, is

$$\sigma = \omega\varepsilon''.$$

In our work, we have measured K' and σ and report them.

THE SAMPLES

The rocks used in this study consist of a suite of igneous and metamorphic rocks. The igneous rocks are a subset of the rocks used by Feves et al. (1977) and described by Richter and Simmons (1977). The metamorphic samples have not been used in previous studies (except 1727); they are described in Appendix A of this report (except 1727). See Padovani et al. (1980) for description of 1727. The location and rock types are given in Table 1.

Table 1.

Samples Examined in this Study

MIT Sample	Location	Rock Type	Comments
83	Troy, OK	Granite	
890	Frederick, MD	Diabase	Petrographic description given by Richter and Simmons (1977). Other physical properties given by Feves et al. (1977).
1331	Mellen, WI	Gabbro	
1370	Red River, WI	Quartz monzonite	
1410	Graniteville, MO	Granite	
1411	Stouts Creek, MO	Rhyolite	
1415	Skrainka, MO	Diabase	
1727	Pennsylvania	Amphibolite	Cracks and petrography discussed by Padovani et al. (1980).
2383	New York (eastern Adirondacks)	Garnet granulite	
2390	New York (eastern Adirondacks)	Garnet granulite	
2422	Central Maine	Phyllite	
2425	Central Maine	Metagranite	
2426	Camden, Maine	Metaquartzite	
2428	Camden, Maine	Metaquartz conglomerate	
2432	Camden, Maine	Metaquartz conglomerate	
2434	Camden, Maine	Calc-silicate	
2439	Central Maine	Quartzo-feldspathic gneiss	
2441	Central Maine	Schist	

EXPERIMENTAL TECHNIQUES AND APPARATUS

Water was removed from the microcracks in each specimen by drying in a vacuum oven at approximately 140°C and 30 mm Hg pressure for several days.

The real part of the dielectric constant (ε') and the dielectric conductivity (σ) were then measured with a General Radio model 1621 capacitance measurement system, described by General Radio (1974, undated) over the frequency range 100-50,000 Hertz. A three-terminal sample holder was used.

A home-made glove box was used to isolate the specimen and specimen holder from the water vapor present in the laboratory air during the time required for each measurement.

THE DATA ON DIELECTRIC PROPERTIES

Values of K', K", tan δ, and σ are given in Appendix B of this report for the suites of igneous and metamorphic rocks.

Plots of K', tan δ, and σ as functions of frequency and a Cole-Cole plot (relative permittivity versus relative loss factor) for each sample are given also in Appendix B.

DISCUSSION

This discussion of the results is considered to be preliminary because the compositions of the major phases, the crack sealing phases, and the fluid inclusions have not yet been determined for the metamorphic samples. Neither has the composition of the fluid inclusions been determined for the igneous rocks. And finally, the degree of alteration of the feldspars, which is expected to be a significant factor in determining the dielectric conductivity, has not been measured. However, some features do appear worthy of mention.

The dielectric conductivities of the igneous and metamorphic rocks are all quite low, of order of 10^{-7} mho/m at 100 Hertz and 10^{-5} mho/m at 50,000 Hertz. Because the samples were chosen to be representative of the rocks in the eastern half of the United States, these values of conductivity are also likely representative.

The igneous rocks, considered as a group, show surprisingly little variation - one order of magnitude for a given frequency. There appears to be little dependence on rock type; the values for gabbro and diabase are approximately equal to the values for granite and rhyolite. Clearly, within the igneous group, the major determinant is not gross lithology.

The dielectric conductivities of the metamorphic rocks are generally lower (by roughly an order of magnitude) than the values for the igneous rocks. Obviously, there exist several exceptions: Troy granite (83) and the calc-silicate rock from Maine (2434).

The thickness of the specimen has little effect on the measured values. Although we measured K' and σ for a 'thick' and a 'thin' disc of each specimen, we report typical values for a single sample only (2426-1 and 2426-2). The two discs were 33 mm and 6 mm thick, respectively. At 100 Hz, the values of σ are 2.2 and 1.9 x 10^{-8} mho/m, respectively. At 50,000 Hertz, they are

1.5 and 1.3 x 10^{-8} mho/m. The chief source of the differences of values between 'thick' and 'thin' specimens is believed to be the presence of trace amounts of water that remained in the microcracks of the 'thick' specimen.

CONCLUSIONS

The dielectric conductivity of igneous and metamorphic rocks from eastern United States is of order 10^{-7} mho/m and 10^{-8} mho/m, respectively, at a frequency of 100 Hertz, temperature of 20°C, and at simulated crustal conditions such that the microcracks are chemically closed.

REFERENCES

Alvarez, R., Complex dielectric permittivity in rocks: A method for its measurement and analysis, Geophysics, 38, 920-940, 1973.

Feves, M., G. Simmons, and R. Siegfried, Microcracks in crustal igneous rocks: Physical properties, in The Earth's Crust: Its Nature and Physical Properties, Geophys. Monogr. Ser., vol. 20, edited by J.G. Heacock, AGU, Washington, DC, 95-117, 1977.

General Radio Company, GR 1616 Precision Capacitance Bridge/GR 1621 Capacitance-Measurement System Instruction Manual, 1974.

General Radio Company, Dielectric Loss and Permittivity Measurements with GenRad Precision Capacitance Bridges: EID 11, undated.

Iglesias, J. and W.B. Westphal, Supplementary Dielectric-Constant and Loss Measurements on High-Temperature Materials, Technical Report 203, Laboratory for Insulation Research, Massachusetts Institute of Technology, 1967.

Olhoeft, G.R., Tables of Room Temperature Electrical Properties for Selected Rocks and Minerals with Dielectric Permittivity Statistics, U.S.G.S. Open File Report 79-993, 1979.

Padovani, E.R., S.B. Shirey, and G. Simmons, Microcracks in amphibolite and granulite facies grade rocks from southeastern Pennsylvania, in preparation, 1980.

Parkohomenko, E.I., Electrical Properties of Rocks, Plenum Press, New York, 1967.

Richter, D. and G. Simmons, Microcracks in crustal igneous rocks: Microscopy, in The Earth's Crust: Its Nature and Physical Properties, Geophys. Monogr. Ser., vol. 20, edited by J.G. Heacock, AGU, Washington, DC, 149-180, 1977.

Saint-Amant, M. and D.W. Strangway, Dielectric properties of dry, geologic materials, Geophysics, 35, 624-645, 1970.

von Hippel, A.R., Dielectrics and Waves, John Wiley and Sons, New York, 1954.

APPENDIX A

Sample Descriptions

Preliminary petrographic and microcrack descriptions of the samples that have not been described previously are included in this appendix. We have examined both polished thin sections and crack sections with the petrographic microscope and the SEM. We follow the terminology and procedures of Simmons and Richter (1976) and Richter and Simmons (1977).

References:

Richter, D. and G. Simmons, Microcracks in crustal igneous rocks: microscopy, in The Earth's Crust: Its Nature and Physical Properties, Geophys. Monogr. Ser., vol. 20, edited by J.G. Heacock, AGU, Washington, DC, 149-180, 1977.

Simmons, G. and D. Richter, Microcracks in rocks, in The Physics and Chemistry of Minerals and Rocks, edited by R.G.J. Strens, Wiley-Interscience, New York, 105-137, 1976.

Sample: 2383

Location: Adirondack Mountains

Petrographic and Microcrack Description:

Sample 2383 is an unequigranular, unfoliated garnet-hornblende-hypersthene (pyroxene)-plagioclase granulite with lesser amounts of clinopyroxene, K-feldspar, and pyrite. Garnet, hornblende, and clinopyroxene occur as subhedral, fine-grained (0.5 mm) aggregates separated by coarse hypersthene and plagioclase. Hypersthene occurs as medium-grained isolated crystals with large zones of abundant inclusions. Plagioclase ranges from coarse, isolated grains with spotty sericitized zones to fine-grained polycrystalline aggregates. Minor biotite is present as clusters of subhedral grains typically associated with pyrite.

Intragrain cracks (IGC) and grain boundary cracks (GBC) are the most abundant crack types. In garnet, open IGC are several microns wide and extend to the grain boundary whereas IGC in plagioclase are short and narrower. Partially healed IGC occur in several hornblende grains and appear as planes of microtubes (figure A-1A). A network of open and sealed GBC ranging in width from 2-20 microns is developed around the garnet-hornblende-clinopyroxene aggregates (figure A-1B). Walls of many of these cracks are jagged and appear to have been widened by alteration and/or dissolution (figure A-1C). Extensive pyrite mineralization has occurred along many grain boundaries (figure A-1D). Occasional isolated fluid inclusions are present in plagioclase and quartz.

Figure A-1A. Sample 2383. Partially healed intragrain crack (IGC) in hornblende. IGCs appear as a set of subparallel microtubes. Scale bar is 40 microns. Transmitted light photomicrograph.

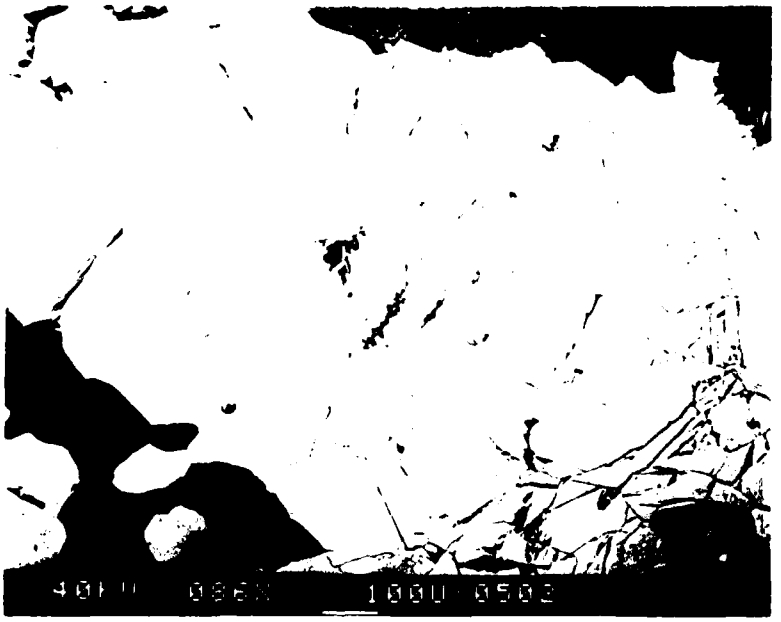

Figure A-1B. Sample 2383. Open grain boundary cracks (GBC) around hornblende-pyroxene aggregate. GBCs in this sample are best developed around these phases. BSEI.

Figure A-1C. Sample 2383. Enlargement of portion of figure A-1B. Grain boundary cracks between adjacent hornblende and pyroxene grains. Walls of the GBC are jagged and appear to have been widened by dissolution. The large bright grain is pyrite. BSEI.

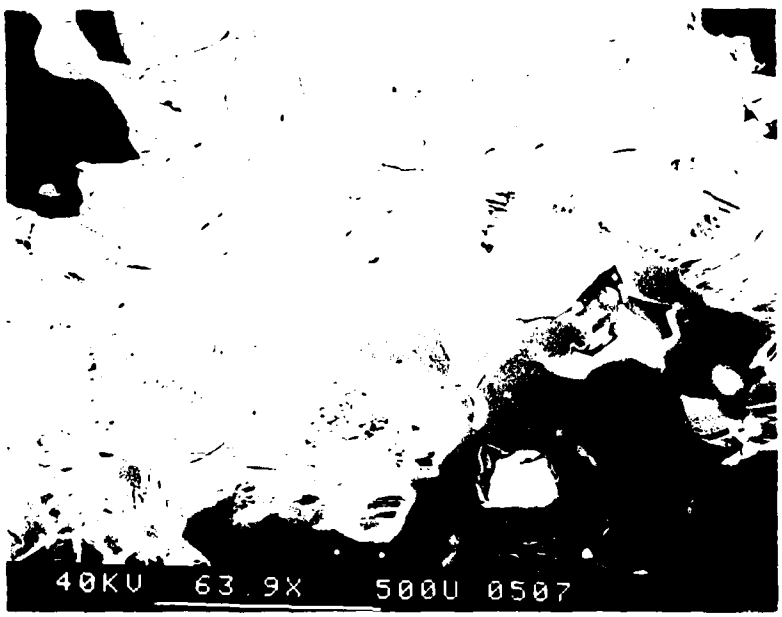

Figure A-1D. Sample 2383. Extensive pyrite mineralization (bright phase) along grain boundary cracks around hornblende-pyroxene-garnet plagioclase aggregates. BSEI.

Sample: 2390

Location: Adirondack Mountains, Northern New York

Petrographic and Microcrack Description:

Sample 2390 is a medium to coarse-grained unfoliated quartz-K feldspar-plagioclase-garnet rock. Figures A-2A and A-2B show typical textures. Quartz and perthite are anhedral, occur as coarse individual grains or medium-grained polygonal aggregates and comprise approximately 80% of the sample. Garnet occurs as coarse (5.0 mm), rounded porphyroblasts containing abundant mineral inclusions. Biotite is present as aggregates of subhedral, elongate crystals and as isolated platy grains. Minor phases include chloritized hornblende, magnetite, rutile, and sphene.

Grain boundary cracks (GBC) around quartz, perthite, and plagioclase and various types of intragrain cracks (IGC) are the most abundant microcracks in this sample. Opened, partially healed (i.e. bubble planes) and rutile sealed IGC are present in quartz (figure A-2C). Bubble planes are typically subparallel, occur in sets and consist of fluid inclusions of varying sizes (figures A-2A and A-2B). Occasional plagioclase grains contain partially healed IGC that appear as bubble planes or as partially sealed cracks (figure A-2D). GBC between quartz and feldspar are 1-3 microns wide and have straight, even walls. Isolated, randomly oriented fluid inclusions occur in quartz and to a lesser degree in plagioclase.

Figure A-2A. Sample 2390. Subparallel set of healed intragrain cracks (i.e. bubble planes) in quartz (central grain). Note the presence of numerous isolated fluid inclusions within this same grain. Transmitted light photomicrograph. Scale bar is 200 microns.

Figure A-2B. Sample 2390. Subparallel planes of fluid inclusions (i.e. bubble plane) in quartz. The bubble plane in the center of the micrograph intersects an open intragrain crack. Open grain boundary cracks between adjacent feldspar grains and between quartz and feldspar are abundant in this sample. BSEI.

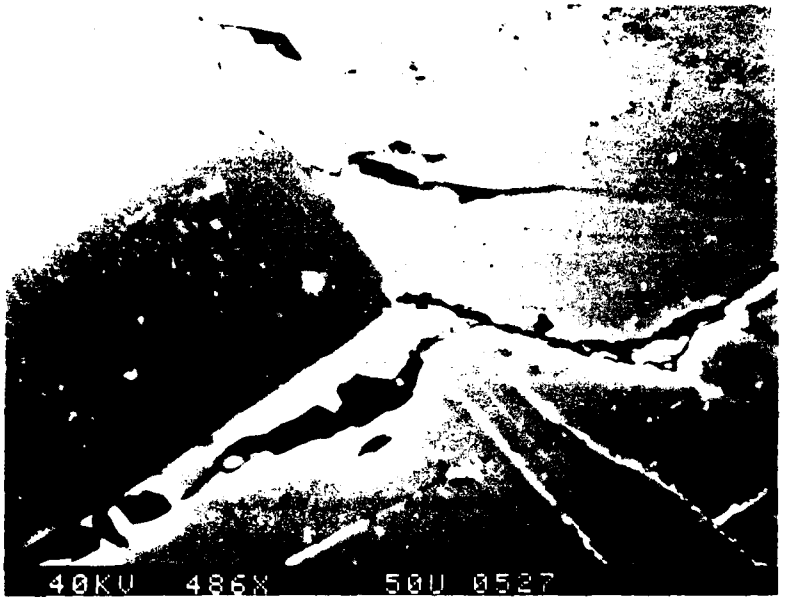

Figure A-2C. Sample 2390. Open grain boundary crack between adjacent quartz and plagioclase grains which is crosscut by a rutile(?) sealed transgranular crack (TGC) in quartz. BSEI.

Figure A-2D-1. Sample 2390. Anhedral plagioclase grain enveloped by a perthitic K-feldspar. Plagioclase contains two partially healed intragrain cracks. BSEI.

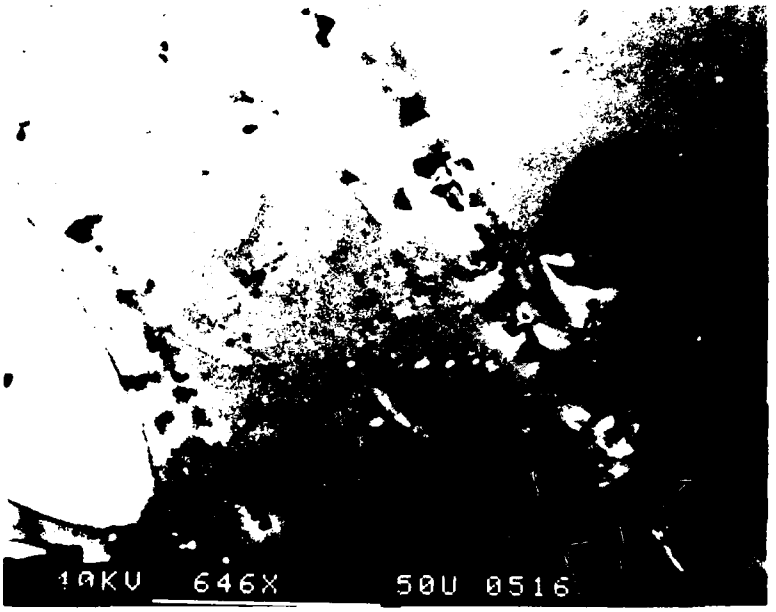

Figure A-2D-2. Sample 2390. Enlargement of the healed IGC. Note the irregular shape of the fluid inclusions along the crack. BSEI.

Sample: 2422

Location: Central Maine

Petrographic and Microcrack Description:

This sample is a fine-grained (less than 0.1 mm), non-foliated calcareous metasandstone (low grade) with small amounts of clay, mica, and an opaque mineral. Calcite occurs as subhedral crystals surrounded by polycrystalline quartz which appears as large continuous grains. Abundant pores, which vary from round to angular, are present in both quartz and calcite.

Grain boundary cracks (GBC) are the most common type of crack in this sample. GBCs between adjacent quartz grains and between quartz and calcite are poorly developed, vary from open to partially healed, and are less than 0.5 microns in width. Occasional intragrain cracks are present in calcite and, to a lesser extent, in quartz.

Sample: 2425

Location: Waterville, Maine

Petrographic and Microcrack Description:

Sample 2425 is a medium-grained, non-foliated quartzo-feldspathic meta-igneous rock. Typical textures are shown in figures A-3A and A-3B. Quartz and plagioclase comprise about 75% of the sample; alkali feldspar, garnet, and biotite are present in lesser amounts. Quartz occurs as individual grains and as coarse, polycrystalline aggregates of optically discontinuous grains. Plagioclase grains are equant to elongate, extremely sausseritized and contain abundant solid and liquid inclusions which account for the highly porous texture observed in SEM micrograph (figure A-3B). Clusters of biotite, chlorite, and sericite occur within these highly altered zones. Radiogenic mineral inclusions are common in biotite.

Intragrain cracks (IGC) and grain boundary cracks (GBC) are abundant in this sample and are best developed within and around quartz, plagioclase, and garnet. GBC between adjacent quartz grains vary from open (5.0 microns) to almost totally healed. Delicate bridges across these GBC and trails of fluid inclusions, which appear continuous with grain boundaries, are common (figure A-3C). Two distinct types of IGC are observed in plagioclase. The first type varies from open to almost totally healed and is coincident with twin planes; these IGC are only a fraction of a micron wide. The second type is 5.0 microns or less in apparent width, are randomly oriented, and either open or partially sealed with blades of chlorite (figure A-3A). Occasional trans-granular cracks (TGC) of varying widths (figure A-3D) occur within this sample. An individual microcrack rarely intersects more than two grain boundaries.

Fluid inclusions are common in quartz (predominantly bubble planes) and extremely abundant in altered plagioclase. Pores in plagioclase are irregular in shape and range in size from 15 microns to tenths of a micron.

Figure A-3A. Sample 2425. Open and chlorite sealed intragrain cracks (IGC) in an altered plagioclase grain. Clusters of fluid inclusions are abundant and unevenly distributed within this grain. BSEI.

Figure A-3B. Sample 2425. Altered plagioclase grain with a high abundance of fluid inclusions. Note the open intragrain cracks which crosscut this grain. BSEI.

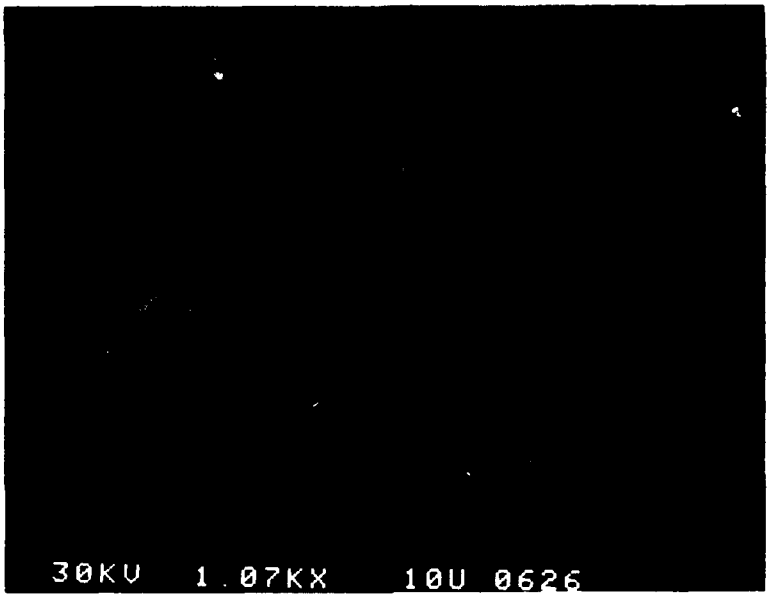

Figure A-3C. Sample 2425. Partially healed grain boundary cracks (GBC) around adjacent quartz grains. Note the delicate mineral bridges which cross the GBC and the trail of fluid inclusions continuous with GBCs. These bridges indicate that the microcracks were open in situ. BSEI.

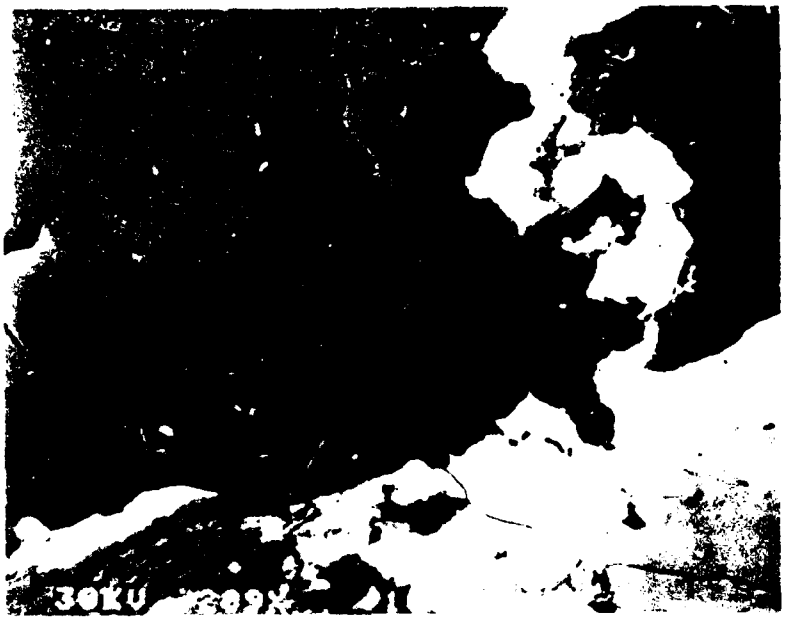

Figure A-3D. Sample 2425. Adjacent quartz (smooth, dark), plagioclase (porous texture), and biotite (bright phase) grains. Note the transgranular crack (TGC) which crosscuts a quartz-biotite grain boundary and the partially healed grain boundary cracks in quartz. Central portion is enlarged in figure A-3C. BSEI.

Sample: 2426

Location: Rockport, Maine

Petrographic and Microcrack Description:

Sample 2426 is a metaquartz conglomerate with a bimodal grain size distribution. Typical micrographs are shown in figure A-4A. Matrix quartz, which is medium-grained (0.2 mm or less), occurs as irregularly shaped, interlocking grains. Rounded, elongated pebbles (greater than 2.0 mm), composed of aggregates of interlocking quartz, are unevenly distributed throughout the sample. The matrix portion is characterized by (1) angular pores which vary from 5 to 75 microns, typically occur at the junction of grain boundaries and are either empty or filled with clusters of a micaceous mineral in association with clay, (2) open or sealed grain boundary cracks (GBC) less than 2 microns in apparent width, the sealing phases are a mica and clay, (3) abundant fluid and mineral inclusions. Figure A-4A illustrates these features.

Microstructurally, the polycrystalline quartz pebbles differ from the matrix quartz in that (1) no intergrain pore spaces are present, (2) GBC are either open or partially healed, i.e. intergrain mica is absent, and (3) fluid and mineral inclusions are less abundant.

An extensive, anastomosing network of sealed multigrain cracks (MGC) extends the entire length of the thin section; the predominant crack sealing phase is an Fe-Mg bearing mineral (figure A-4B). The MGC intersects several coarse (2.0-5.0 mm) prismatic Fe-Mg sulfide crystals which are rimmed and brecciated by the Fe-Mg crack sealing phase. Occasional fractured, elongated muscovite grains occur within the MGC.

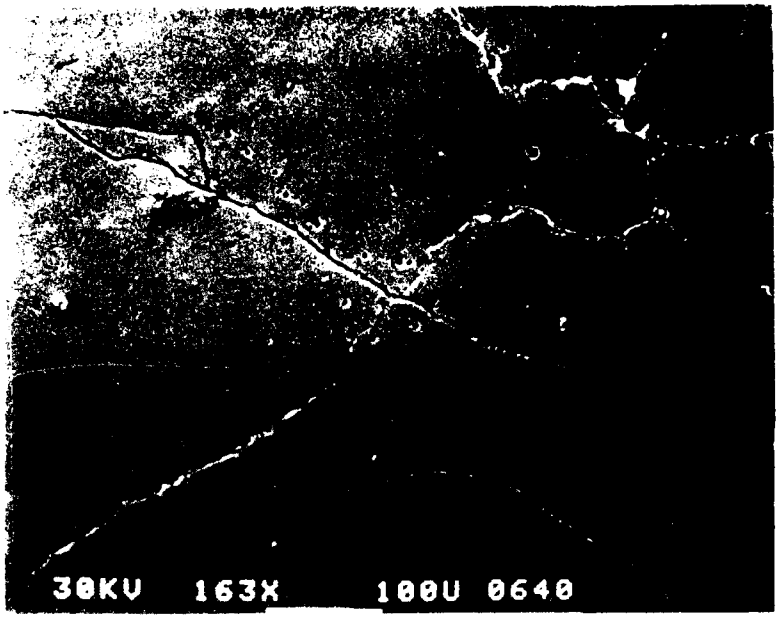

Figure A-4A-1. Sample 2426. Representative area of the matrix quartz fraction of the metaconglomerate. Muscovite (brighter phase) occurs as clusters between quartz grains and occasionally along grain boundaries.

Figure A-4A-2. Sample 2426. Enlargement of portion of figure A-4A-1. Grain boundary cracks vary from open to partially healed. BSEI.

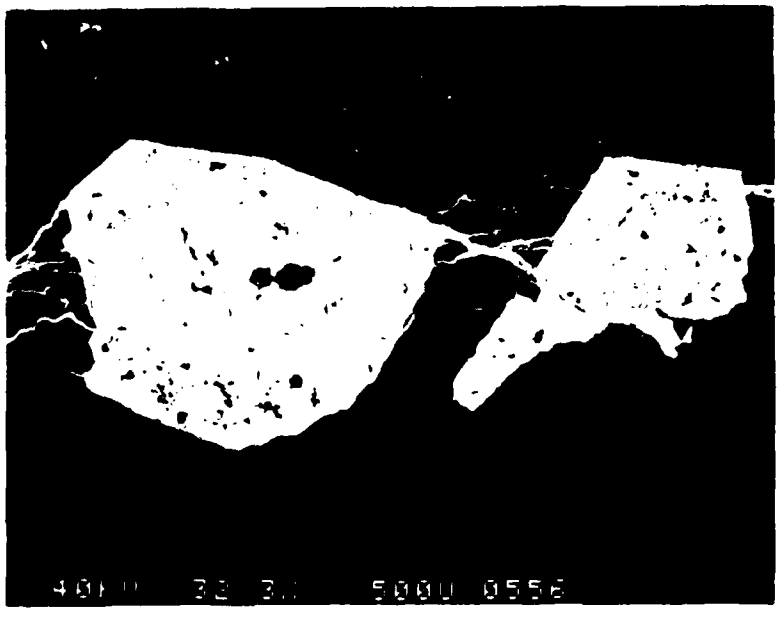

Figure A-4B-1. Sample 2426. Extensive, anastomosing multigrain crack (MGC) network intersecting prismatic Fe-Mg sulfide crystals. The sulfide crystals are rimmed and fractured by an Fe-Mg crack sealing phase (see figure A-4B-3 for EDS pattern) which is the major crack sealing phase. BSEI.

Figure A-4B-2. Sample 2426. Enlargement of an area in figure A-4B-1. The bright phase is composed of Fe and Mg. Occasional muscovite (elongate crystal) occurs within the MGC network. The dot marks the location of the EDS analysis given in figure A-4B-3. BSEI.

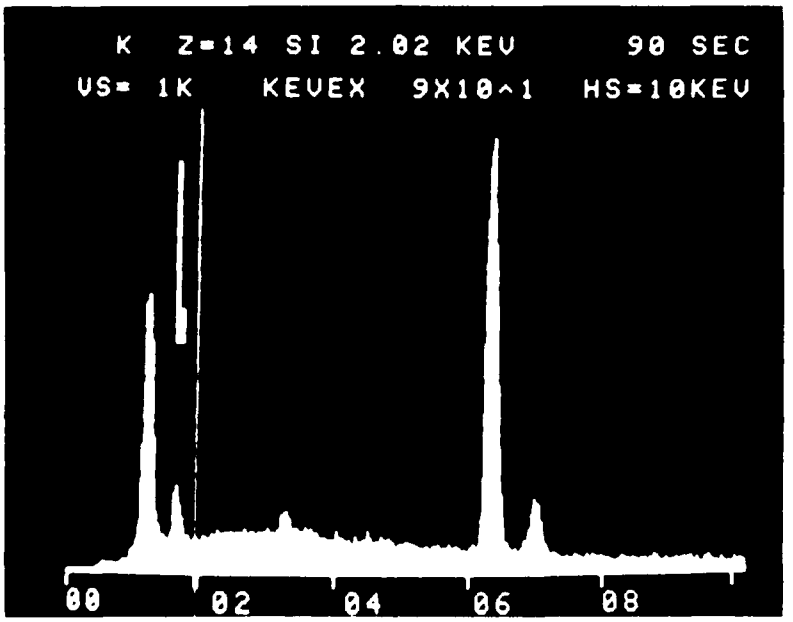

Figure A-4B-3. Sample 2426. EDS spectrum of crack sealing phase shown in figure A-4B-2. The peaks (left to right) are MgK (1.3 Kev), SiK (1.7 Kev), KK_{α} (3.3 Kev), FeK_{α} (6.4 Kev), and FeK_{β} (7.1 Kev).

Sample: 2428

Location: Camden, Maine

Petrographic and Microcrack Description:

Sample 2428 is a metaquartz conglomerate with a bimodal grain size distribution. Typical micrographs are given in figures A-5A and A-5B. The matrix quartz fraction is composed of irregularly shaped, interlocking grains with apparent grain sizes between 0.2 and 0.4 mm. The pebble fraction consists of coarse (greater than 2.0 mm) rounded, elongated, polycrystalline grains which can be subdivided into two types based on the size of individual quartz grains. The first type is fine-grained (0.1 to 0.2 mm), occurs in irregularly shaped pebbles and contains abundant inclusions. The second type is coarser-grained (0.6 to 1.0 mm), occurs in well-rounded pebbles and contains fewer inclusions. Biotite and muscovite are present as platy or elongated crystals within grain boundaries or as irregularly shaped clusters (figure A-5B); occasional pyrite occurs within these clusters.

Grain boundary cracks are the most abundant crack type in this sample. GBC around matrix quartz and fine-grained polycrystalline grains vary from open to sealed, have apparent width less than 0.5 microns, and contain abundant biotite and muscovite (figure A-5C). Many of the GBC are continuous around irregularly shaped pores, which are abundant in this sample. GBC around the coarse, polycrystalline grains are wider (0.5 to 10 microns) and contain open or partially sealed (with rutile) segments (figure A-5D); interstitial muscovite and biotite are absent. Occasional intragrain cracks, which appear as planes of fluid inclusions, occur only within the coarser fraction (figure A-5A).

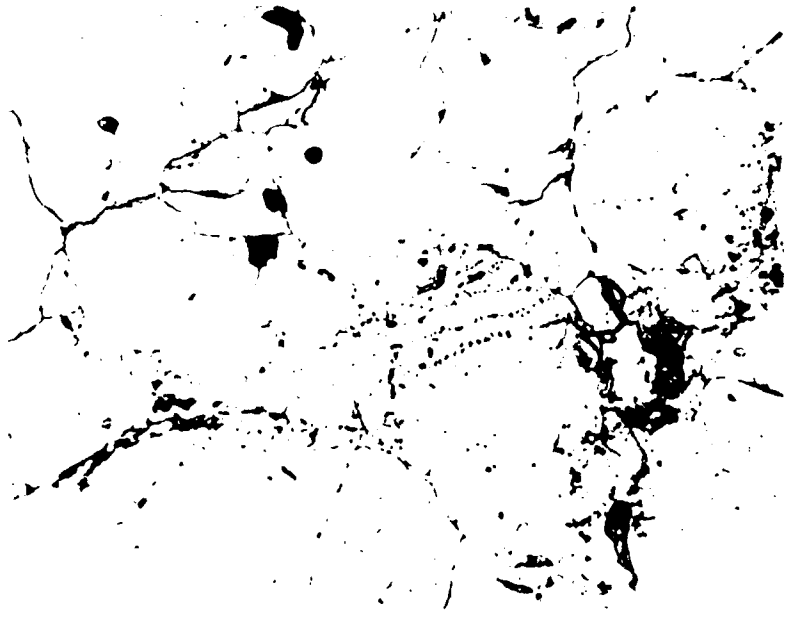

Figure A-5A. Sample 2428. Subparallel set of bubble planes which are continuous across a quartz-quartz grain boundary. Area is within a polycrystalline quartz pebble. Transmitted light micrograph. Scale bar is 200 microns.

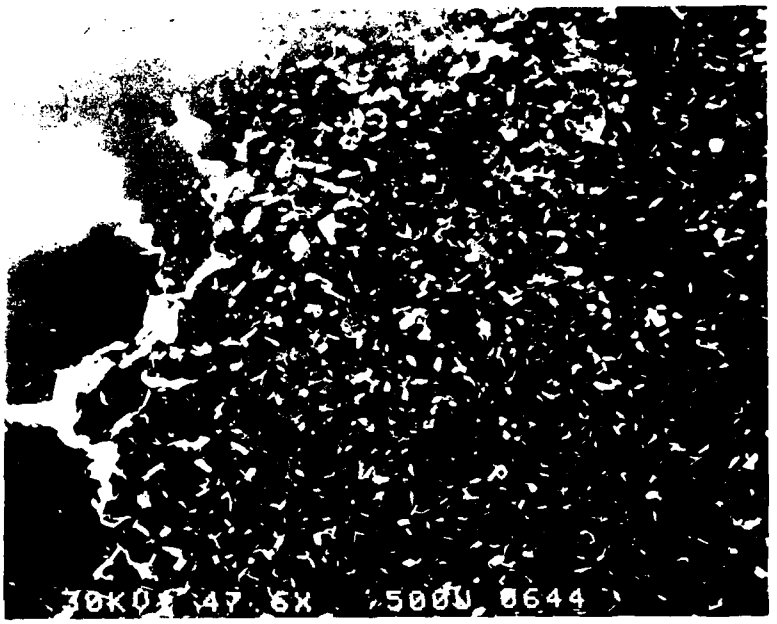

Figure A-5B. Sample 2428. Matrix (right) and pebble (left). This micrograph illustrates the great variation in abundance and distribution of (a) interstitial biotite (bright phase) and muscovite (light gray) and (b) pores between the matrix and pebble fractions. A typical area in the matrix is enlarged in figure A-5C. BSEI.

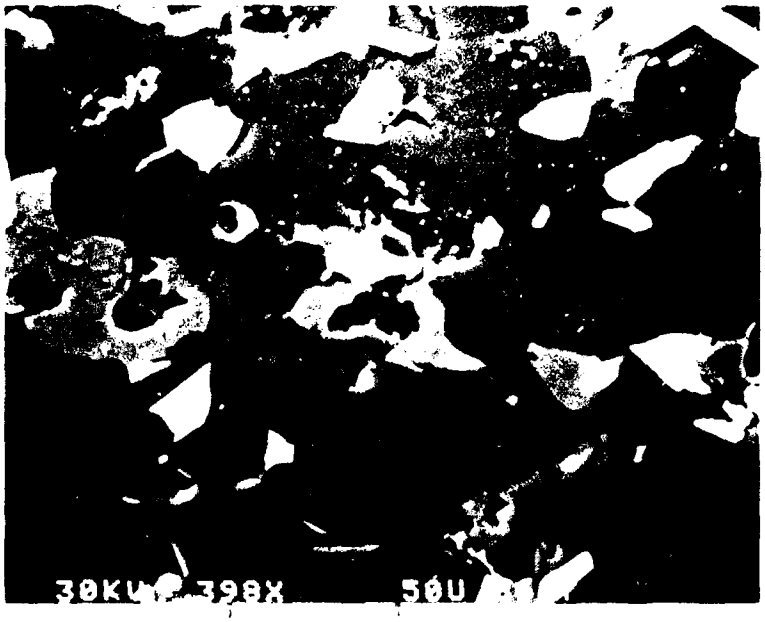

Figure A-5C. Sample 2428. Grain boundary cracks (GBC) around matrix quartz grains. GBCs vary from open to partially healed and commonly terminate at the intersection of a biotite or muscovite grain. BSEI.

Figure A-5D-1. Sample 2428. Grain boundary cracks (GBC) and intragrain cracks (IGC) associated with polycrystalline quartz grains in the pebbles. GBCs are partially sealed with rutile (bright phase). A plane of fluid inclusions trends subparallel to an open GBC. BSEI.

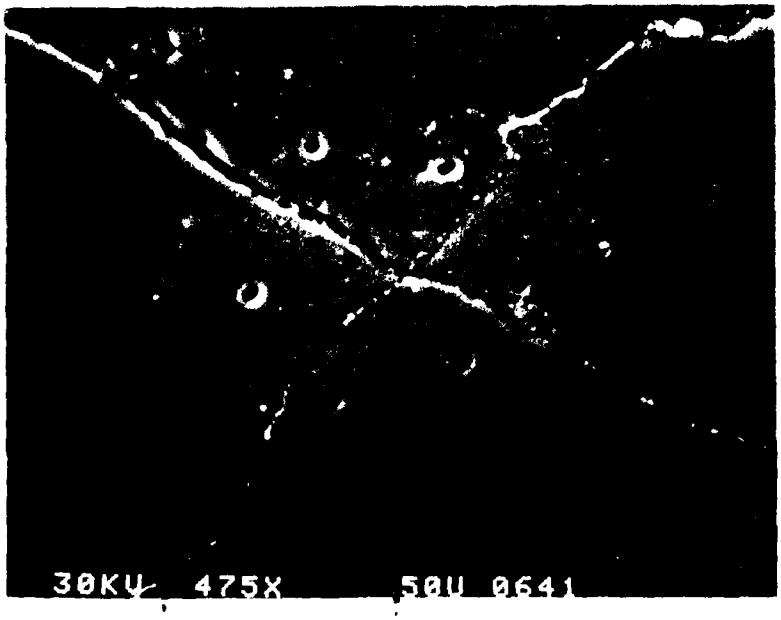

Figure A-5D-2. Sample 2428. Enlargement of the central area of figure A-5D-1. Note the presence of several, randomly oriented fluid inclusions. BSEI.

Sample: 2432

Location: Camden, Maine

Petrographic and Microcrack Description:

Sample 2432 is a foliated metaquartz conglomerate composed of elongate, polycrystalline pebbles (individual grains are 0.3 mm) in a fine-grained (less than 0.15 mm) matrix of quartz and muscovite. Muscovite occurs as aggregates of blade-like crystals which appear as subparallel, discontinuous grains aligned with schistosity between quartz grains; these aggregates vary from 0.01 to 0.20 mm in apparent width. A typical view of quartz grains and matrix is shown in figure A-6A. Numerous angular cavities (less than 75 microns) occur in the matrix fraction (figure A-6B) and to a lesser extent in the polycrystalline pebbles. These cavities vary from empty to totally filled with intergrown muscovite and clay (figure A-6B). Isolated pyrite crystals occur in association with these phases.

Grain boundary cracks (GBC) are the most abundant type of crack in this sample. GBC around matrix quartz grains are less than 0.5 microns in apparent width, vary from partially healed to partially sealed with muscovite blades, and typically terminate at a cavity wall (figures A-6A and A-6C). GBC around quartz pebbles are wider (2-15 microns) and contain abundant muscovite and clay (figure A-6A). Solid and fluid inclusions are abundant in both matrix and pebble quartz grains.

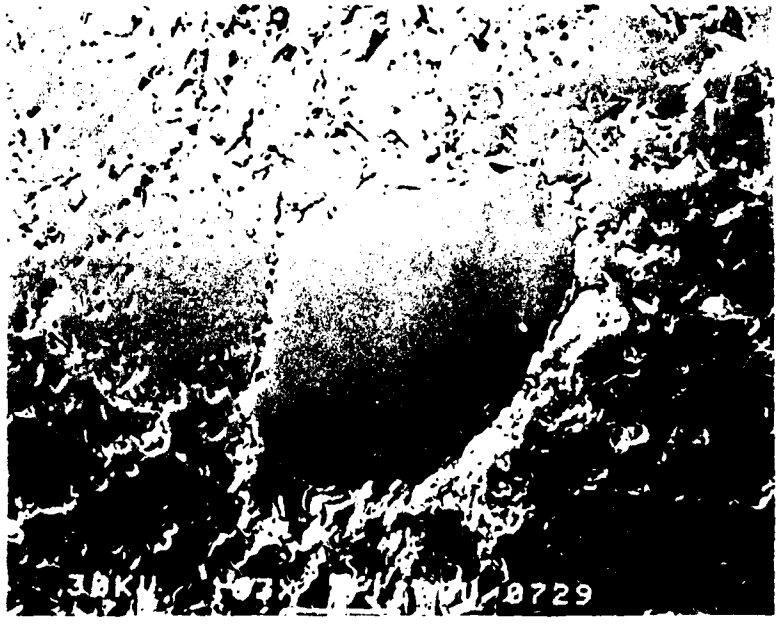

Figure A-6A. Sample 2432. Muscovite-clay sealed grain boundary crack around a rounded, slightly elongate quartz grain. Note the low density solid or fluid inclusions in this grain. BSEI.

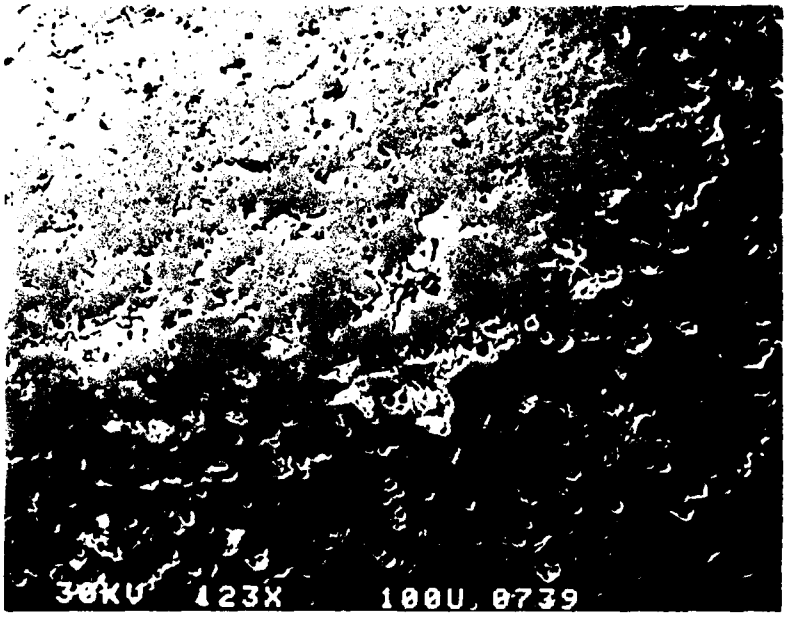

Figure A-6B-1. Sample 2432. Representative area in fine-grained matrix portion of this sample. Grain boundary cracks between adjacent quartz grains are poorly developed. Note the abundance of angular cavities. BSEI.

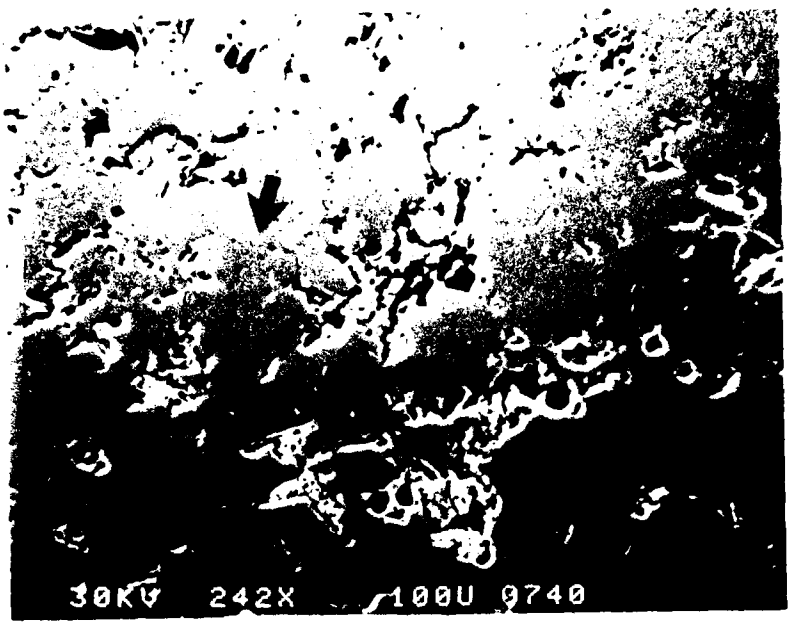

Figure A-6B-2. Sample 2432. Enlargement of central portion of figure A-6B-1. Cavities range from empty to filled with clay and/or muscovite. Arrow denotes location of figure A-6C. BSEI.

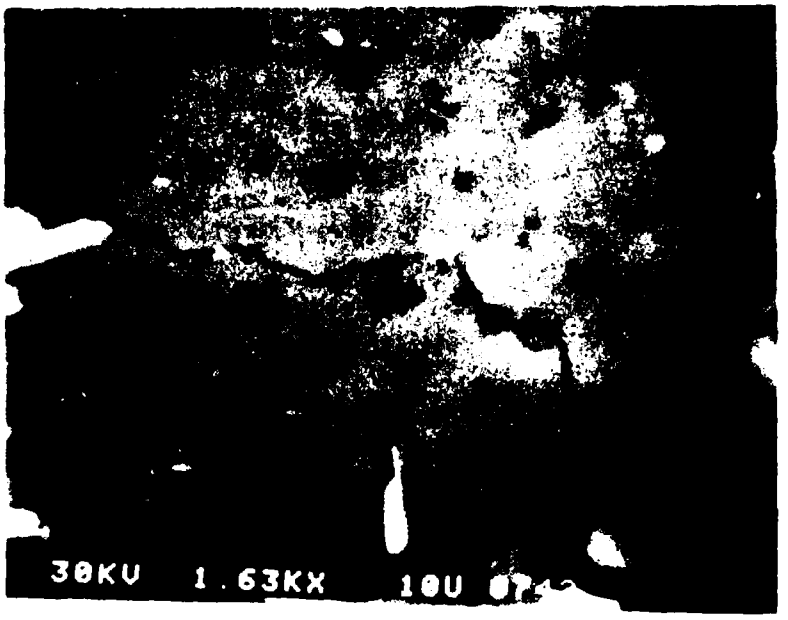

Figure A-6C. Sample 2432. Partially healed grain boundary crack between adjacent quartz grains in the matrix. Abundant fluid inclusions are present in quartz. BSEI.

Sample: 2434

Location: Camden, Maine

Petrographic and Microcrack Description:

Sample 2434 is a metamorphosed, extremely fine-grained (less than 0.1 mm) interbedded siliceous limestone (i.e. calc-silicate). Compositional bands are discontinuous, are highly contorted and irregular, range in thickness from 0.75 to 10 mm and are divisible into three general types of mineral assemblages. The most abundant type consists of interlocking angular calcite, rounded quartz grains, and biotite blades (figure A-7A). Numerous intragrain and interstitial pores occur in and between calcite grains. The second type consists of intergrown clay and biotite and diopsidic pyroxene with lesser amounts of quartz, calcite, and sphene (figure A-7B). The third type, which occurs as narrow (0.4 mm or less) bands, consists of rounded quartz grains and muscovite with minor amounts of clay and sphene (figure A-7C). Contacts between adjacent compositional layers range from sharp to gradational.

Grain boundary cracks around adjacent calcite grains and intragrain cracks in calcite are the only microcracks in this sample. The GBC vary from open to partially healed and have apparent widths less than 0.5 microns (figure A-7D). All IGC appear as bubble planes which terminate at a grain boundary.

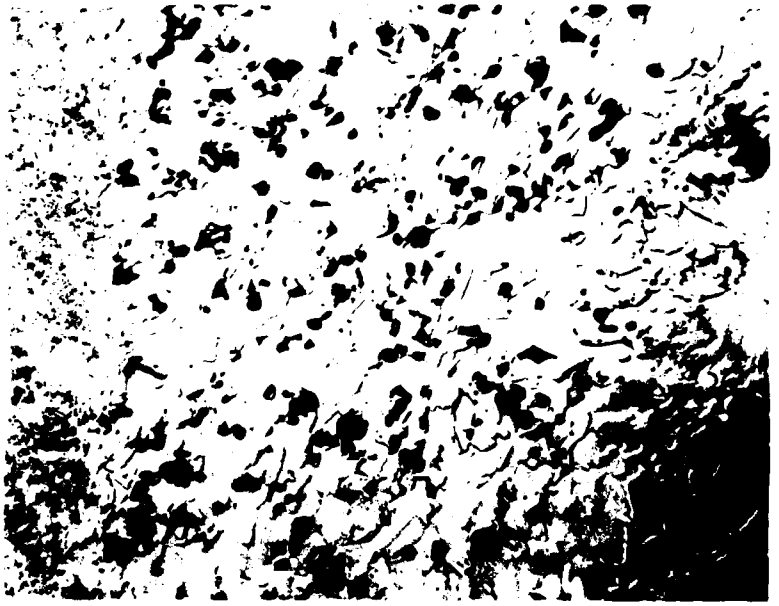

Figure A-7A. Sample 2434. Calcite-quartz-biotite compositional layer containing abundant angular pores. Quartz (dark phase) and biotite are evenly distributed throughout the layer. This unit grades into a more quartz-biotite rich layer to the right; the left boundary is defined by a sharp contact with a calc-silicate band containing sphene and diopsidic pyroxene. BSEI.

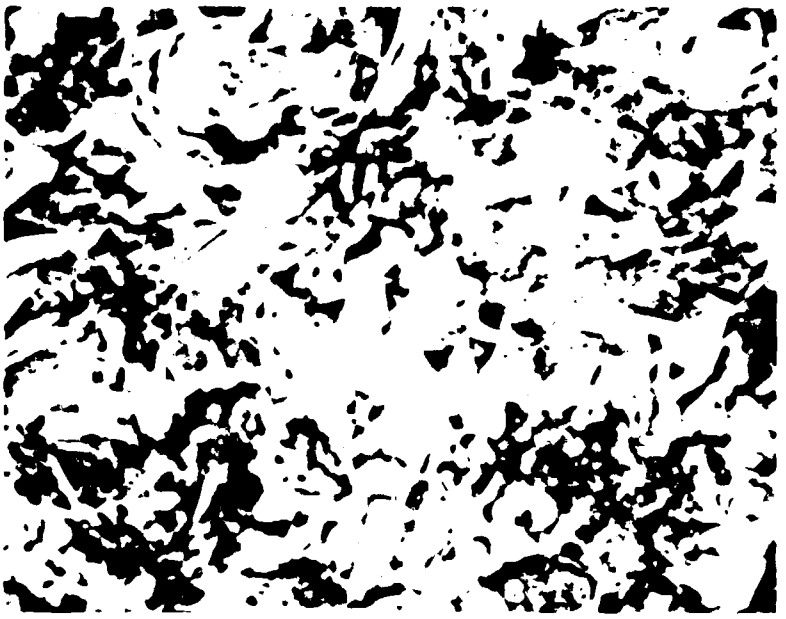

Figure A-7B. Sample 2434. Calc-silicate layer containing diopsidic pyroxene, sphene and intergrown clay (possibly an alteration product of muscovite) and biotite. This unit is completely devoid of any microcrack. Note the presence of clusters of fluid inclusions. BSEI.

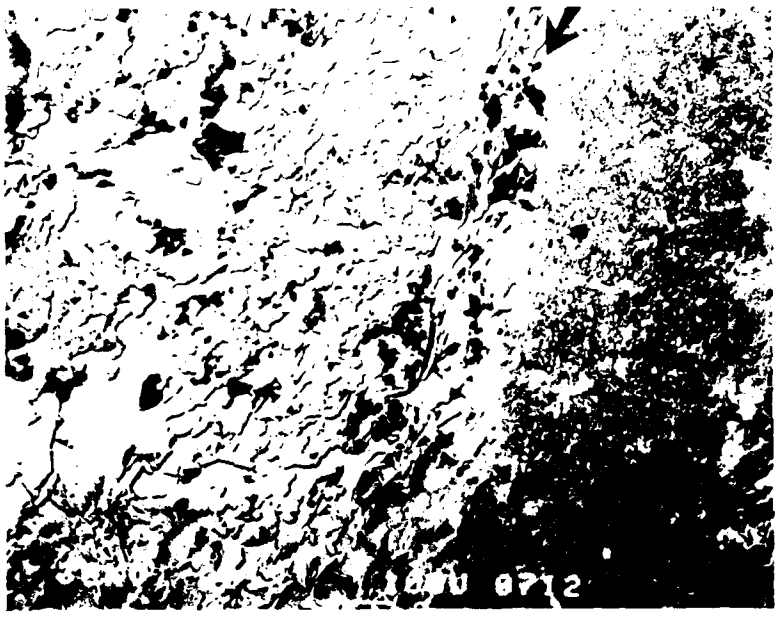

Figure A-7C. Sample 2434. Quartz-muscovite rich layer (arrow) sandwiched between a calc-silicate unit (right) and a calcite-rich layer (left). The quartz-muscovite mineral assemblage is present in thin, discontinuous bands. BSEI.

Figure A-7D-1. Sample 2434. Open grain boundary cracks and healed intragrain cracks (IGC) associated with calcite. These cracks are the only cracks observed in this sample. BSEI.

Figure A-7D-2. Sample 2434. Enlargement of an area in figure A-7D-1. The healed IGCs appear as planes of fluid inclusions. BSEI.

Sample: 2439

Location: Central Maine

Petrographic and Microcrack Description:

Sample 2439 is a medium to coarse-grained quartzo-feldspathic, biotitic migmatite. Compositional bands are continuous, range in width from 2-10 cm, and are divisible into two types of mineral assemblages. The first type, which is medium-grained, consists of quartz, plagioclase, and biotite with lesser amounts of muscovite and garnet. Parallel alignment of biotite, which occurs as clusters of subhedral, blade-shaped crystals, defines a well-developed foliation. Quartz grains tend to be elongated in the direction of foliation. Porphyroblasts of plagioclase are partially sericitized. The second type, which is medium to coarse-grained, consists of K-feldspar, quartz, and plagioclase interlayered with thin bands composed of muscovite intergrown with sillimanite needles, garnet porphyroblasts and thin granulose quartz bands. Alkali feldspar is coarse, sometimes polycrystalline and slightly sericitized.

Intragrain cracks are the most abundant crack type in this sample. Two types of IGC occur in quartz: (1) anastomosing microcracks with open and partially sealed segments, many of which are bound on either end by abrupt changes in microcrack direction (figure A-8A) and (2) healed microcracks (i.e. planes of fluid inclusions) (figure A-8B). In K-feldspar, IGC are typically isolated, subparallel and open (figure A-8B).

Fluid inclusions in K-feldspar occur as (1) distinct planes within individual grains (figure A-8B), (2) broad bands which parallel grain boundaries (figure A-8C), (3) isolated clusters unevenly distributed within grains. Plagioclase grains contain abundant inclusions, many of which are filled with sericite (figure A-8B). Poorly developed grain boundary cracks occur between adjacent quartz grains and at the borders of feldspar (potassium and plagioclase) and quartz grains.

Figure A-8A-1. Sample 2439. Anastomosing intragrain cracks (IGC) in quartz. IGCs in quartz contain both open and partially sealed segments. They typically terminate on other cracks with low angle intersections. BSEI.

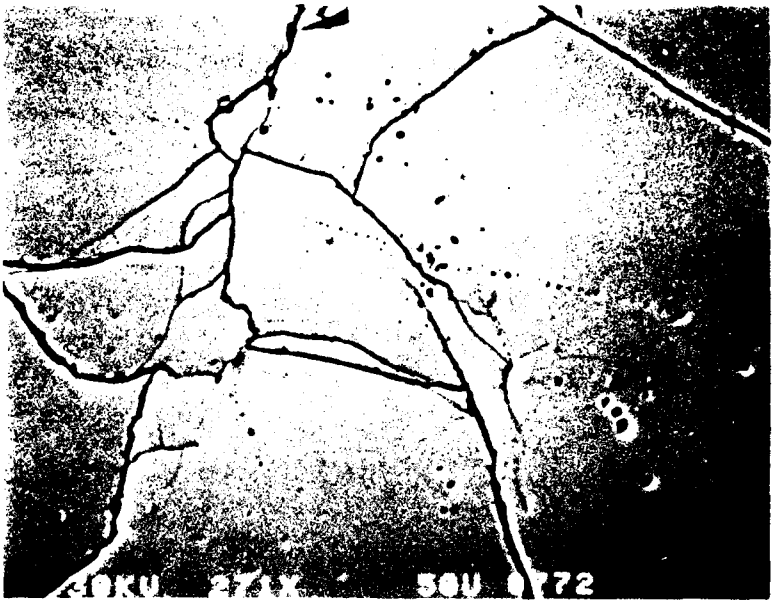

Figure A-8A-2. Sample 2439. Enlargement of central area of figure A-8A-1. Note the abundance of fluid inclusions. BSEI.

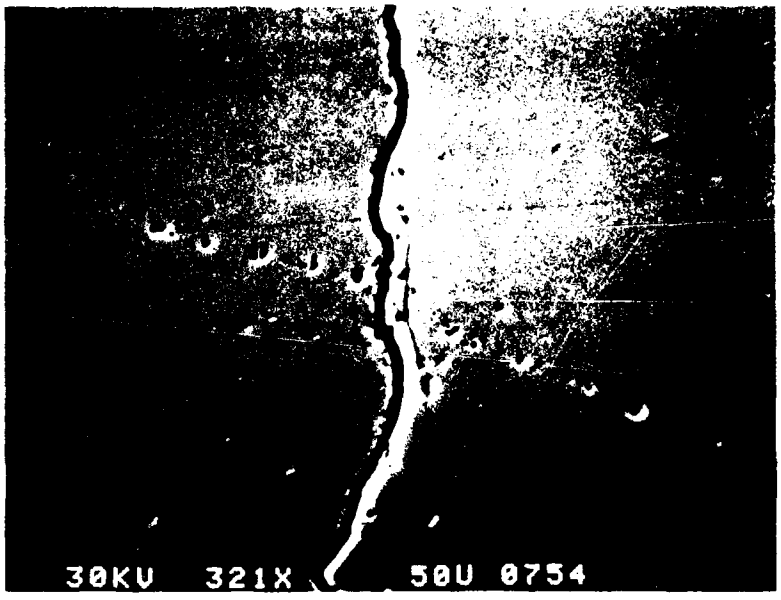

Figure A-8B-1. Sample 2439. Intersection between a partially healed (i.e. bubble plane) intragrain crack (IGC) and an open IGC in quartz. The left end of the partially healed crack is enlarged in A-8B-2. BSEI.

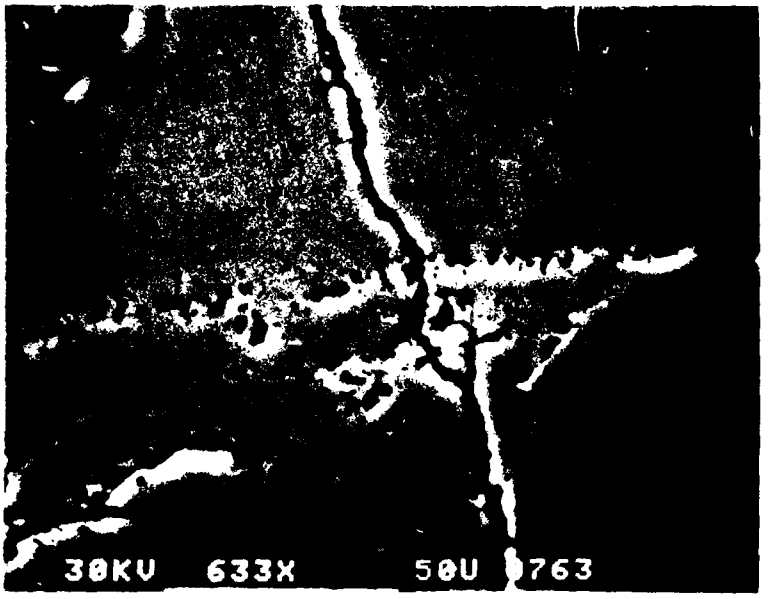

Figure A-8B-2. Sample 2439. Intersection between a partially healed (i.e. bubble plane) intragrain crack (IGC) and an open IGC in quartz. Enlargement of segment of bubble plane seen in figure A-8B-1. At this location, the healed IGC is defined by a series of short, overlapping bubble planes (i.e. en echelon cracks). BSEI.

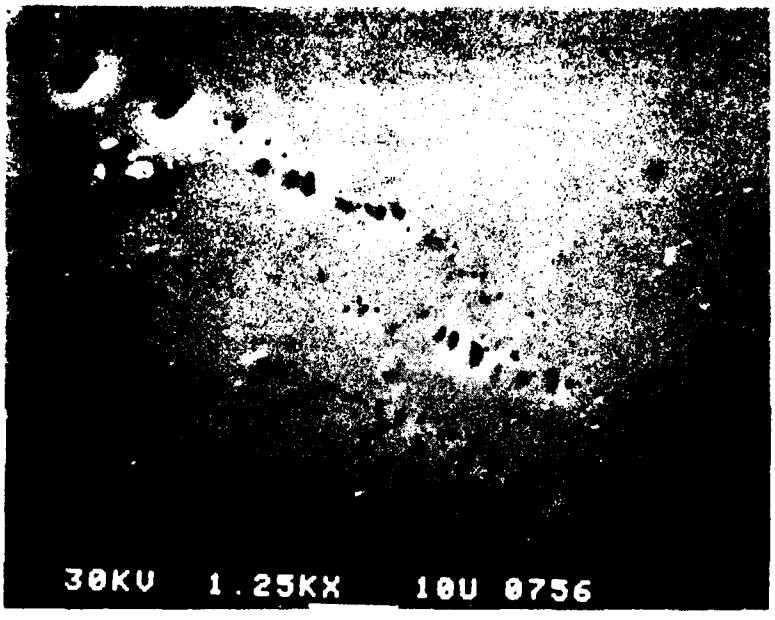

Figure A-8B-3. Sample 2439. Intersection between a partially healed (i.e. bubble plane) intragrain crack (IGC) and an open IGC in potassium feldspar. Note the thin dark parallel lines which indicate cleavage. Absence of surfaces on sides of the large crack, the generally smooth surface of the crack, the failure of the 10μ-size fragment to break along cleavage directions are evidence that the crack was present in the rock in situ and was not produced by sample collecting, handling, or preparation.

Figure A-8C-1. Sample 2439. Plagioclase (porous phase) contains abundant solid and fluid inclusions. Arrow indicates area seen in figure A-8C-2. BSEI.

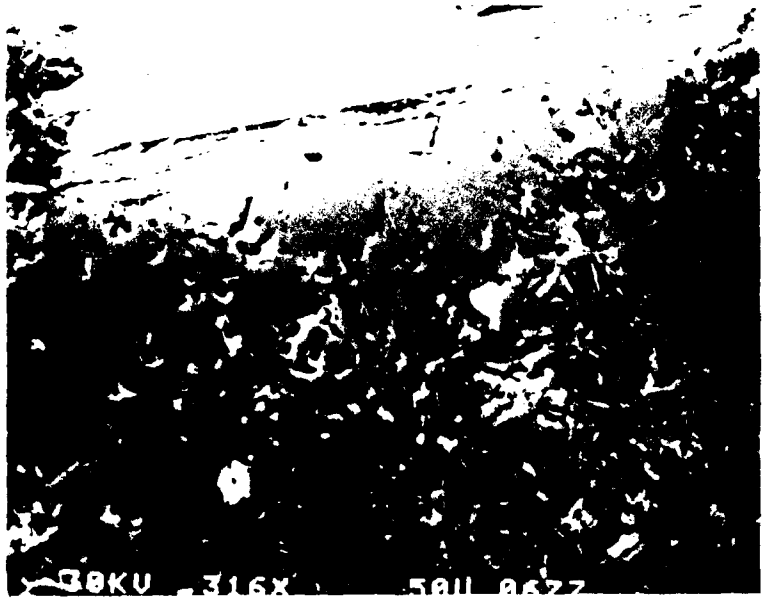

Figure A-8C-2. Sample 2439. Enlargement of inclusions in plagioclase. BSEI.

Figure A-8D. Sample 2439. Agglomeration of fluid inclusions around the periphery of a potassium feldspar grain. The elongate mineral is muscovite. BSEI.

Sample: 2441

Location: Camden, Maine

Petrographic and Microcrack Description:

Sample 2441 is a quartz-plagioclase-biotite-andalusite schist with a well-developed foliation defined by the parallel alignment of subhedral blades of biotite (figure A-9A). Elongate aggregates of columnar andalusite crystals occur in association with biotite. Quartz is present as coarse, elongate grains and as finer-grained, irregularly shaped crystals which together comprise quartzose bands (several mm wide) which parallel the foliation. Plagioclase is coarse, sometimes polycrystalline with large zones of extensive sericitization.

Grain boundary cracks (GBC) are best developed around andalusite and quartz (figure A-9A). GBC range from 1 to 10 microns in width, typically have jagged walls, and are either open or sealed with a clay phase (figure A-9A). Occasional GBC between plagioclase and andalusite contain brecciated material enveloped by clay and platy muscovite crystals. Quartz contains numerous open intragrain cracks (IGC) which extend from the grain boundary and terminate within the grain before intersecting another grain boundary (figures A-9B and A-9C). Many of the IGC are oriented perpendicular to the direction of elongation. Abundant subparallel sets of healed IGC (i.e. planes of fluid inclusions) are ubiquitous in quartz (figure A-9C).

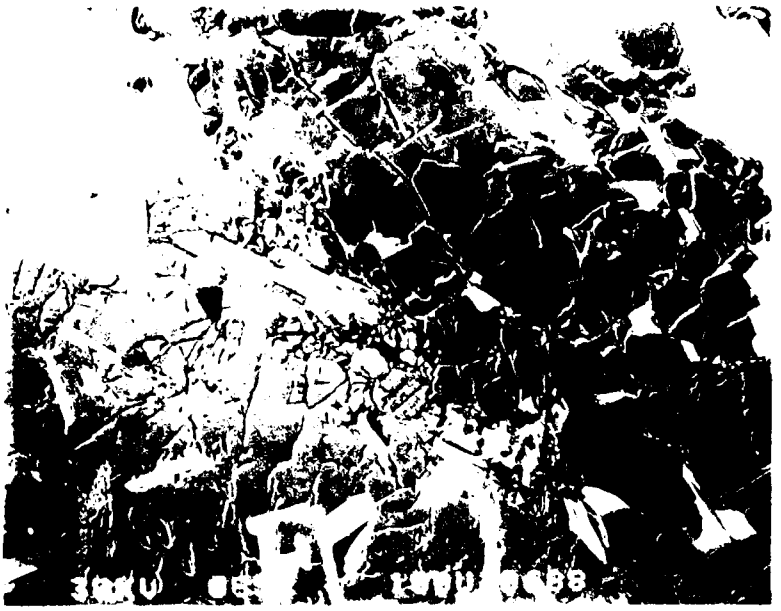

Figure A-9A-1. Sample 2441. Representative area of this sample, illustrating the textural relationships between andalusite (dark gray), plagioclase (light gray), biotite (bright phase), and muscovite. Sealed grain boundary cracks (GBC) occur around columnar andalusite crystals and polycrystalline plagioclase. Central portion is enlarged in figure A-9A-2. BSEI.

Figure A-9A-2. Sample 2441. Enlargement of clay-sealed GBCs around andalusite crystals. BSEI.

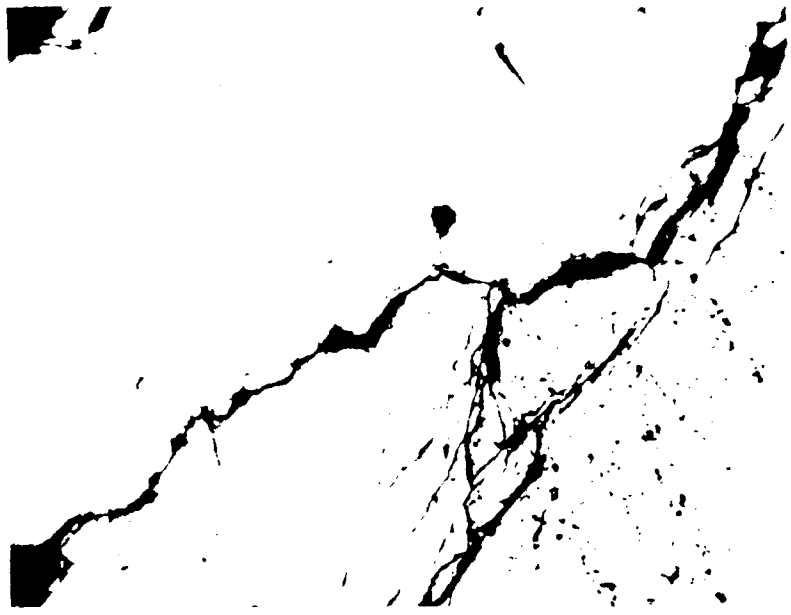

Figure A-9B. Sample 2441. Open grain boundary crack (GBC) and intragrain crack in quartz. Note the abundance of fluid inclusions. Transmitted light micrograph. Scale bar is 200 microns.

Figure A-9C-1. Sample 2441. Open and partially healed intragrain cracks (IGC) in quartz. Healed IGCs (bubble planes) typically occur in subparallel sets.

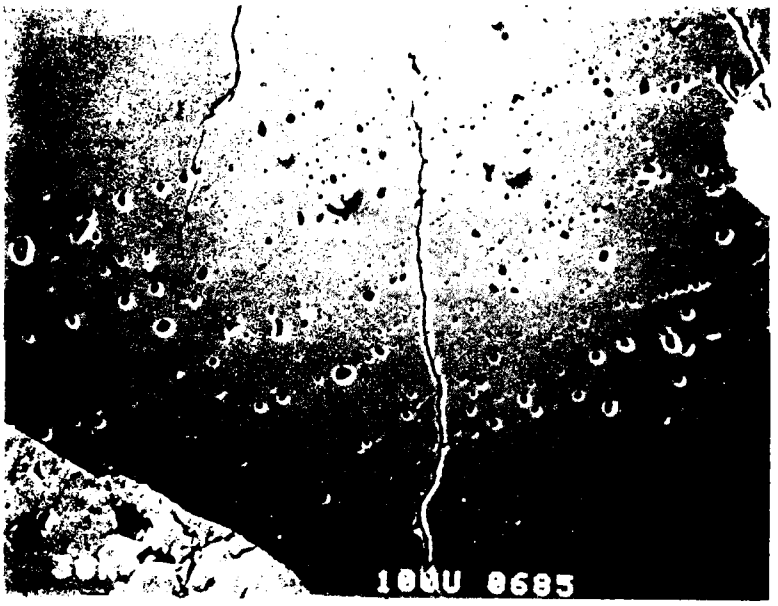

Figure A-9C-2. Sample 2441. Enlargement of central area of figure A-9C-1. These fluid inclusions record many episodes of fracturing and sealing.

APPENDIX B

Dielectric Properties of Selected Igneous and Metamorphic Rocks

A table of data on the dielectric property (permittivity and dielectric conductivity) as a function of frequency is given for each specimen. The data are also given in graphical form.

SAMPLE 83

FREQUENCY (HERTZ)	RELATIVE DIELECTRIC CONSTANT	CONDUC-TIVITY (MHO/M)	LOSS TANGENT	LOSS FACTOR
100.	5.707	0.2884E-09	0.3003E-01	0.1714E 00
200.	5.635	0.5391E-09	0.2843E-01	0.1602E 00
300.	5.594	0.7889E-09	0.2794E-01	0.1563E 00
400.	5.566	0.1026E-08	0.2738E-01	0.1524E 00
500.	5.545	0.1262E-08	0.2706E-01	0.1500E 00
800.	5.502	0.1941E-08	0.2621E-01	0.1442E 00
1000.	5.483	0.2401E-08	0.2603E-01	0.1427E 00
2000.	5.421	0.4619E-08	0.2532E-01	0.1373E 00
3000.	5.388	0.6723E-08	0.2472E-01	0.1332E 00
4000.	5.362	0.8844E-08	0.2451E-01	0.1314E 00
5000.	5.344	0.1095E-07	0.2435E-01	0.1301E 00
8000.	5.306	0.1708E-07	0.2392E-01	0.1269E 00
10000.	5.290	0.2094E-07	0.2353E-01	0.1245E 00
15000.	5.259	0.3094E-07	0.2331E-01	0.1226E 00
20000.	5.236	0.4058E-07	0.2303E-01	0.1206E 00
25000.	5.216	0.4996E-07	0.2277E-01	0.1188E 00
30000.	5.205	0.5960E-07	0.2269E-01	0.1181E 00
40000.	5.180	0.7845E-07	0.2250E-01	0.1166E 00
50000.	5.162	0.9686E-07	0.2230E-01	0.1151E 00
1000.	5.483	0.2406E-08	0.2608E-01	0.1430E 00

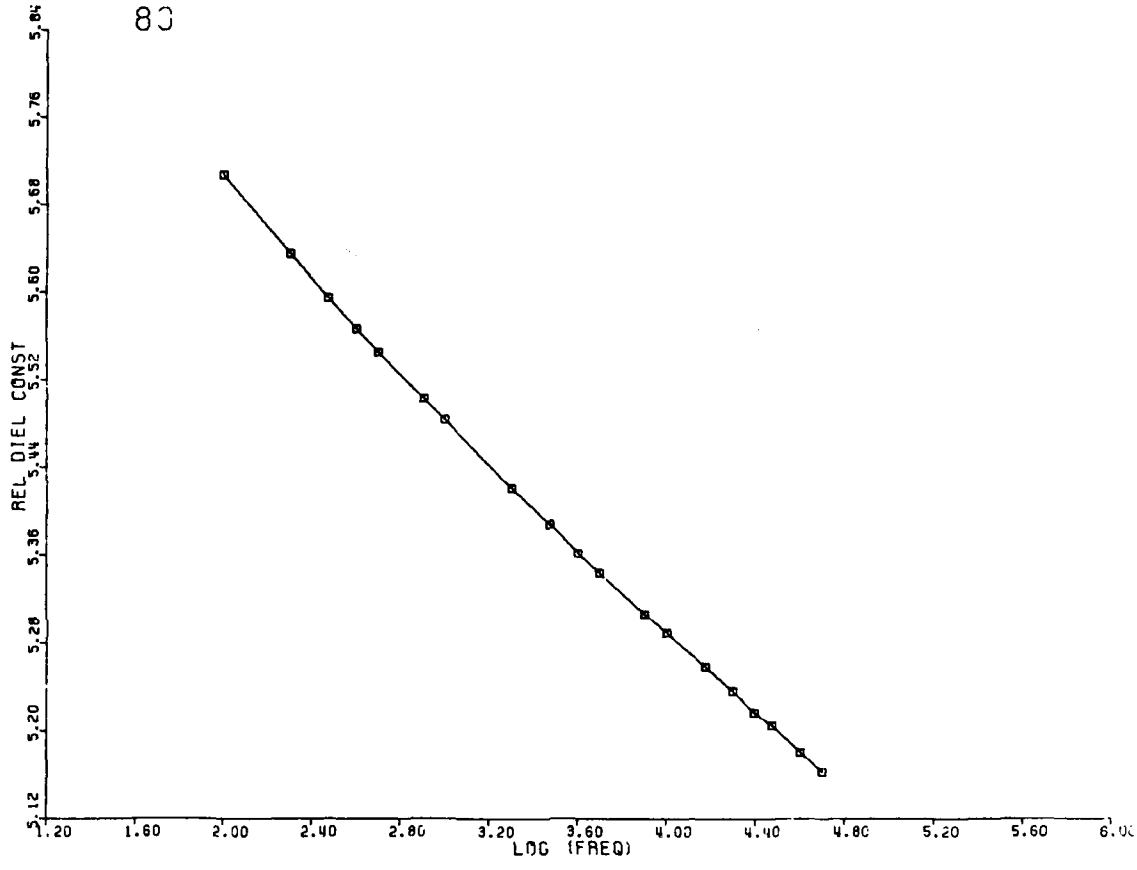

Figure B-1A. Relative permittivity (ε') of sample 83, granite from Troy, Oklahoma, as a function of frequency.

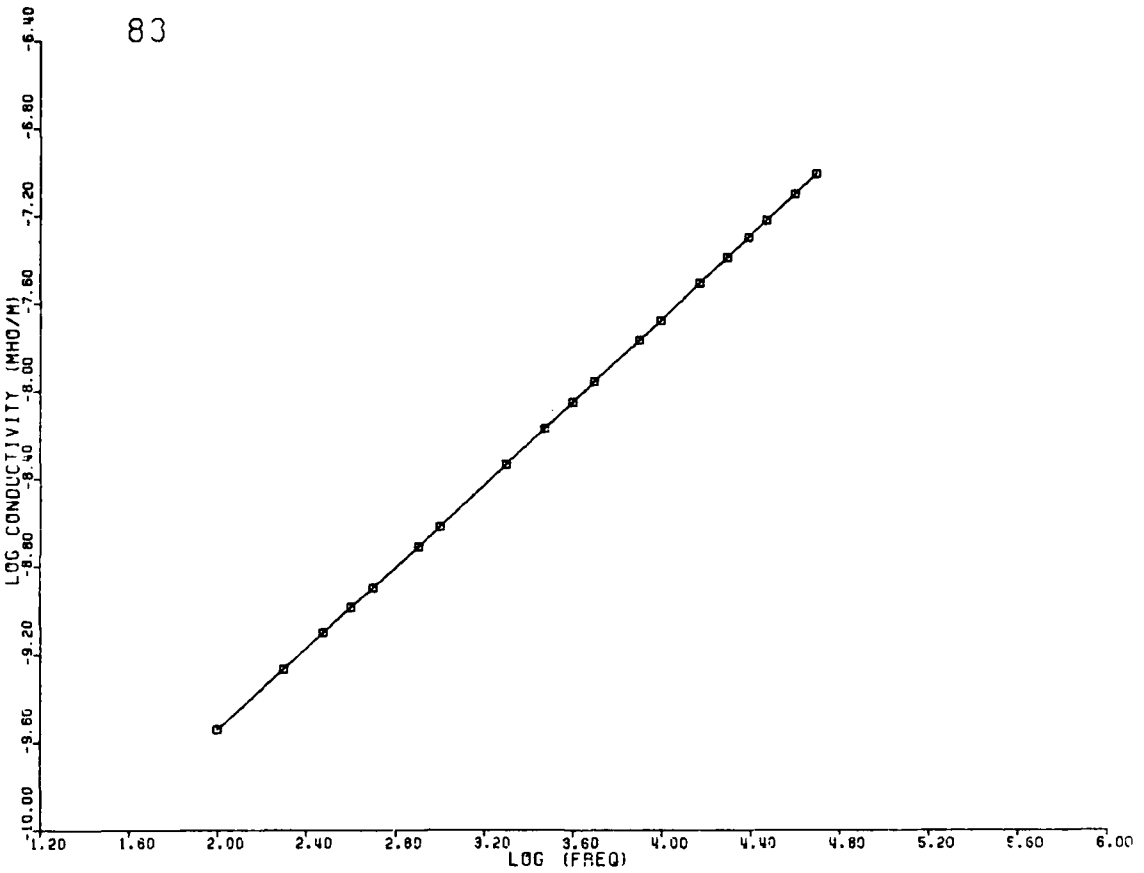

Figure B-1B. Dielectric conductivity ($\sigma = \omega\varepsilon''$) of sample 83, granite from Troy, Oklahoma, as a function of frequency.

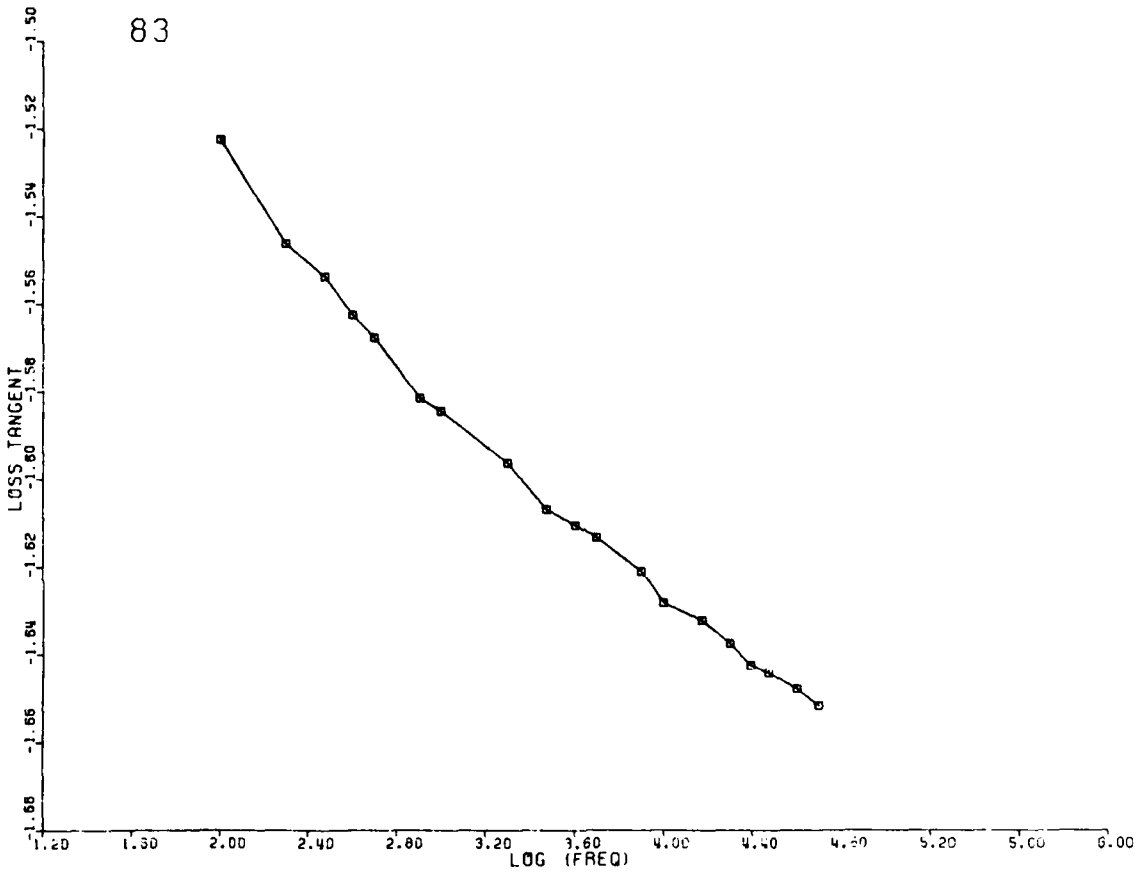

Figure B-1C. Loss tangent of sample 83, granite from Troy, Oklahoma, as a function of frequency.

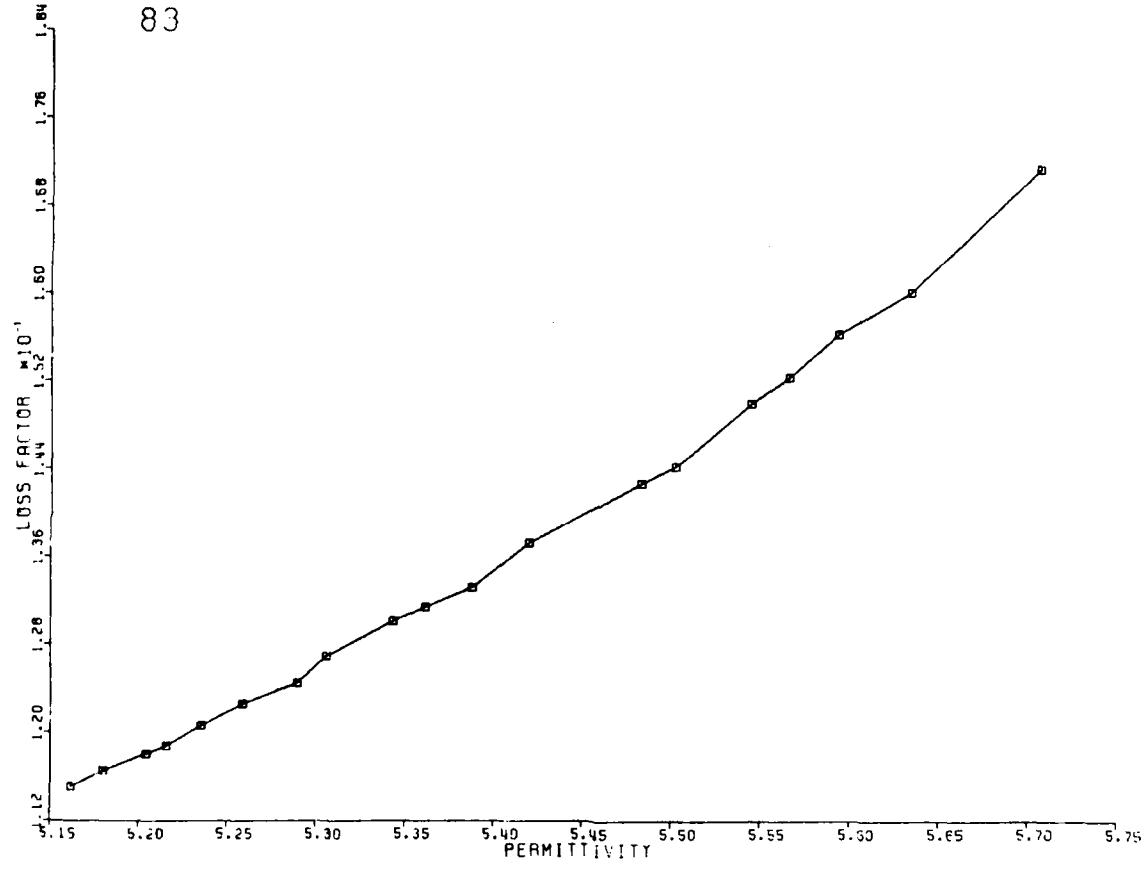

Figure B-1D. Cole-Cole plot, relative loss factor versus relative permittivity, of sample 83, granite from Troy, Oklahoma.

SAMPLE 890

FREQUENCY (HERTZ)	RELATIVE DIELECTRIC CONSTANT	CONDUC-TIVITY (MHO/M)	LOSS TANGENT	LOSS FACTOR
100.	9.373	0.2811E-08	0.5403E-01	0.5064E 00
200.	9.208	0.4452E-08	0.4355E-01	0.4010E 00
300.	9.123	0.5986E-08	0.3940E-01	0.3595E 00
400.	9.068	0.7386E-08	0.3668E-01	0.3327E 00
500.	9.032	0.8776E-08	0.3501E-01	0.3162E 00
800.	8.953	0.1277E-07	0.3213E-01	0.2876E 00
1000.	8.917	0.1539E-07	0.3110E-01	0.2773E 00
2000.	8.808	0.2811E-07	0.2875E-01	0.2532E 00
3000.	8.748	0.4051E-07	0.2781E-01	0.2433E 00
4000.	8.705	0.5307E-07	0.2746E-01	0.2390E 00
5000.	8.669	0.6521E-07	0.2710E-01	0.2349E 00
8000.	8.603	0.1010E-06	0.2644E-01	0.2275E 00
10000.	8.572	0.1235E-06	0.2595E-01	0.2224E 00
15000.	8.512	0.1801E-06	0.2541E-01	0.2163E 00
20000.	8.469	0.2341E-06	0.2490E-01	0.2109E 00
25000.	8.439	0.2875E-06	0.2455E-01	0.2072E 00
30000.	8.409	0.3373E-06	0.2408E-01	0.2025E 00
40000.	8.373	0.4335E-06	0.2332E-01	0.1952E 00
50000.	8.342	0.5190E-06	0.2241E-01	0.1870E 00
1000.	8.917	0.1539E-06	0.3110E 00	0.2773E 01

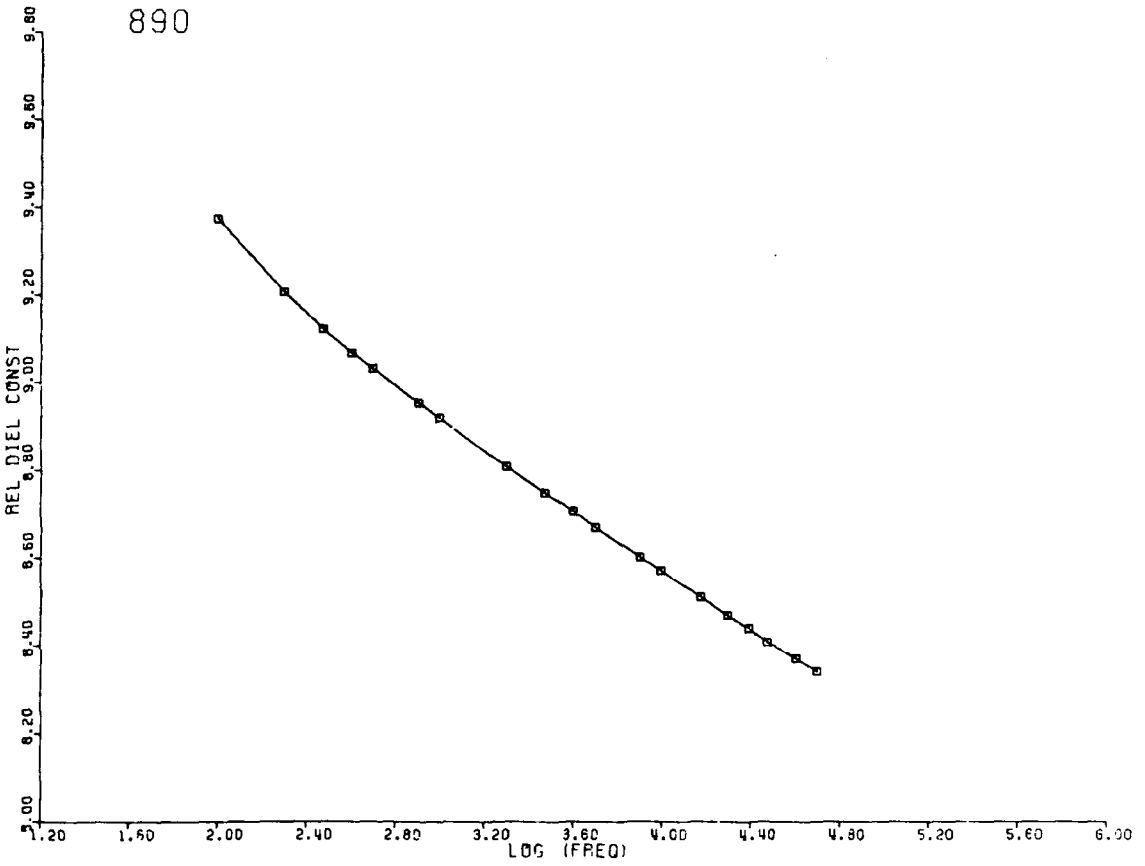

Figure B-2A. Relative permittivity (ε') of sample 890, diabase from Frederick, Maryland, as a function of frequency.

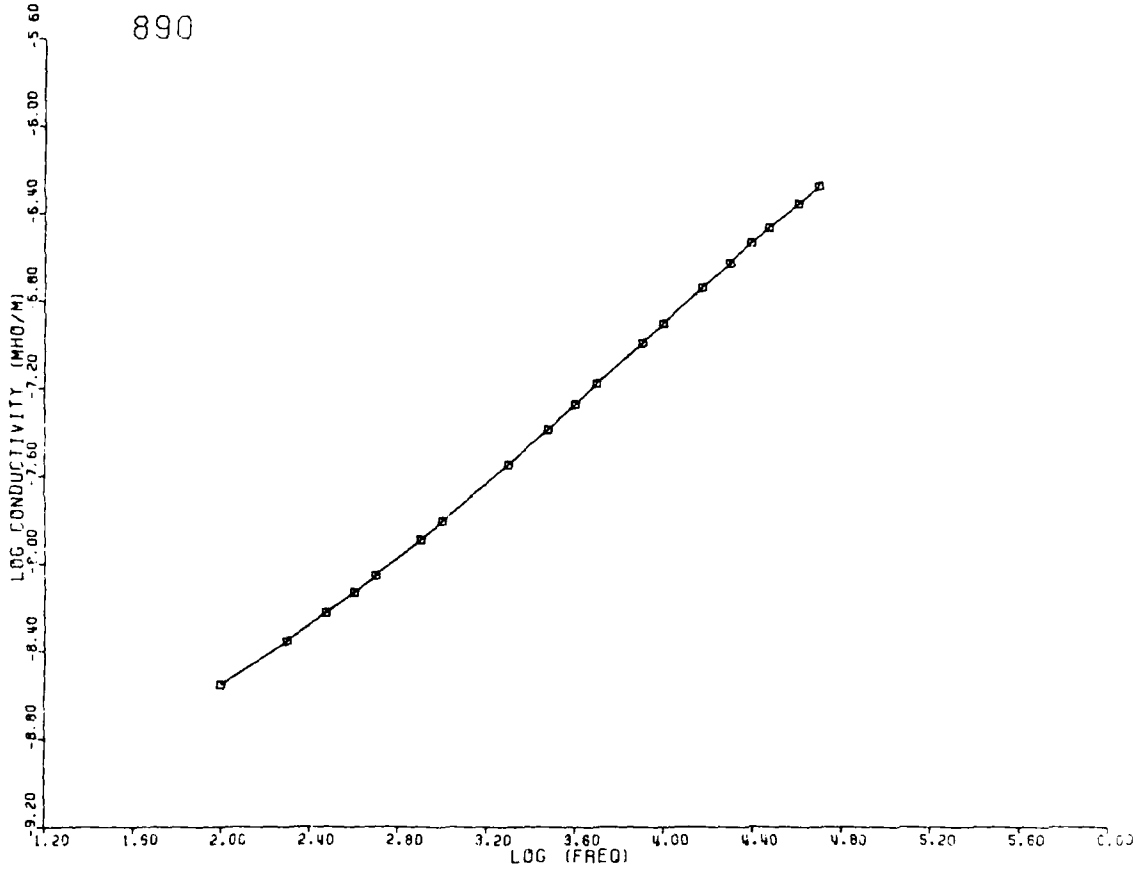

Figure B-2B. Dielectric conductivity ($\sigma = \omega\varepsilon''$) of sample 890, diabase from Frederick, Maryland, as a function of frequency.

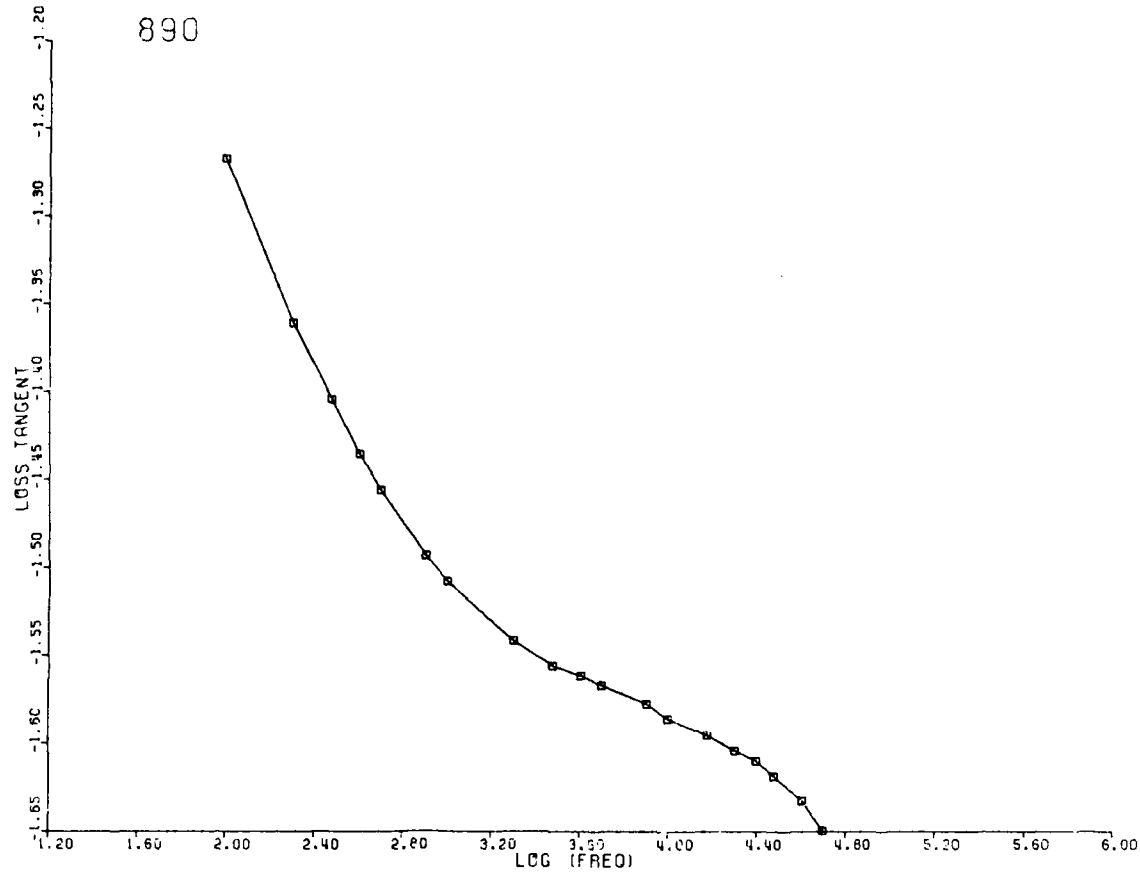

Figure B-2C. Loss tangent of sample 890, diabase from Frederick, Maryland, as a function of frequency.

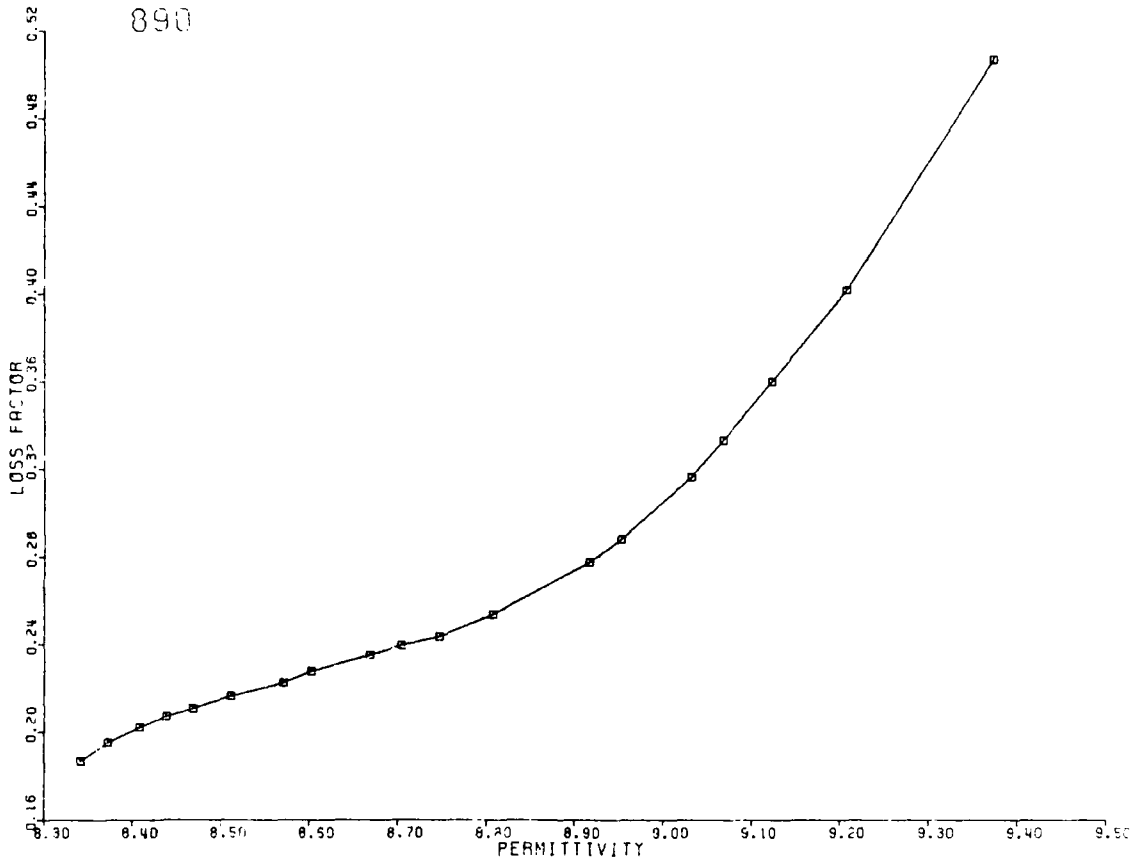

Figure B-2D. Cole-Cole plot, relative loss factor versus relative permittivity, of sample 890, diabase from Frederick, Maryland.

SAMPLE 1331

FREQUENCY (HERTZ)	RELATIVE DIELECTRIC CONSTANT	CONDUC-TIVITY (MHO/M)	LOSS TANGENT	LOSS FACTOR
100.	6.881	0.2370E-08	0.5517E-01	0.3796E 00
200.	6.743	0.4148E-08	0.4926E-01	0.3322E 00
300.	6.663	0.5686E-08	0.4556E-01	0.3036E 00
400.	6.617	0.7281E-08	0.4406E-01	0.2916E 00
500.	6.571	0.8854E-08	0.4316E-01	0.2836E 00
800.	6.491	0.1322E-07	0.4077E-01	0.2647E 00
1000.	6.456	0.1594E-07	0.3955E-01	0.2553E 00
2000.	6.353	0.2940E-07	0.3706E-01	0.2354E 00
3000.	6.296	0.4216E-07	0.3575E-01	0.2251E 00
4000.	6.250	0.5356E-07	0.3431E-01	0.2145E 00
5000.	6.227	0.6609E-07	0.3400E-01	0.2117E 00
8000.	6.170	0.9914E-07	0.3217E-01	0.1985E 00
10000.	6.135	0.1162E-06	0.3034E-01	0.1862E 00
15000.	6.089	0.1618E-06	0.2837E-01	0.1728E 00
20000.	6.055	0.2074E-06	0.2743E-01	0.1661E 00
25000.	6.021	0.2427E-06	0.2583E-01	0.1555E 00
30000.	6.009	0.2769E-06	0.2460E-01	0.1478E 00
40000.	5.986	0.3418E-06	0.2287E-01	0.1369E 00
50000.	5.963	0.3988E-06	0.2142E-01	0.1278E 00
1000.	6.456	0.1594E-07	0.3955E-01	0.2553E 00

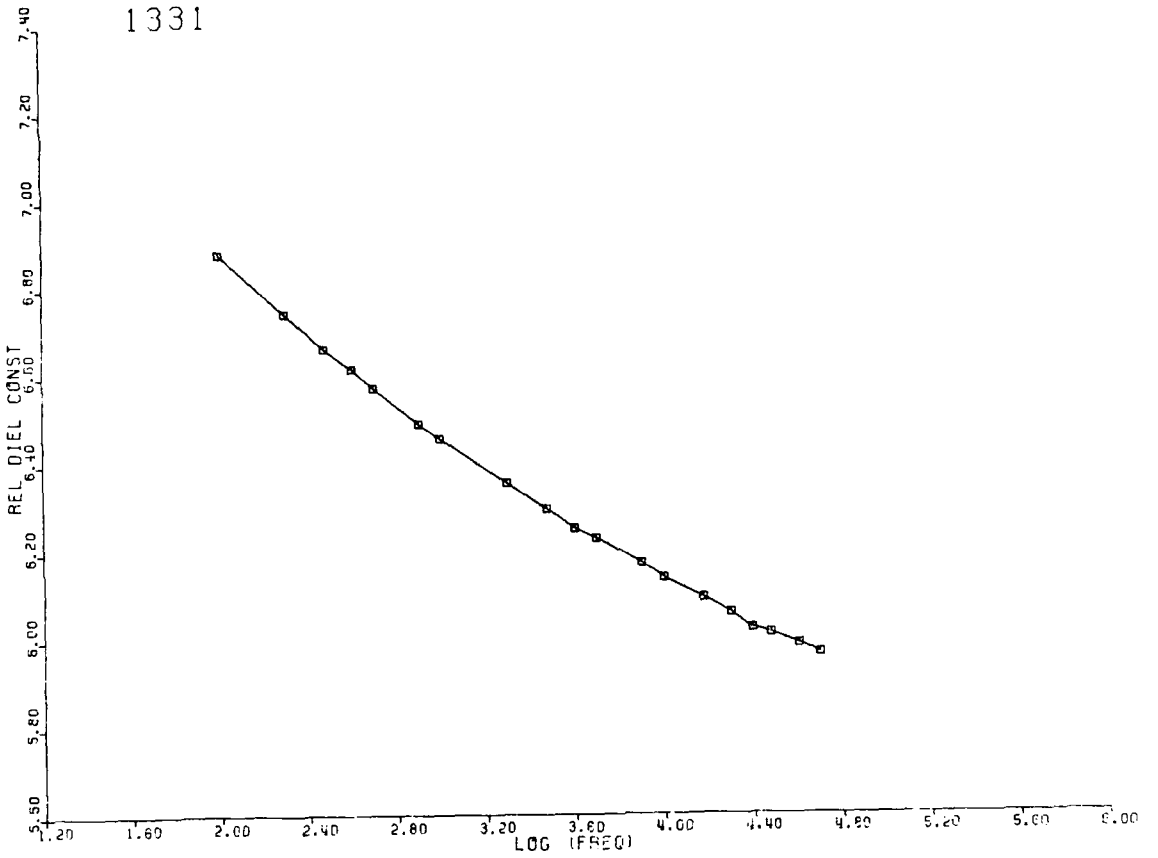

Figure B-3A. Relative permittivity (ε') of sample 1331, gabbro from Mellen, Wisconsin, as a function of frequency.

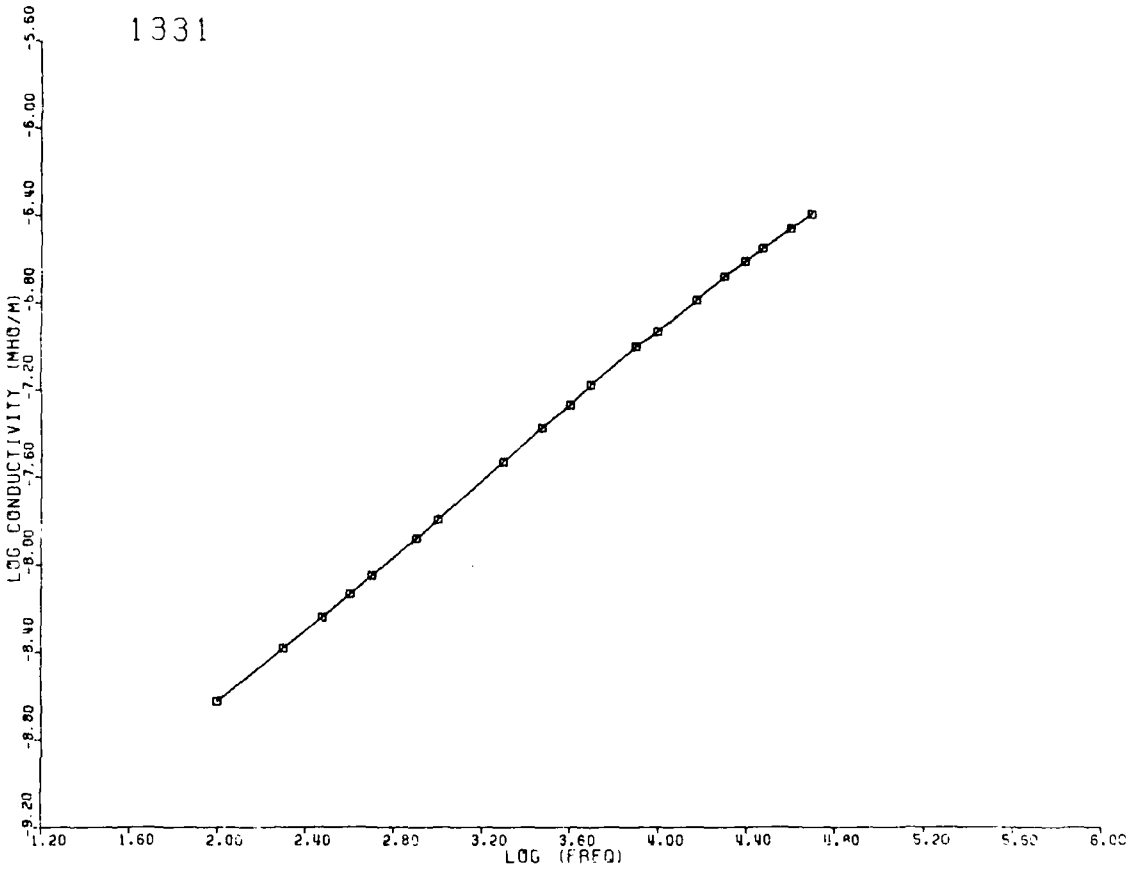

Figure B-3B. Dielectric conductivity ($\sigma = \omega\varepsilon''$) of sample 1331, gabbro from Mellen, Wisconsin, as a function of frequency.

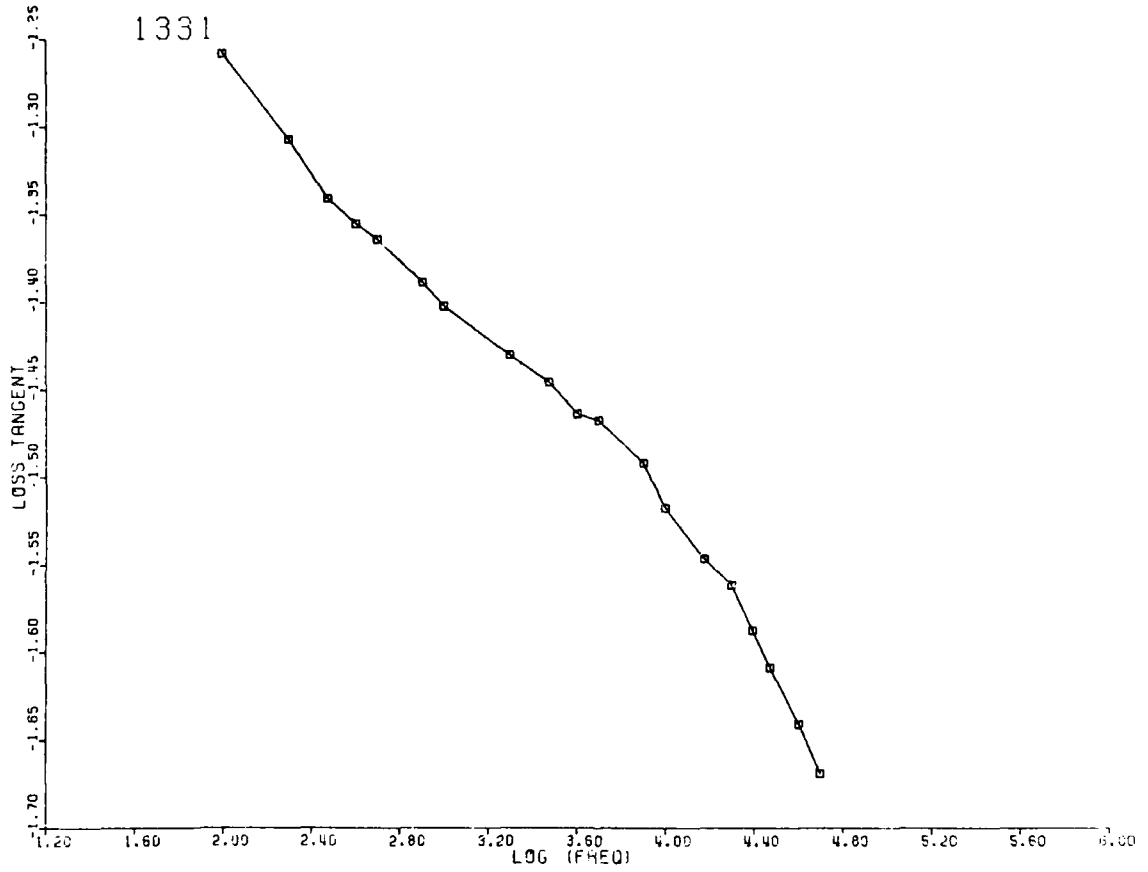

Figure B-3C. Loss tangent of sample 1331, gabbro from Mellen, Wisconsin, as a function of frequency.

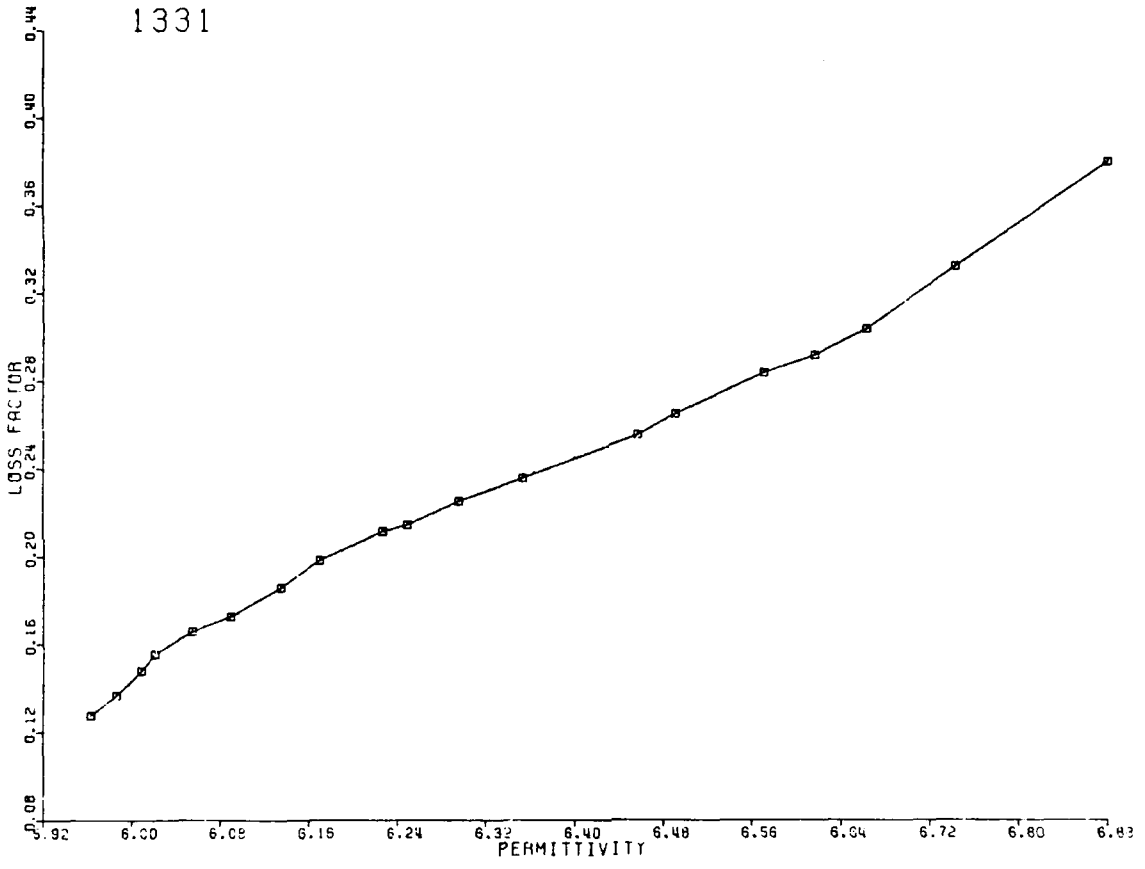

Figure B-3D. Cole-Cole plot, relative loss factor versus relative permittivity, of sample 1331, gabbro from Mellen, Wisconsin.

SAMPLE 1370

FREQUENCY (HERTZ)	RELATIVE DIELECTRIC CONSTANT	CONDUC-TIVITY (MHO/M)	LOSS TANGENT	LOSS FACTOR
100.	16.785	0.7572E-08	0.7086E-01	0.1189E 01
200.	16.332	0.1316E-07	0.6329E-01	0.1034E 01
300.	16.096	0.1834E-07	0.5966E-01	0.9604E 00
400.	15.939	0.2341E-07	0.5768E-01	0.9194E 00
500.	15.821	0.2829E-07	0.5618E-01	0.8889E 00
800.	15.575	0.4244E-07	0.5350E-01	0.8333E 00
1000.	15.457	0.5200E-07	0.5285E-01	0.8169E 00
2000.	15.123	0.9733E-07	0.5055E-01	0.7645E 00
3000.	14.936	0.1406E-06	0.4928E-01	0.7360E 00
4000.	14.808	0.1823E-06	0.4835E-01	0.7160E 00
5000.	14.710	0.2222E-06	0.4745E-01	0.6980E 00
8000.	14.513	0.3387E-06	0.4583E-01	0.6651E 00
10000.	14.425	0.4105E-06	0.4470E-01	0.6448E 00
15000.	14.258	0.5898E-06	0.4332E-01	0.6176E 00
20000.	14.149	0.7631E-06	0.4236E-01	0.5994E 00
25000.	14.071	0.9325E-06	0.4164E-01	0.5859E 00
30000.	14.002	0.1106E-05	0.4135E-01	0.5790E 00
40000.	13.894	0.1445E-05	0.4083E-01	0.5673E 00
50000.	13.805	0.1763E-05	0.4013E-01	0.5540E 00
1000.	15.467	0.5260E-05	0.5342E 01	0.8263E 02

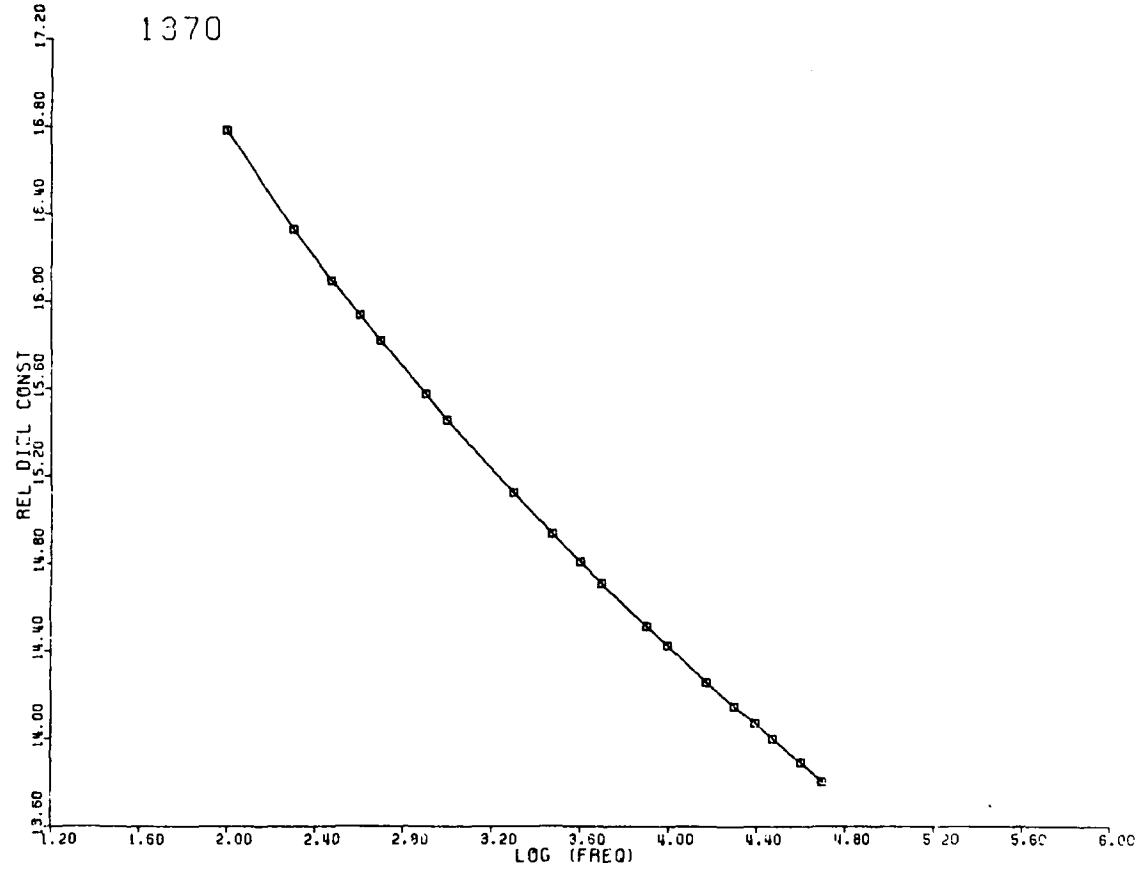

Figure B-4A. Relative permittivity (ε') of sample 1370, quartz monzonite from Red River, Wisconsin, as a function of frequency.

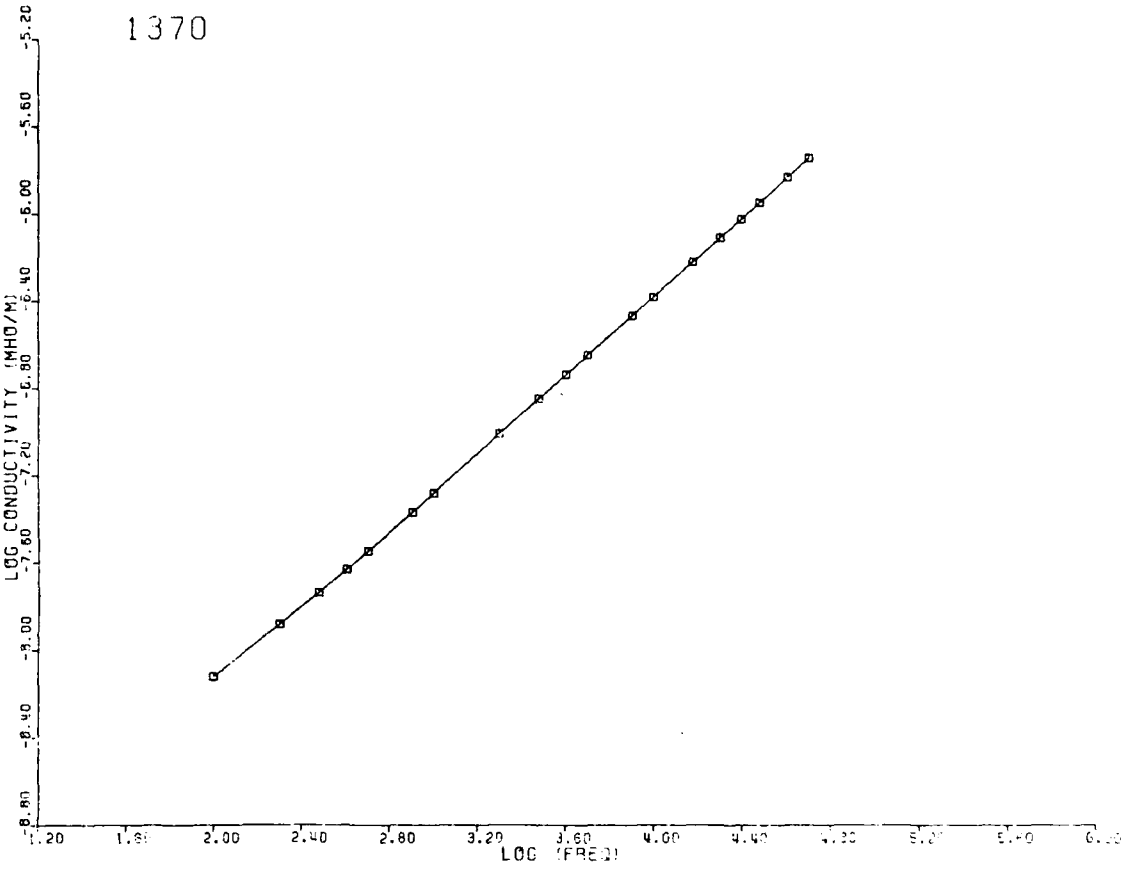

Figure B-4B. Dielectric conductivity ($\sigma = \omega\varepsilon''$) of sample 1370, quartz monzonite from Red River, Wisconsin, as a function of frequency.

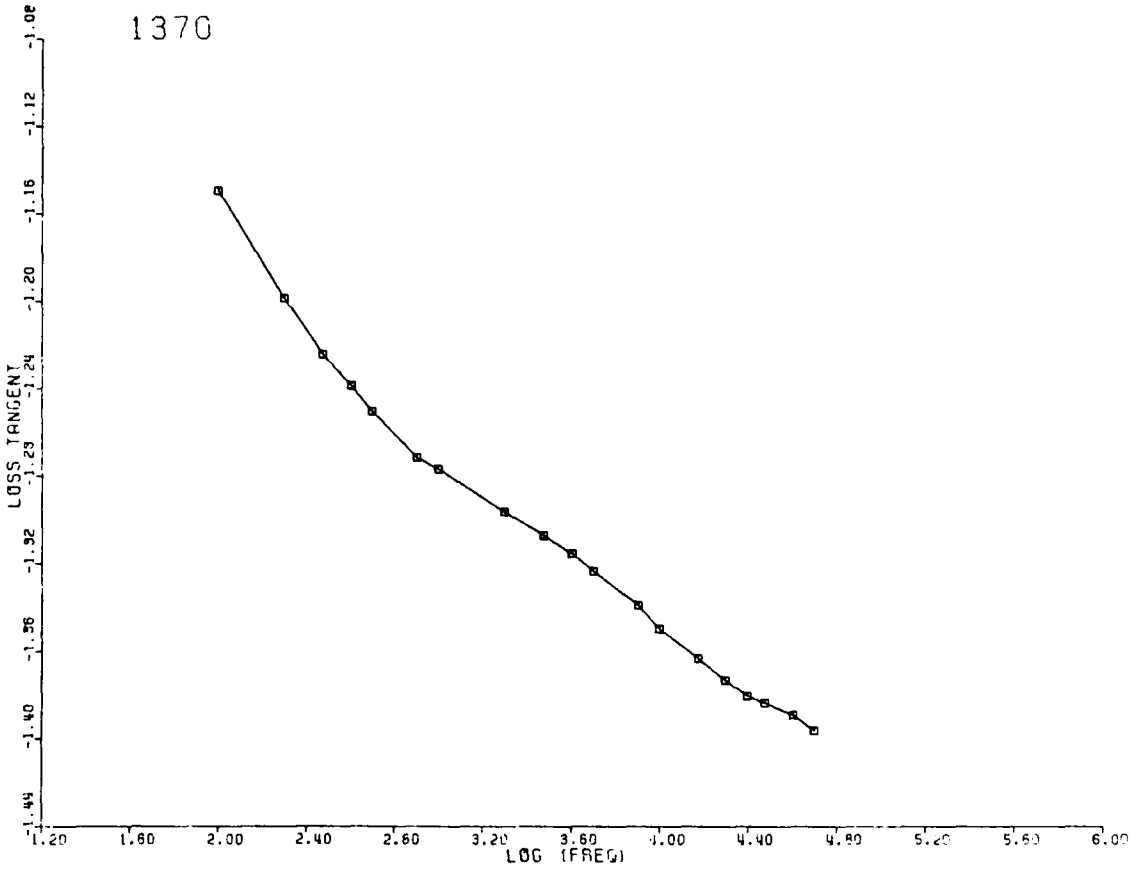

Figure B-4C. Loss tangent of sample 1370, quartz monzonite from Red River, Wisconsin, as a function of frequency.

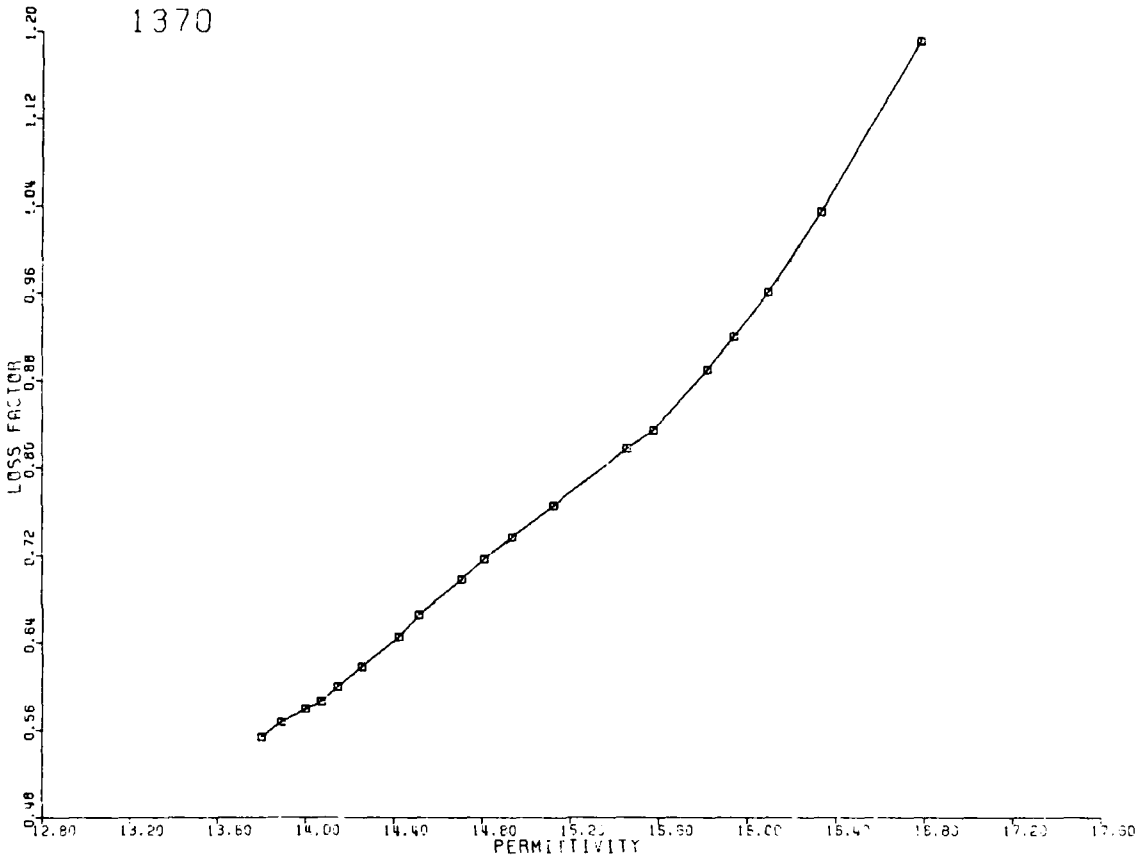

Figure B-4D. Cole-Cole plot, relative loss factor versus relative permittivity, of sample 1370, quartz monzonite from Red River, Wisconsin.

SAMPLE 1410

FREQUENCY (HERTZ)	RELATIVE DIELECTRIC CONSTANT	CONDUC-TIVITY (MHO/M)	LOSS TANGENT	LOSS FACTOR
100.	7.400	0.1242E-08	0.3078E-01	0.2277E 00
200.	7.304	0.2303E-08	0.2891E-01	0.2111E 00
300.	7.253	0.3315E-08	0.2793E-01	0.2026E 00
400.	7.218	0.4326E-08	0.2747E-01	0.1983E 00
500.	7.189	0.5323E-08	0.2715E-01	0.1952E 00
800.	7.134	0.8198E-08	0.2634E-01	0.1879E 00
1000.	7.108	0.1010E-07	0.2605E-01	0.1851E 00
2000.	7.030	0.1947E-07	0.2538E-01	0.1784E 00
3000.	6.985	0.2875E-07	0.2515E-01	0.1757E 00
4000.	6.954	0.3797E-07	0.2503E-01	0.1741E 00
8000.	6.881	0.7541E-07	0.2512E-01	0.1728E 00
15000.	6.815	0.1411E-06	0.2531E-01	0.1725E 00
25000.	6.758	0.2367E-06	0.2569E-01	0.1736E 00
30000.	6.738	0.2868E-06	0.2601E-01	0.1752E 00
40000.	6.705	0.3861E-06	0.2640E-01	0.1770E 00
50000.	6.678	0.4873E-06	0.2675E-01	0.1787E 00
80000.	6.619	0.8038E-06	0.2783E-01	0.1842E 00

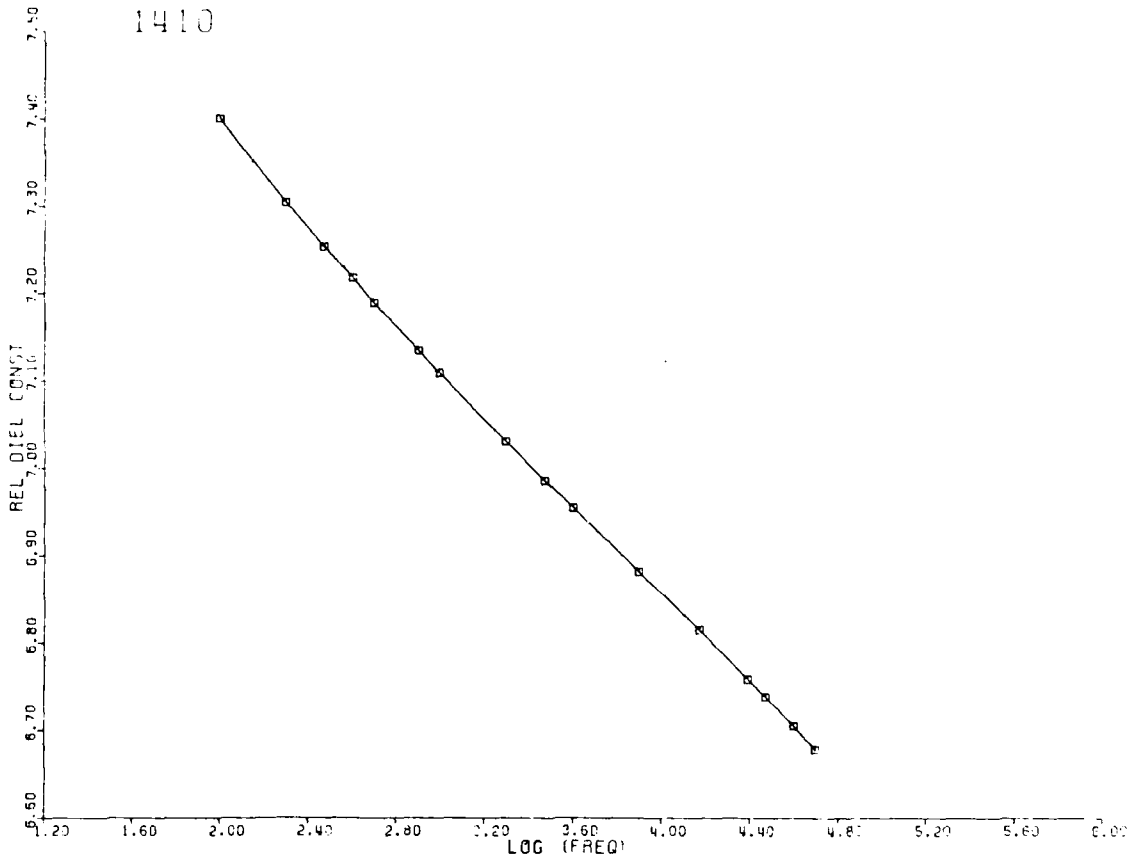

Figure B-5A. Relative permittivity (ε') of sample 1410, granite from Graniteville, Missouri, as a function of frequency.

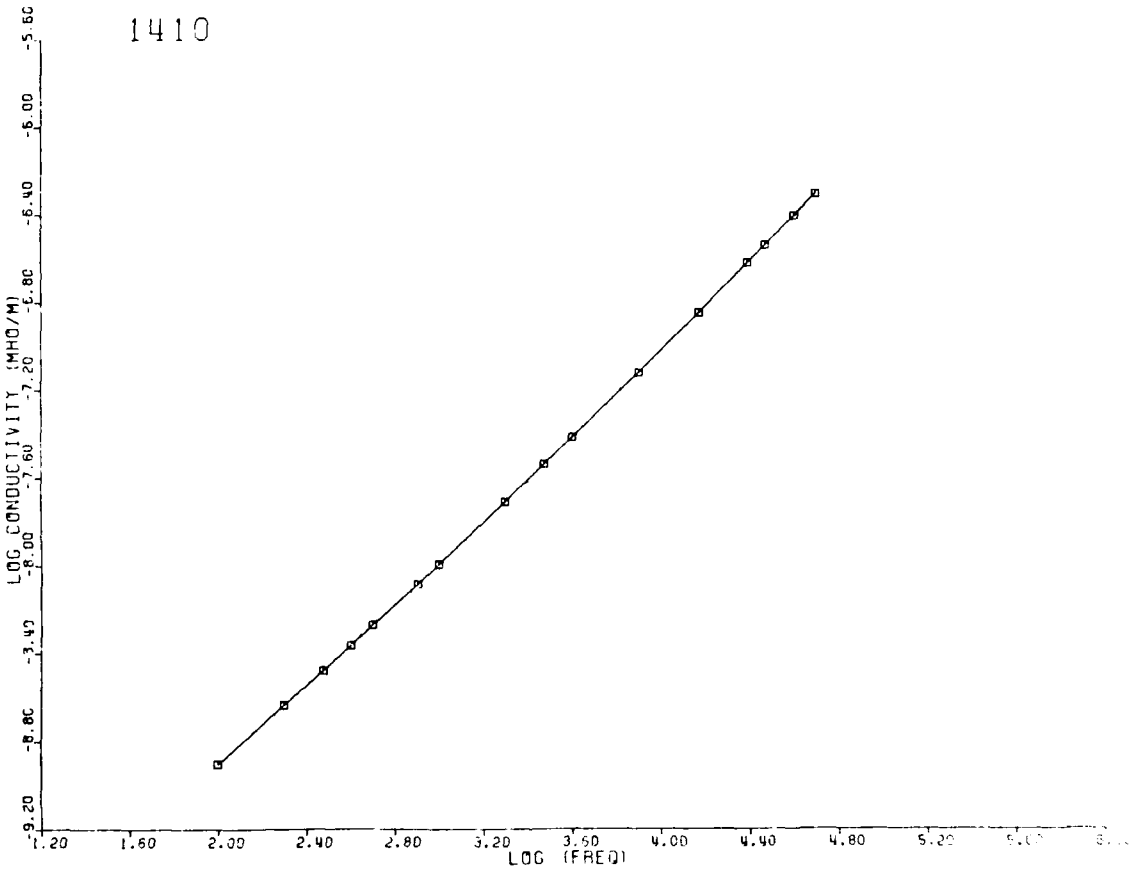

Figure B-5B. Dielectric conductivity ($\sigma = \omega\varepsilon''$) of sample 1410, granite from Graniteville, Missouri, as a function of frequency.

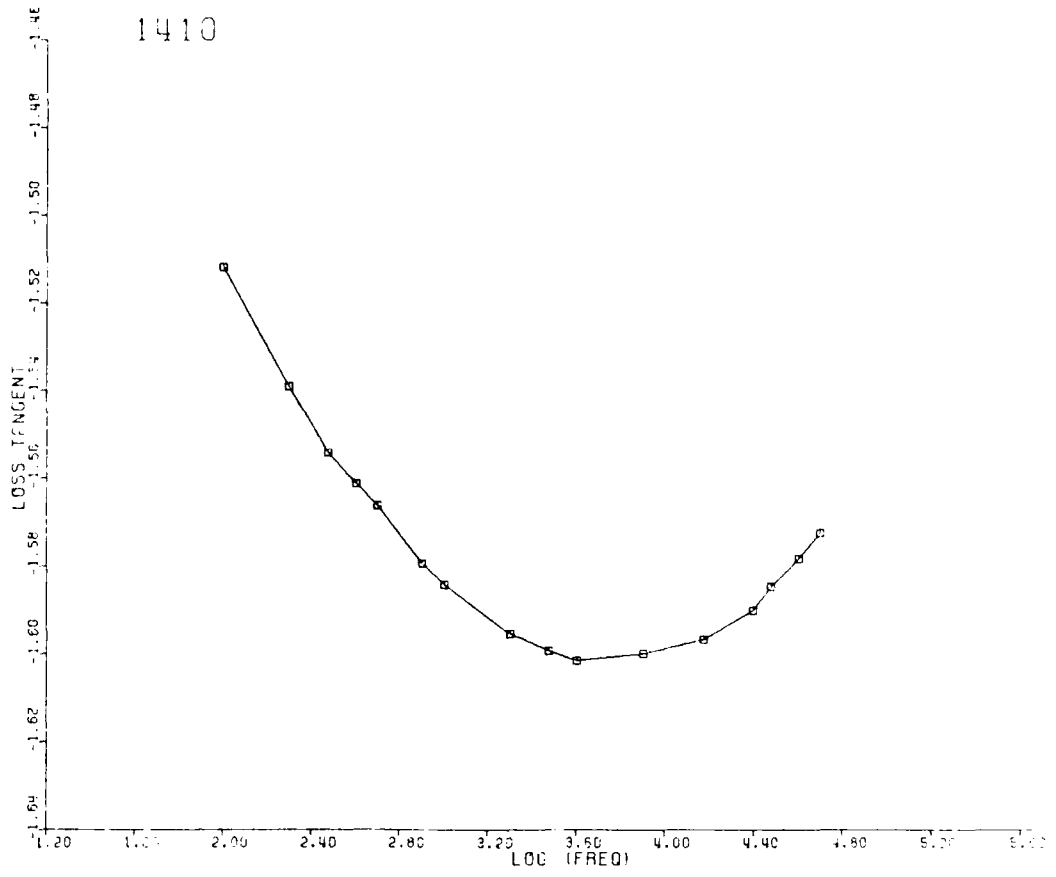

Figure B-5C. Loss tangent of sample 1410, granite from Graniteville, Missouri, as a function of frequency.

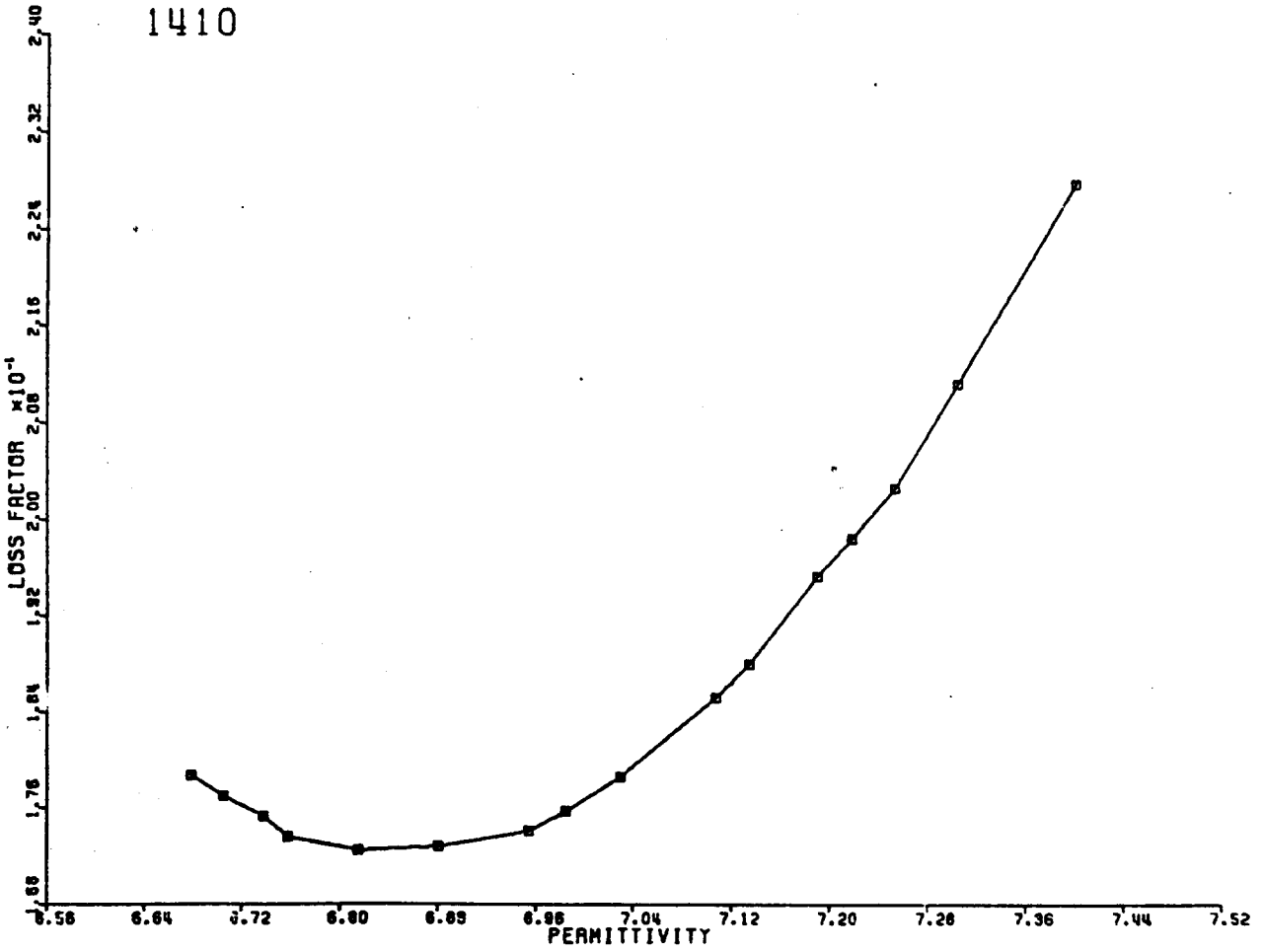

Figure B-5D. Cole-Cole plot, relative loss factor versus relative permittivity, of sample 1410, granite from Graniteville, Missouri.

SAMPLE 1411

FREQUENCY (HERTZ)	RELATIVE DIELECTRIC CONSTANT	CONDUC-TIVITY (MHO/M)	LOSS TANGENT	LOSS FACTOR
100.	7.455	0.4746E-08	0.9564E-01	0.7131E 00
200.	7.167	0.8421E-08	0.8826E-01	0.6325E 00
300.	7.016	0.1179E-07	0.8413E-01	0.5902E 00
400.	6.915	0.1512E-07	0.8213E-01	0.5679E 00
500.	6.836	0.1829E-07	0.8038E-01	0.5495E 00
800.	6.684	0.2759E-07	0.7753E-01	0.5182E 00
1000.	6.613	0.3364E-07	0.7642E-01	0.5054E 00
2000.	6.404	0.6234E-07	0.7312E-01	0.4683E 00
3000.	6.286	0.8932E-07	0.7117E-01	0.4473E 00
4000.	6.205	0.1157E-06	0.7003E-01	0.4345E 00
5000.	6.145	0.1413E-06	0.6909E-01	0.4246E 00
8000.	6.020	0.2131E-06	0.6648E-01	0.4002E 00
10000.	5.966	0.2561E-06	0.6448E-01	0.3847E 00
15000.	5.868	0.3628E-06	0.6192E-01	0.3634E 00
20000.	5.801	0.4622E-06	0.5985E-01	0.3472E 00
25000.	5.753	0.5568E-06	0.5817E-01	0.3346E 00
30000.	5.710	0.6499E-06	0.5700E-01	0.3255E 00
40000.	5.653	0.8236E-06	0.5472E-01	0.3093E 00
50000.	5.609	0.9787E-06	0.5243E-01	0.2941E 00
1000.	7.073	0.3366E-07	0.7149E-01	0.5057E 00

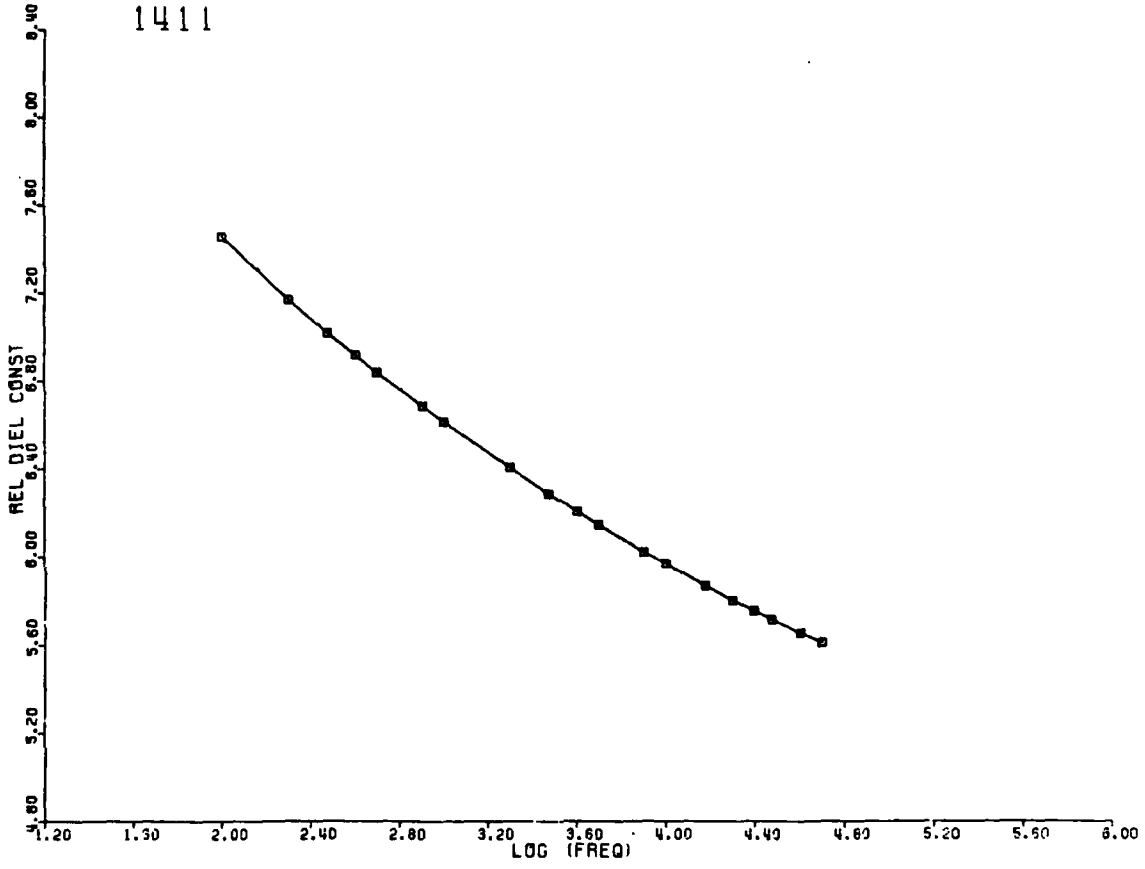

Figure B-6A. Relative permittivity (ε') of sample 1411, rhyolite from Stouts Creek, Missouri, as a function of frequency.

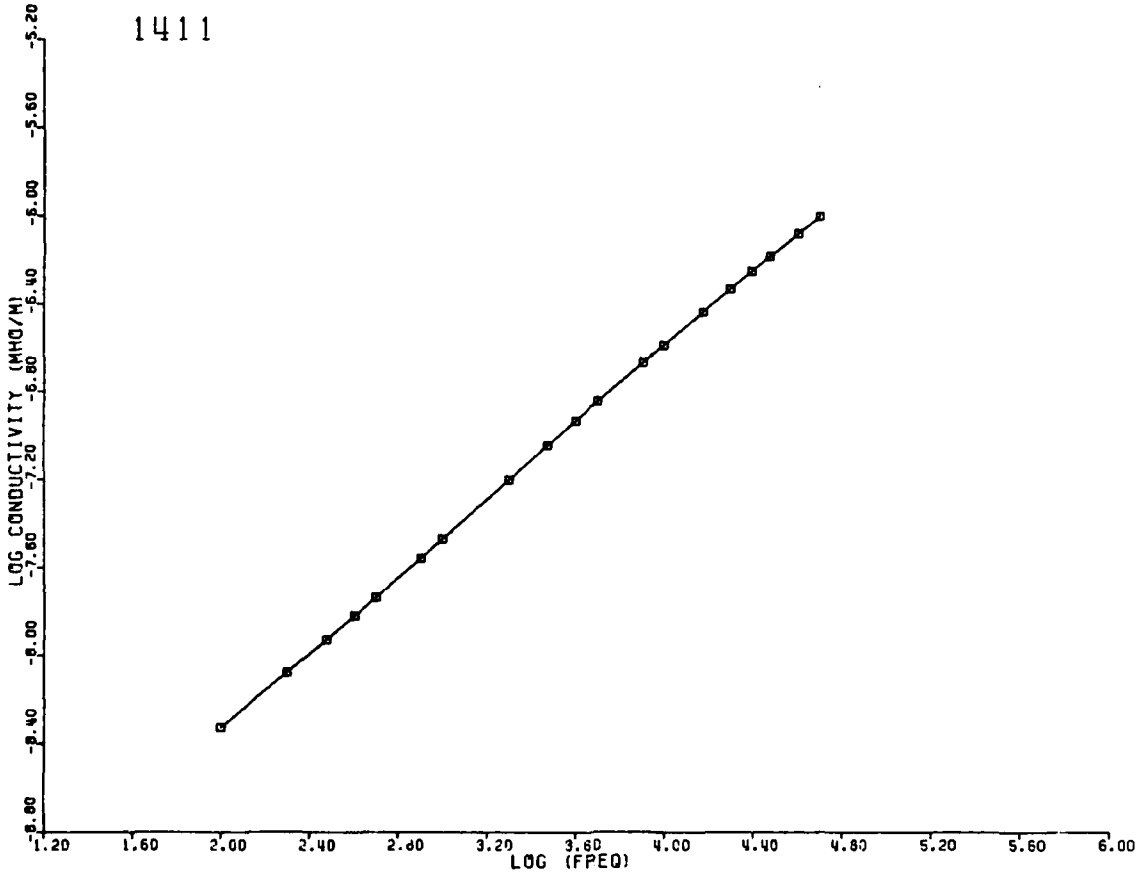

Figure B-6B. Dielectric conductivity ($\sigma = \omega\varepsilon''$) of sample 1411, rhyolite from Stouts Creek, Missouri, as a function of frequency.

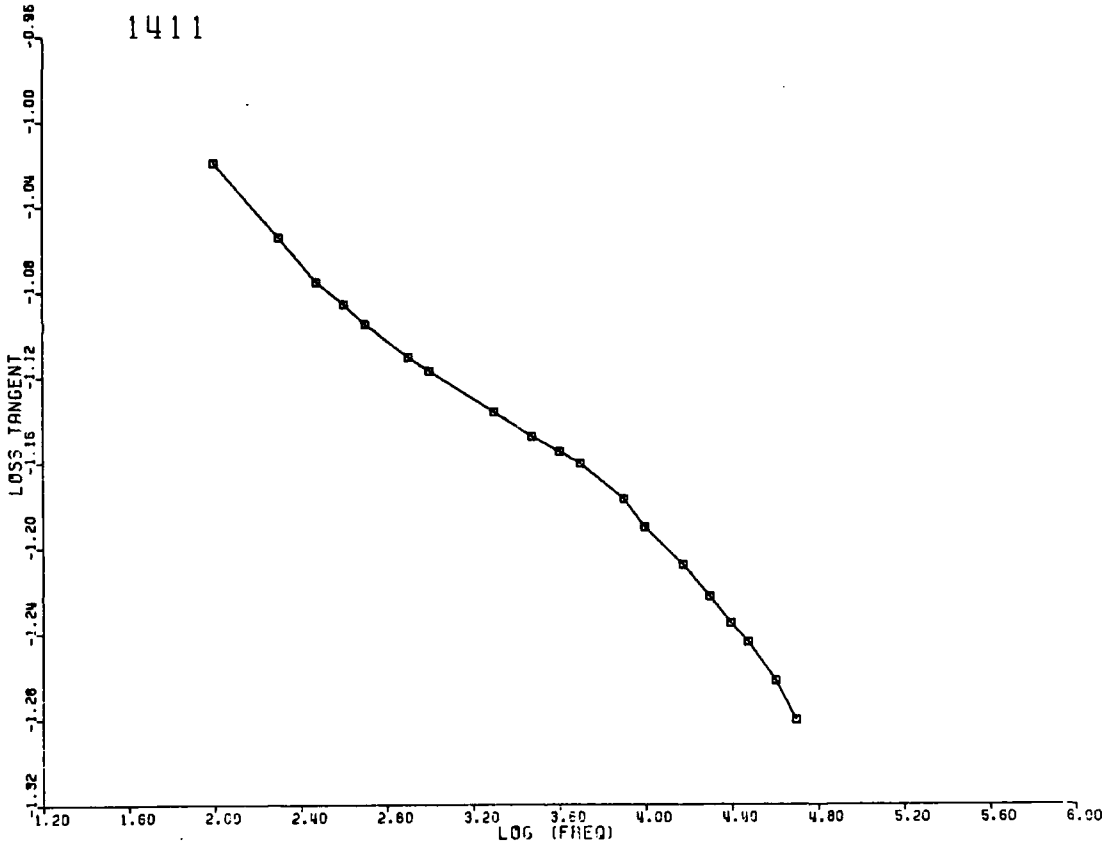

Figure B-6C. Loss tangent of sample 1411, rhyolite from Stouts Creek, Missouri, as a function of frequency.

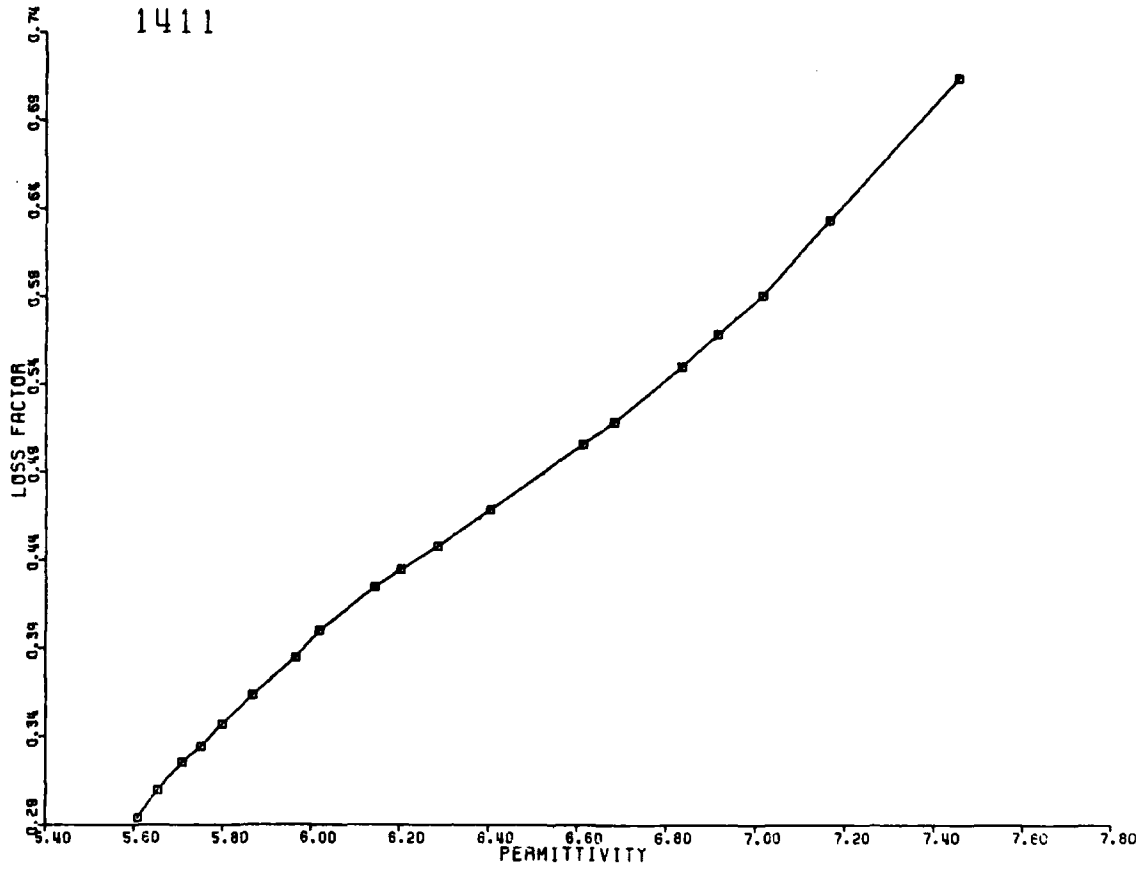

Figure B-6D. Cole-Cole plot, relative loss factor versus relative permittivity, of sample 1411, rhyolite from Stouts Creek, Missouri.

SAMPLE 1415

FREQUENCY (HERTZ)	RELATIVE DIELECTRIC CONSTANT	CONDUC-TIVITY (MHO/M)	LOSS TANGENT	LOSS FACTOR
100.	10.767	0.7668E-08	0.1328E 00	0.1429E 01
200.	10.283	0.1225E-07	0.1110E 00	0.1142E 01
300.	10.040	0.1630E-07	0.1009E 00	0.1013E 01
400.	9.879	0.2016E-07	0.9510E-01	0.9395E 00
500.	9.768	0.2387E-07	0.9109E-01	0.8897E 00
800.	9.536	0.3420E-07	0.8358E-01	0.7970E 00
1000.	9.435	0.4075E-07	0.8051E-01	0.7596E 00
2000.	9.142	0.7185E-07	0.7325E-01	0.6697E 00
3000.	8.981	0.1005E-06	0.6956E-01	0.6247E 00
4000.	8.880	0.1287E-06	0.6755E-01	0.5998E 00
5000.	8.799	0.1550E-06	0.6567E-01	0.5778E 00
8000.	8.638	0.2326E-06	0.6275E-01	0.5420E 00
10000.	8.567	0.2783E-06	0.6055E-01	0.5187E 00
15000.	8.436	0.3903E-06	0.5749E-01	0.4850E 00
20000.	8.345	0.4937E-06	0.5514E-01	0.4601E 00
25000.	8.274	0.5902E-06	0.5318E-01	0.4400E 00
30000.	8.234	0.6849E-06	0.5169E-01	0.4256E 00
40000.	8.153	0.8573E-06	0.4900E-01	0.3995E 00
50000.	8.093	0.1024E-05	0.4715E-01	0.3816E 00
1000.	9.435	0.4075E-07	0.8051E-01	0.7596E 00

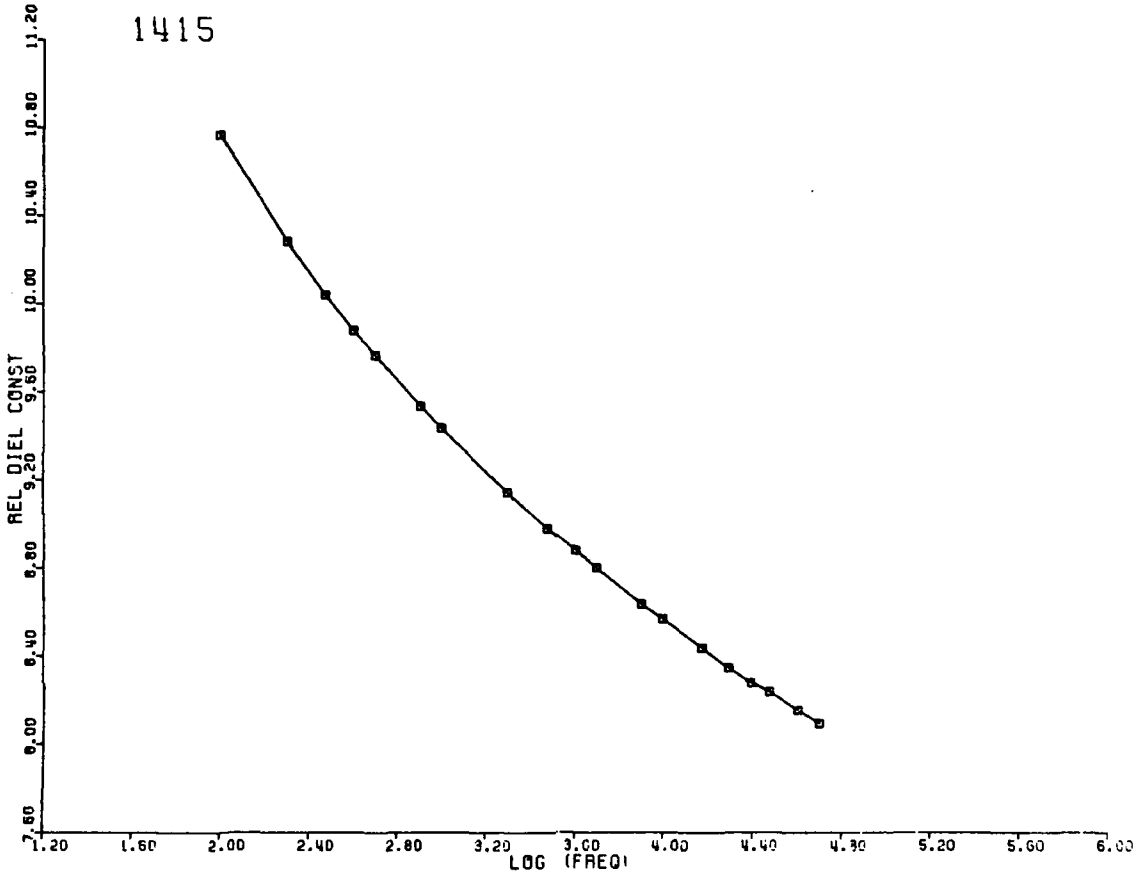

Figure B-7A. Relative permittivity (ε') of sample 1415, diabase from Skrainka, Missouri, as a function of frequency.

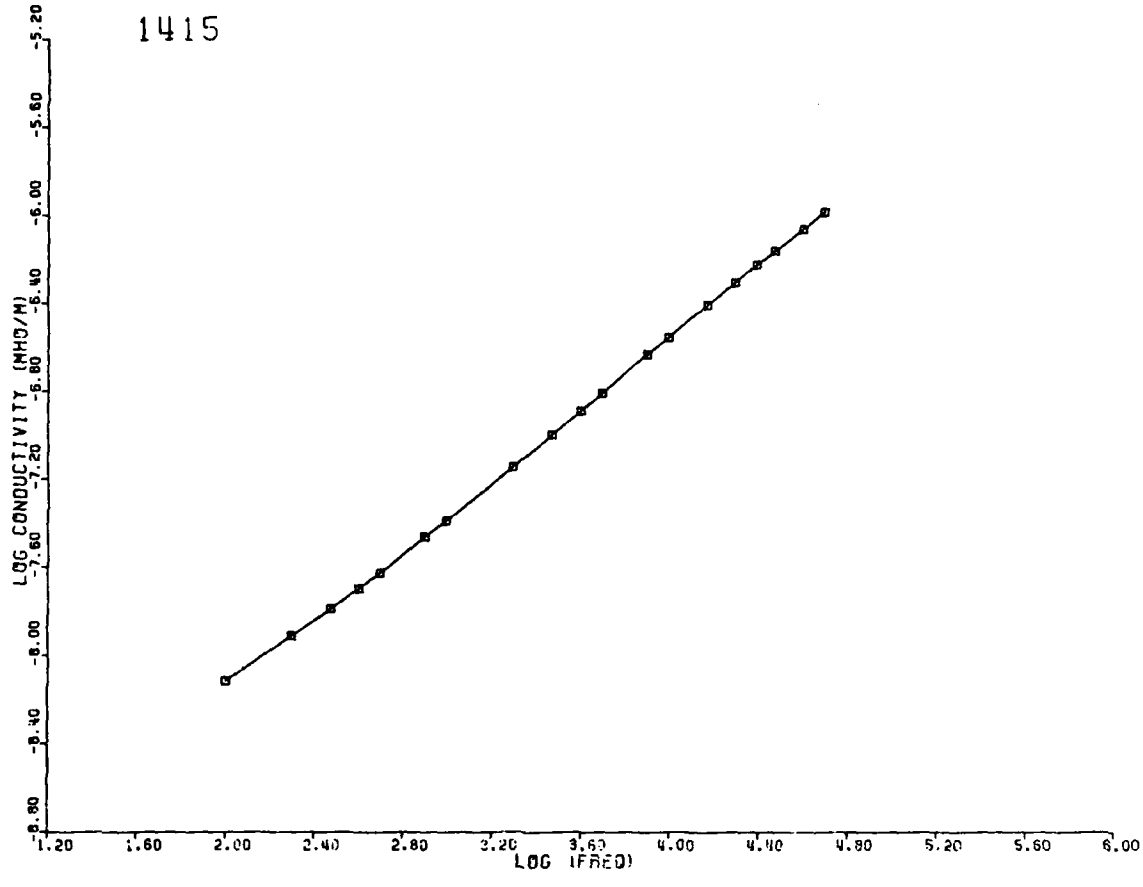

Figure B-7B. Dielectric conductivity ($\sigma = \omega\varepsilon''$) of sample 1415, diabase from Skrainka, Missouri, as a function of frequency.

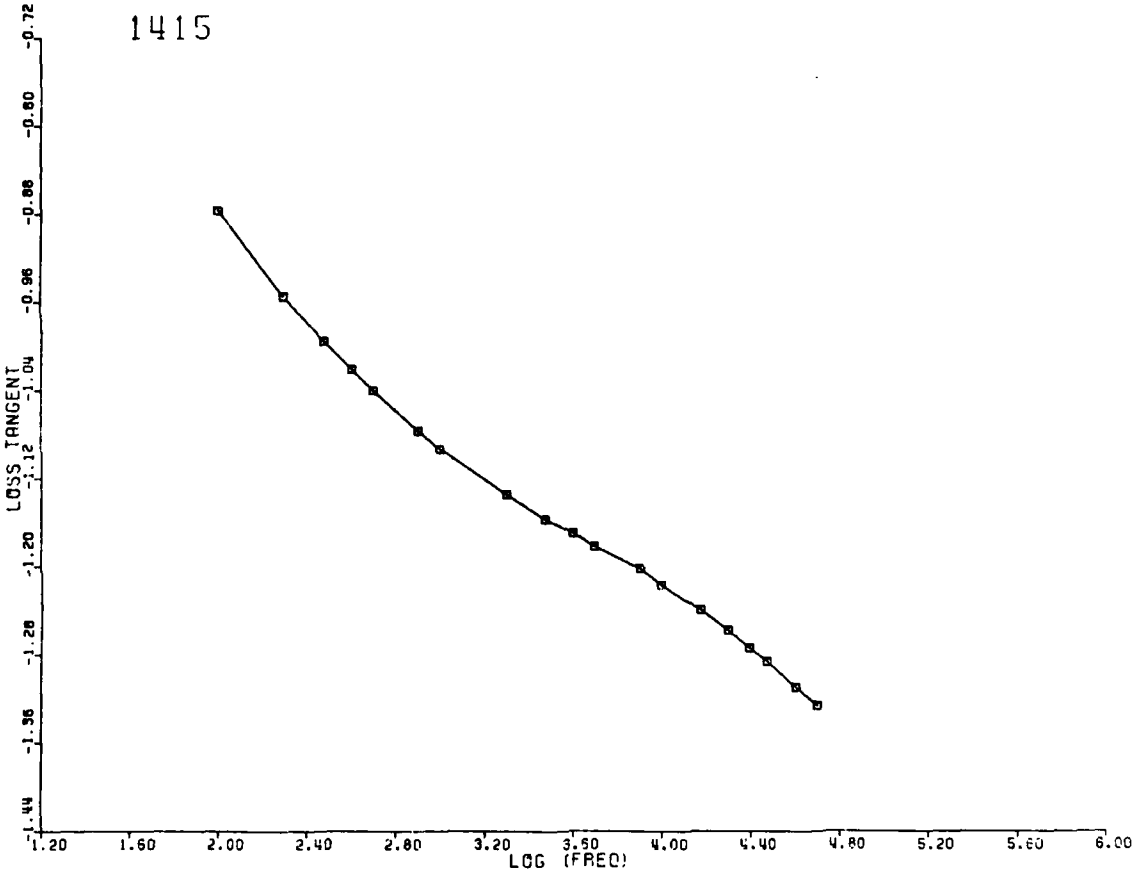

Figure B-7C. Loss tangent of sample 1415, diabase from Skrainka, Missouri, as a function of frequency.

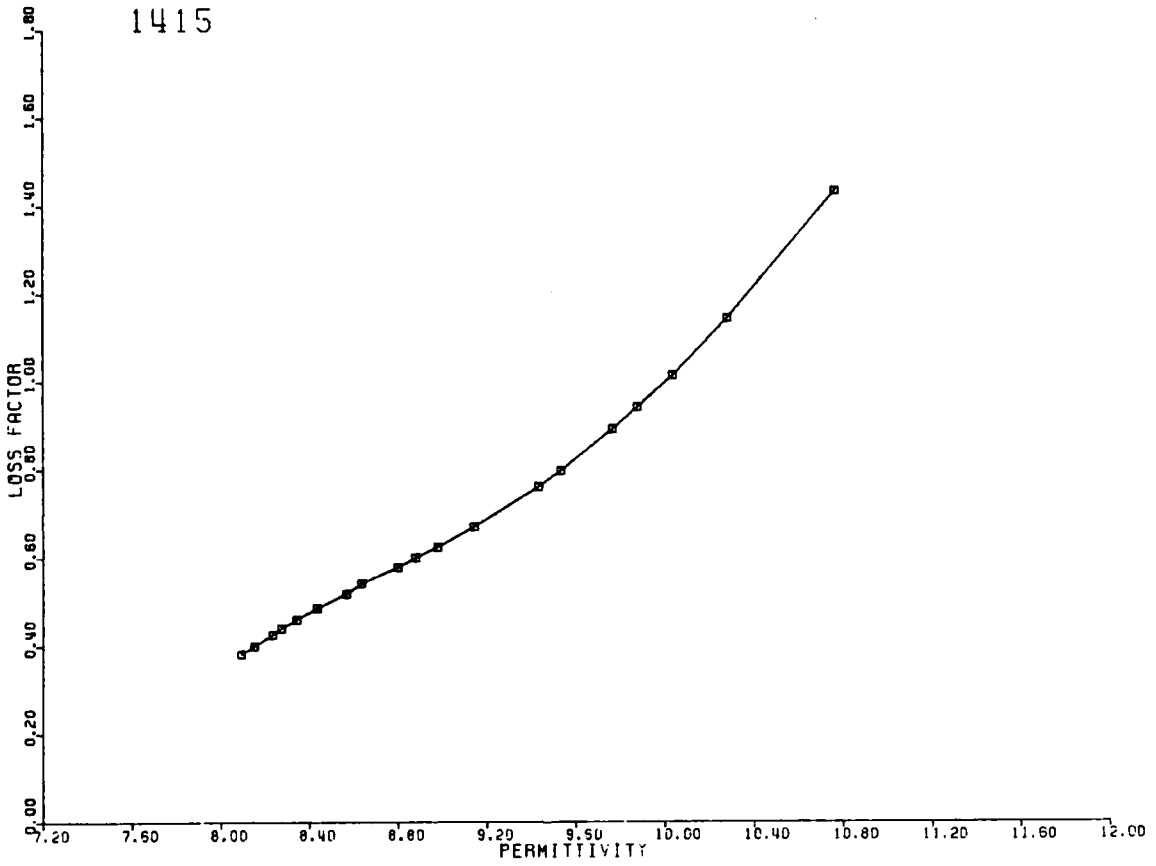

Figure B-7D. Cole-Cole plot, relative loss factor versus relative permittivity, of sample 1415, diabase from Skrainka, Missouri.

SAMPLE 1727

FREQUENCY (HERTZ)	RELATIVE DIELECTRIC CONSTANT	CONDUC-TIVITY (MHO/M)	LOSS TANGENT	LOSS FACTOR
100.	10.907	0.4135E-08	0.6894E-01	0.7520E 00
200.	10.580	0.8312E-08	0.7144E-01	0.7558E 00
300.	10.386	0.1255E-07	0.7327E-01	0.7610E 00
400.	10.246	0.1682E-07	0.7462E-01	0.7645E 00
500.	10.135	0.2108E-07	0.7563E-01	0.7665E 00
600.	10.045	0.2530E-07	0.7636E-01	0.7670E 00
700.	9.968	0.2950E-07	0.7689E-01	0.7665E 00
800.	9.901	0.3369E-07	0.7735E-01	0.7659E 00
900.	9.842	0.3784E-07	0.7769E-01	0.7646E 00
1000.	9.788	0.4200E-07	0.7804E-01	0.7638E 00
1500.	9.582	0.6218E-07	0.7868E-01	0.7539E 00
2000.	9.437	0.8149E-07	0.7851E-01	0.7409E 00
2500.	9.327	0.9995E-07	0.7795E-01	0.7270E 00
3000.	9.239	0.1177E-06	0.7724E-01	0.7136E 00
4000.	9.101	0.1512E-06	0.7553E-01	0.6874E 00
5000.	9.000	0.1825E-06	0.7376E-01	0.6638E 00
8000.	8.801	0.2659E-06	0.6867E-01	0.6044E 00
10000.	8.718	0.3132E-06	0.6533E-01	0.5696E 00
15000.	8.574	0.4210E-06	0.5954E-01	0.5105E 00
20000.	8.483	0.5142E-06	0.5512E-01	0.4676E 00
25000.	8.420	0.5971E-06	0.5158E-01	0.4343E 00
30000.	8.371	0.6726E-06	0.4871E-01	0.4077E 00
40000.	8.302	0.8068E-06	0.4418E-01	0.3668E 00
50000.	8.254	0.9264E-06	0.4082E-01	0.3370E 00
80000.	8.161	0.1224E-05	0.3409E-01	0.2782E 00

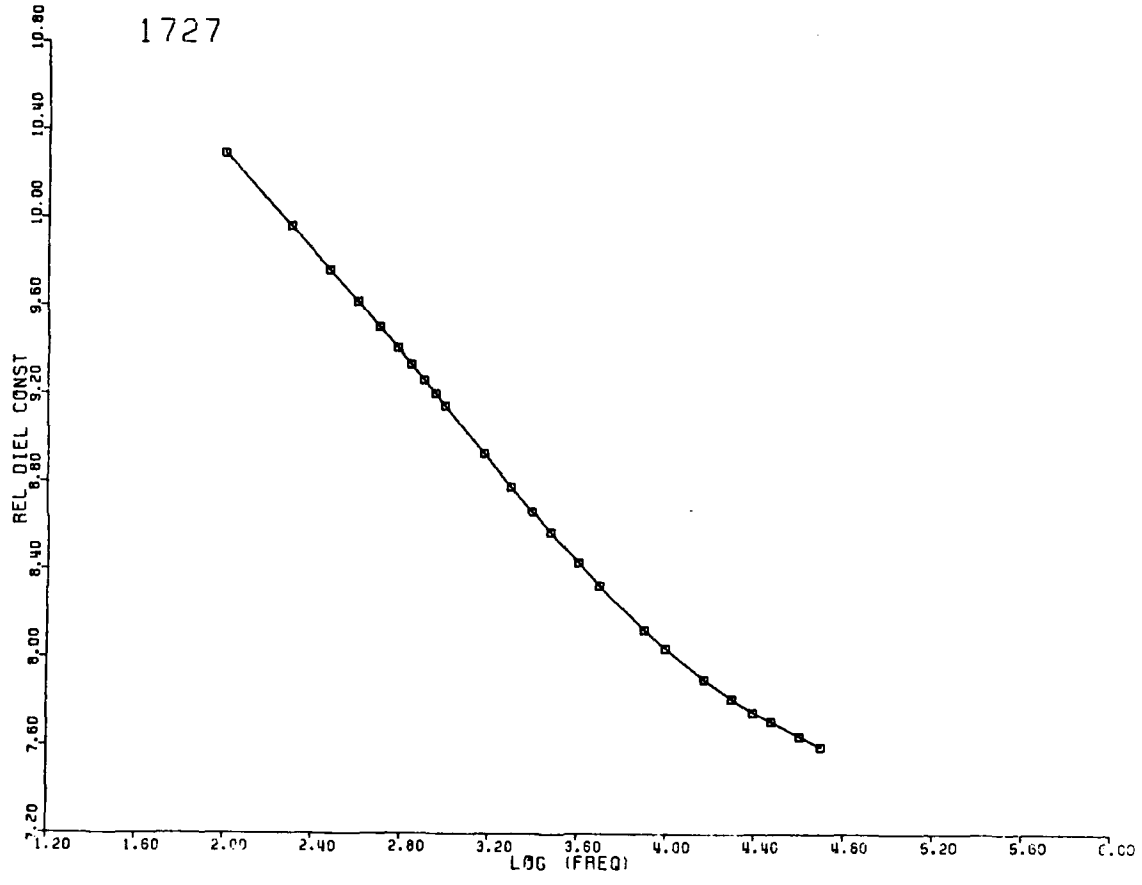

Figure B-8A. Relative permittivity (ε') of sample 1727, amphibolite from Pennsylvania, as a function of frequency.

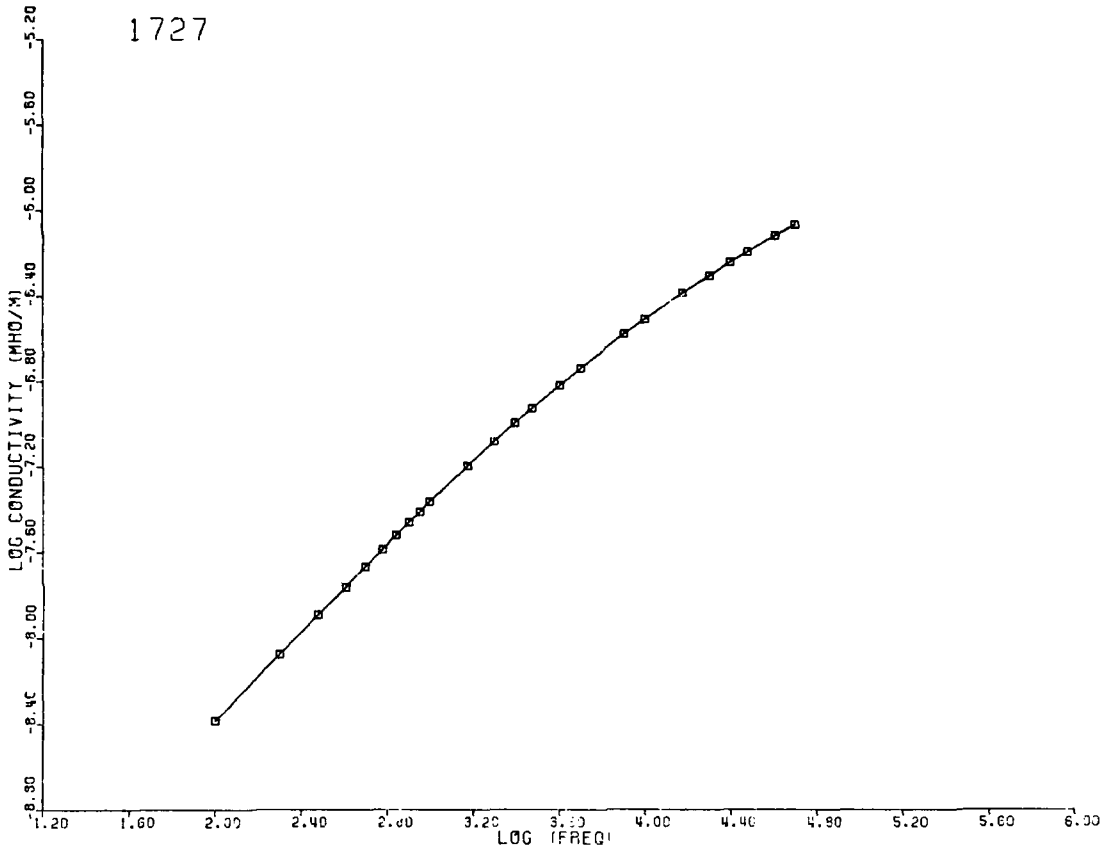

Figure B-8B. Dielectric conductivity ($\sigma = \omega\epsilon''$) of sample 1727, amphibolite from Pennsylvania, as a function of frequency.

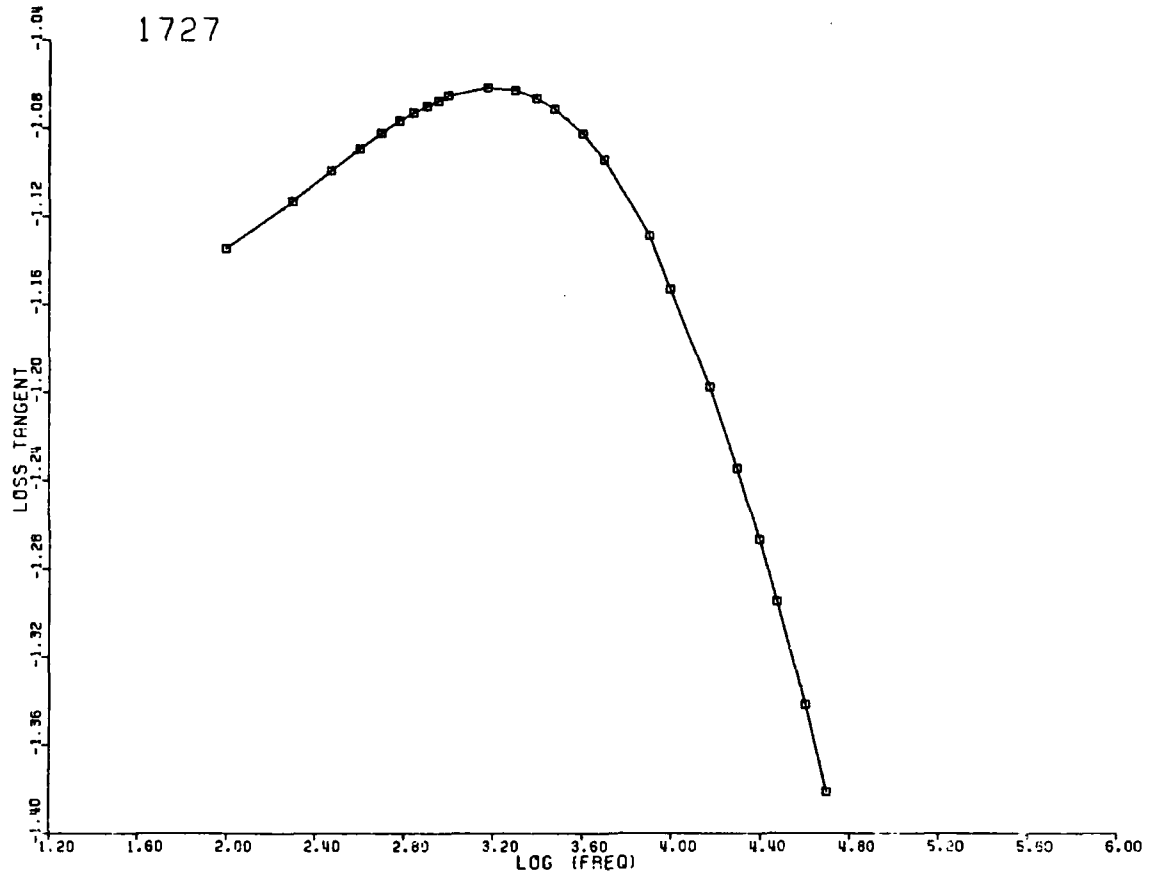

Figure B-8C. Loss tangent of sample 1727, amphibolite from Pennsylvania, as a function of frequency.

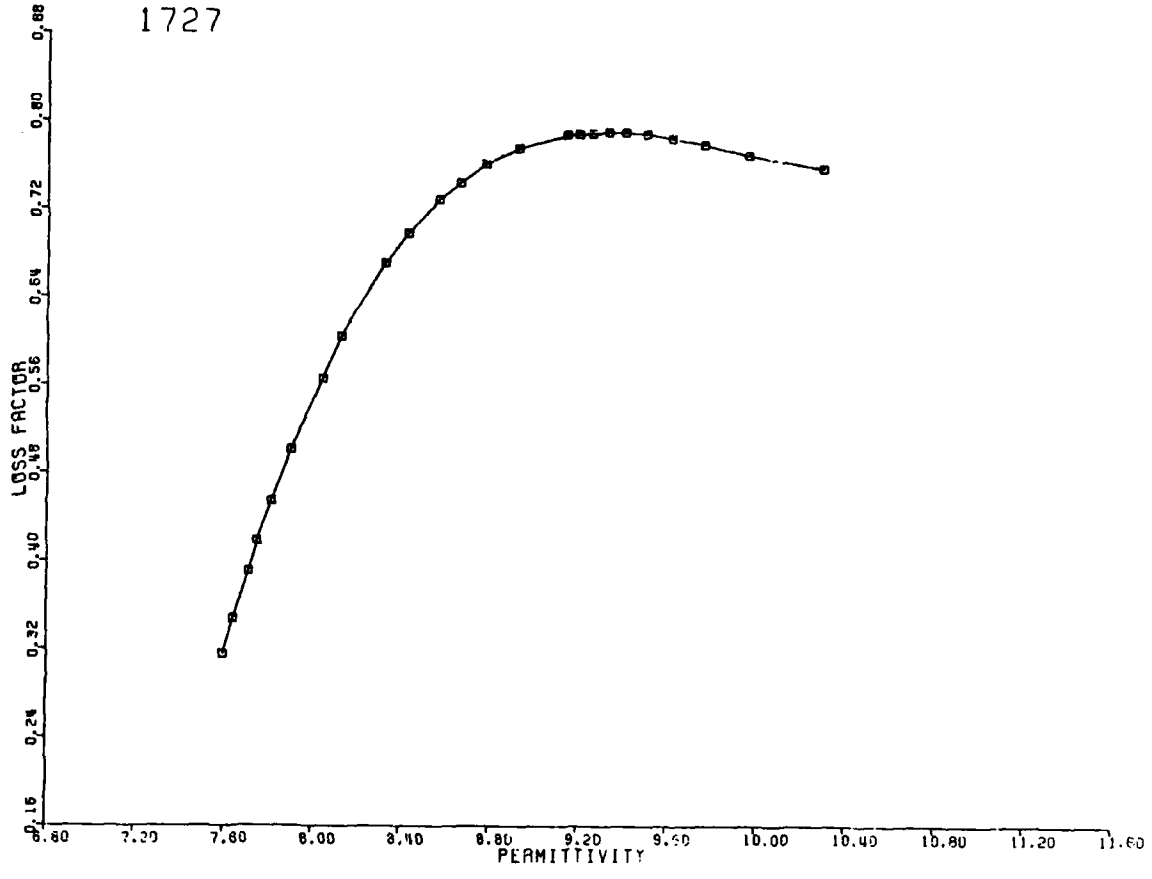

Figure B-8D. Cole-Cole plot, relative loss factor versus relative permittivity, of sample 1727, amphibolite from Pennsylvania.

SAMPLE 2383

FREQUENCY (HERTZ)	RELATIVE DIELECTRIC CONSTANT	CONDUC-TIVITY (MHO/M)	LOSS TANGENT	LOSS FACTOR
500.	10.638	0.1140E-07	0.3890E-01	0.4138E 00
600.	10.595	0.1334E-07	0.3807E-01	0.4033E 00
700.	10.559	0.1527E-07	0.3748E-01	0.3957E 00
800.	10.524	0.1731E-07	0.3729E-01	0.3925E 00
900.	10.498	0.1925E-07	0.3695E-01	0.3880E 00
1000.	10.485	0.2090E-07	0.3616E-01	0.3792E 00
1500.	10.392	0.2981E-07	0.3469E-01	0.3605E 00
2000.	10.325	0.3780E-07	0.3320E-01	0.3429E 00
2500.	10.280	0.4579E-07	0.3232E-01	0.3323E 00
3000.	10.241	0.5264E-07	0.3108E-01	0.3183E 00
4000.	10.198	0.6690E-07	0.2975E-01	0.3034E 00
5000.	10.149	0.8003E-07	0.2861E-01	0.2904E 00
8000.	10.071	0.1166E-06	0.2624E-01	0.2643E 00
10000.	10.044	0.1394E-06	0.2518E-01	0.2529E 00
15000.	9.986	0.1997E-06	0.2419E-01	0.2415E 00
20000.	9.948	0.2511E-06	0.2289E-01	0.2278E 00
25000.	9.919	0.3054E-06	0.2234E-01	0.2216E 00
30000.	9.895	0.3625E-06	0.2215E-01	0.2192E 00
40000.	9.856	0.4709E-06	0.2167E-01	0.2136E 00
50000.	9.824	0.5879E-06	0.2171E-01	0.2133E 00
80000.	9.750	0.9184E-06	0.2136E-01	0.2083E 00

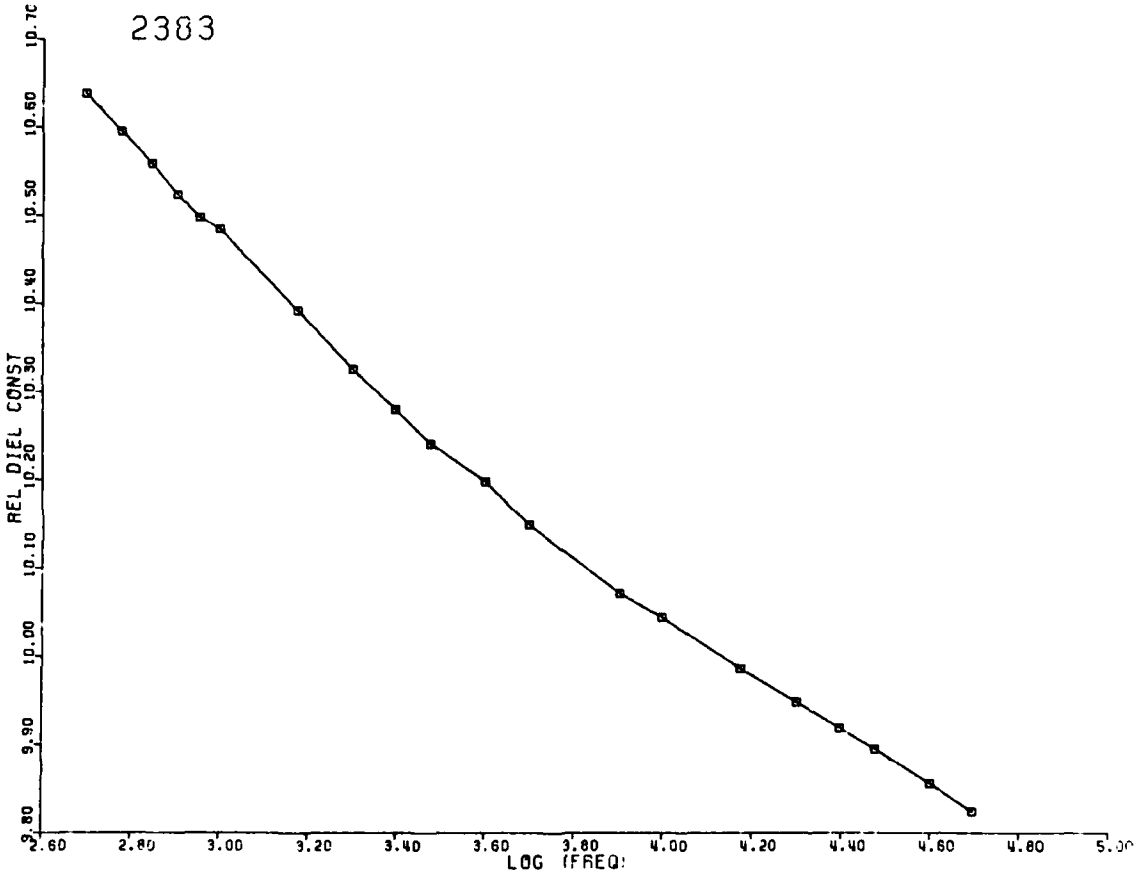

Figure B-9A. Relative permittivity (ε') of sample 2383, garnet granulite from eastern Adirondacks, New York, as a function of frequency.

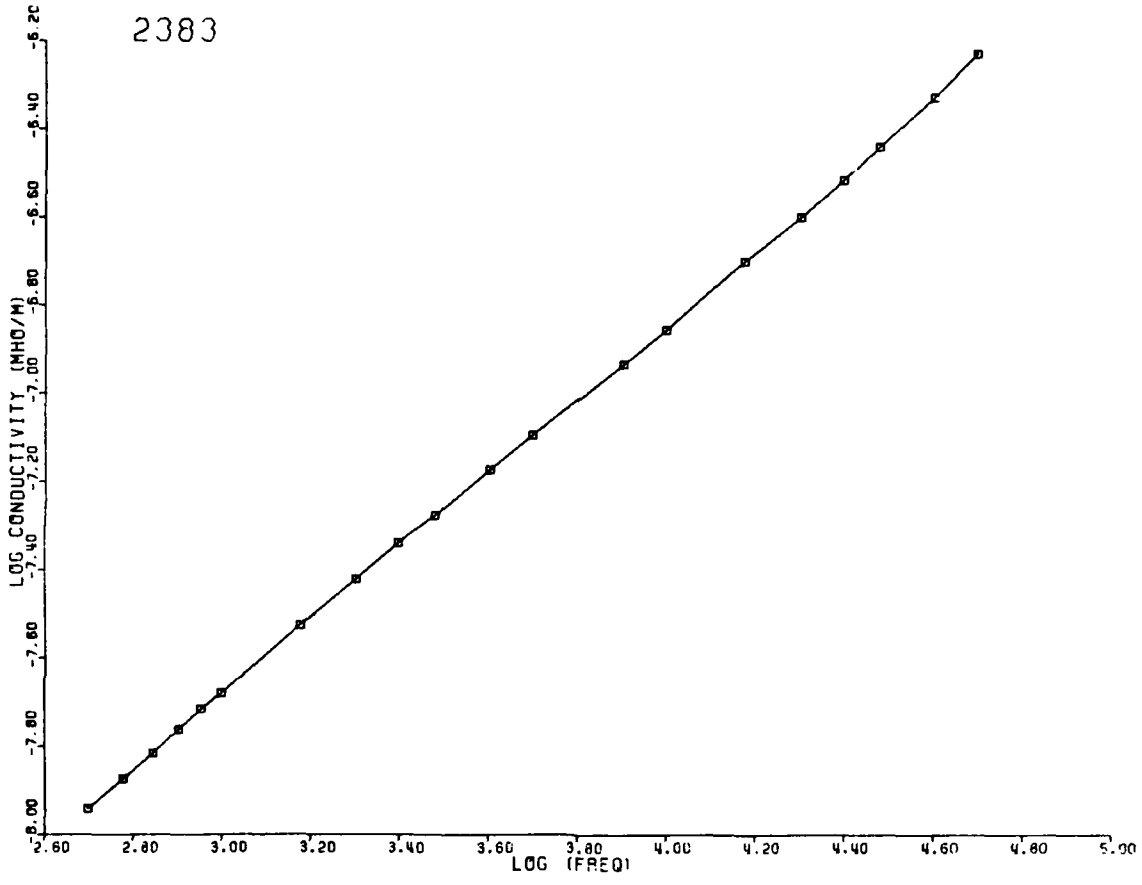

Figure B-9B. Dielectric conductivity ($\sigma = \omega\varepsilon''$) of sample 2383, garnet granulite from eastern Adirondacks, New York, as a function of frequency.

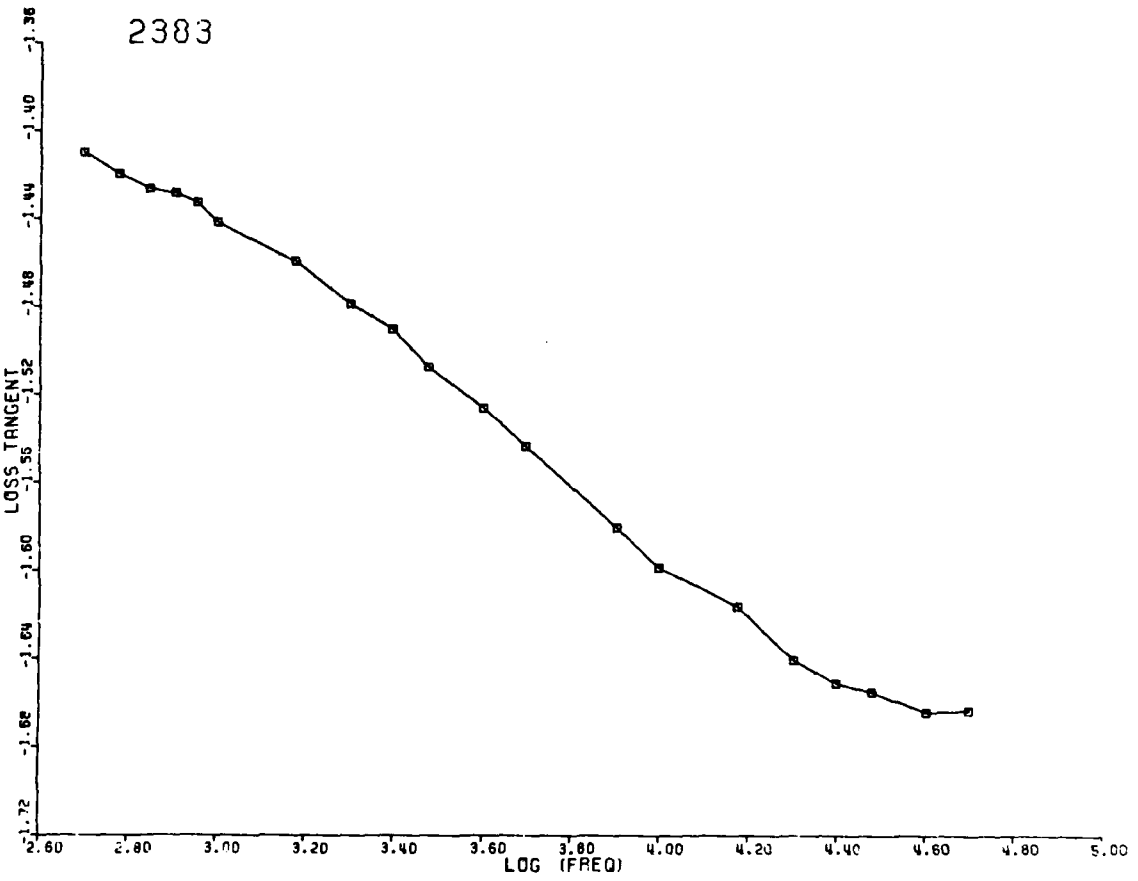

Figure B-9C. Loss tangent of sample 2383, garnet granulite from eastern Adirondacks, New York, as a function of frequency.

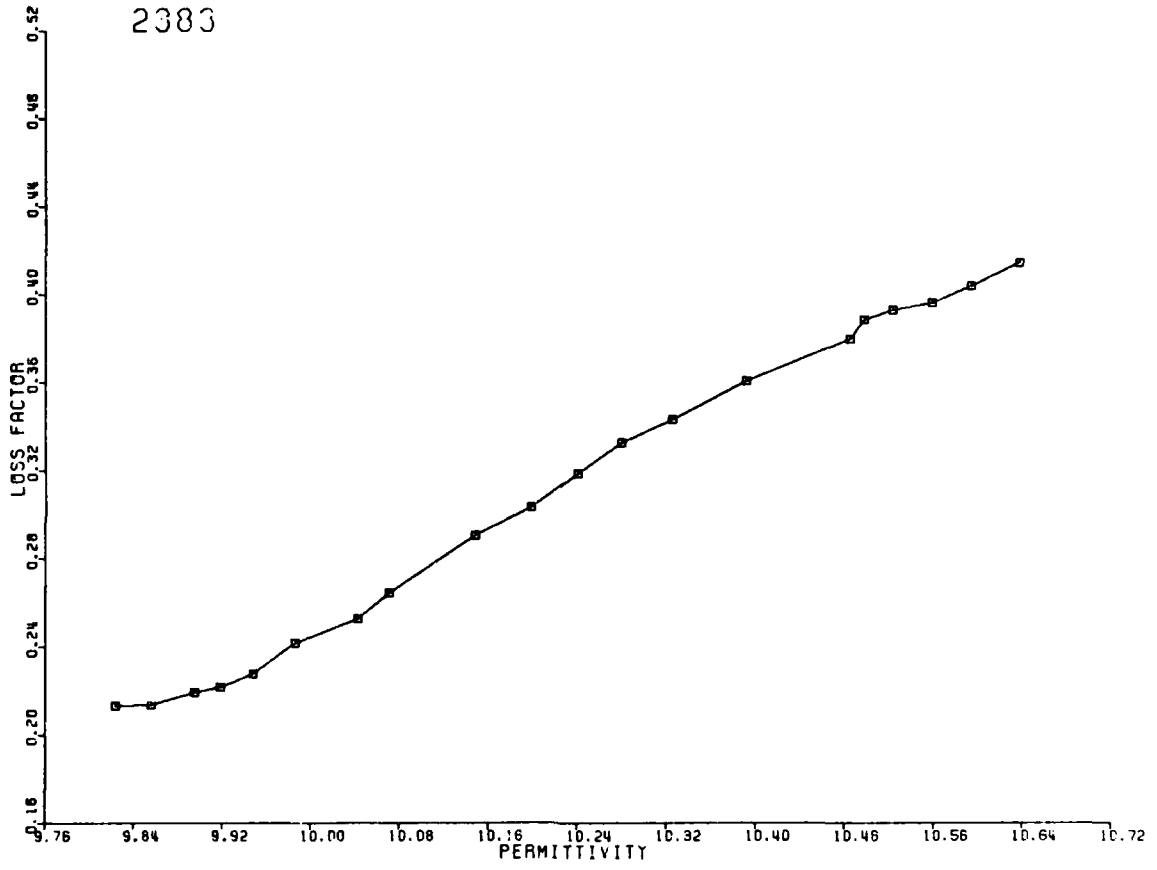

Figure B-9D. Cole-Cole plot, relative loss factor versus relative permittivity, of sample 2383, garnet granulite from eastern Adirondacks, New York.

SAMPLE 2390

FREQUENCY (HERTZ)	RELATIVE DIELECTRIC CONSTANT	CONDUC-TIVITY (MHO/M)	LOSS TANGENT	LOSS FACTOR
100.	6.507	0.1206E-08	0.3430E-01	0.2232E 00
200.	6.418	0.2103E-08	0.3033E-01	0.1946E 00
300.	6.372	0.2912E-08	0.2821E-01	0.1797E 00
400.	6.341	0.3674E-08	0.2682E-01	0.1700E 00
500.	6.318	0.4405E-08	0.2582E-01	0.1631E 00
600.	6.300	0.5105E-08	0.2500E-01	0.1575E 00
700.	6.285	0.5784E-08	0.2434E-01	0.1530E 00
800.	6.273	0.6457E-08	0.2382E-01	0.1494E 00
900.	6.262	0.7116E-08	0.2337E-01	0.1464E 00
1000.	6.253	0.7756E-08	0.2296E-01	0.1436E 00
1500.	6.219	0.1089E-07	0.2160E-01	0.1343E 00
2000.	6.196	0.1387E-07	0.2072E-01	0.1284E 00
2500.	6.179	0.1679E-07	0.2012E-01	0.1243E 00
3000.	6.165	0.1967E-07	0.1969E-01	0.1214E 00
4000.	6.145	0.2509E-07	0.1889E-01	0.1161E 00
5000.	6.130	0.3050E-07	0.1843E-01	0.1129E 00
8000.	6.098	0.4616E-07	0.1751E-01	0.1068E 00
10000.	6.084	0.5583E-07	0.1699E-01	0.1034E 00
15000.	6.059	0.8076E-07	0.1645E-01	0.9966E-01
20000.	6.041	0.1050E-06	0.1609E-01	0.9723E-01
25000.	6.028	0.1290E-06	0.1585E-01	0.9554E-01
30000.	6.017	0.1528E-06	0.1567E-01	0.9430E-01
40000.	6.000	0.1999E-06	0.1542E-01	0.9251E-01
50000.	5.985	0.2385E-06	0.1475E-01	0.8828E-01
80000.	5.956	0.3618E-06	0.1406E-01	0.8372E-01

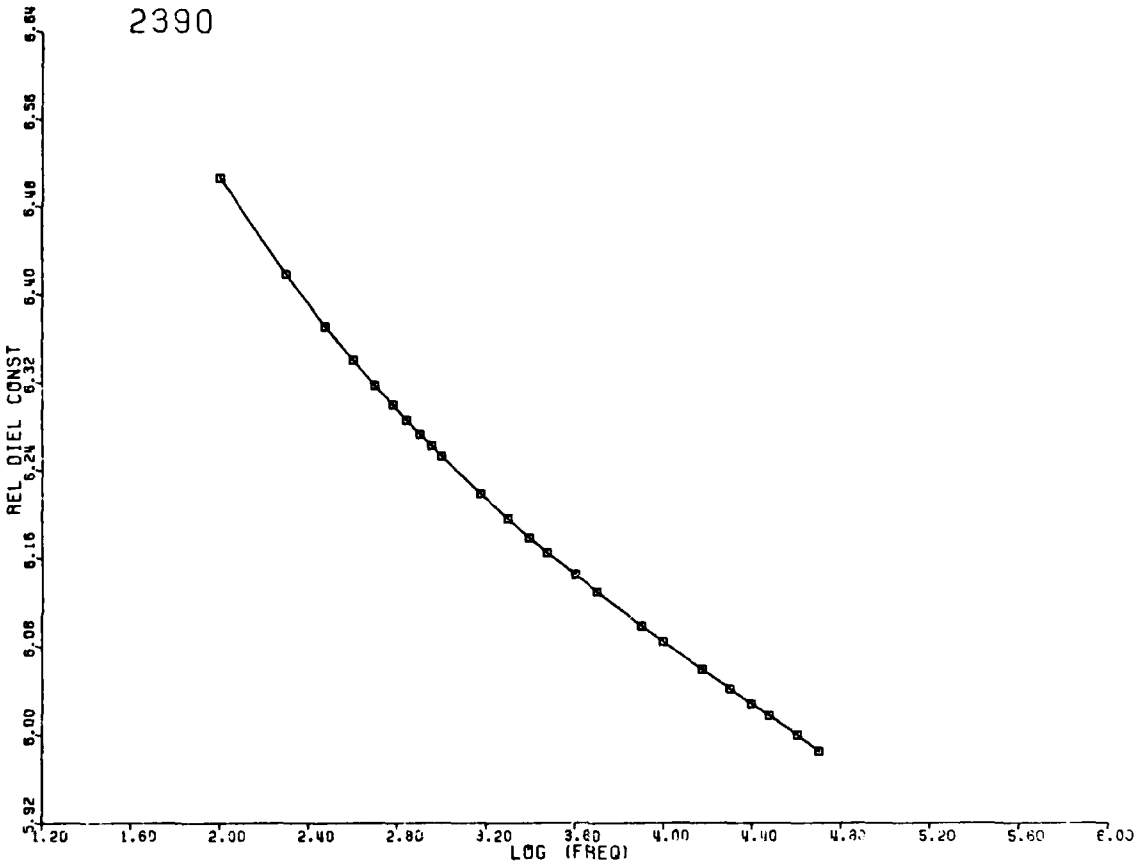

Figure B-10A. Relative permittivity (ε') of sample 2390, garnet granulite from eastern Adirondacks, New York, as a function of frequency.

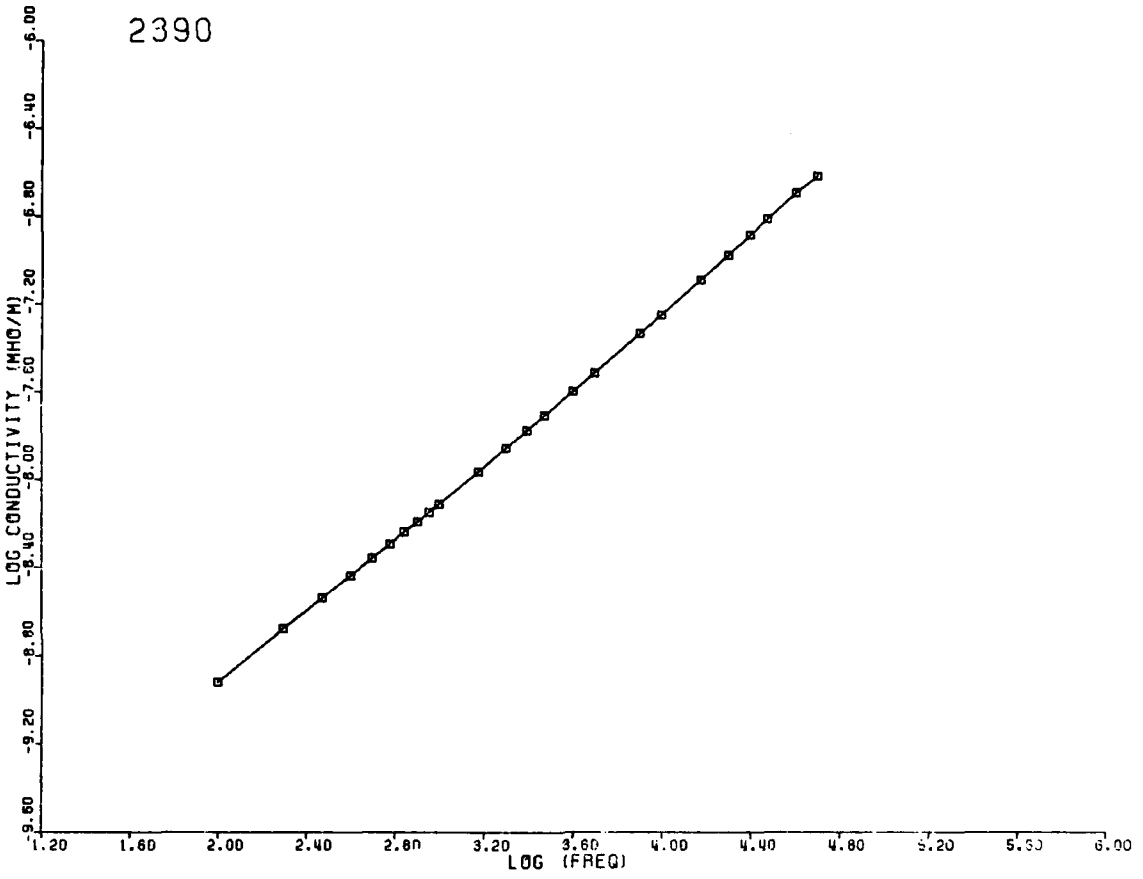

Figure B-10B. Dielectric conductivity ($\sigma = \omega\varepsilon''$) of sample 2390, garnet granulite from eastern Adirondacks, New York, as a function of frequency.

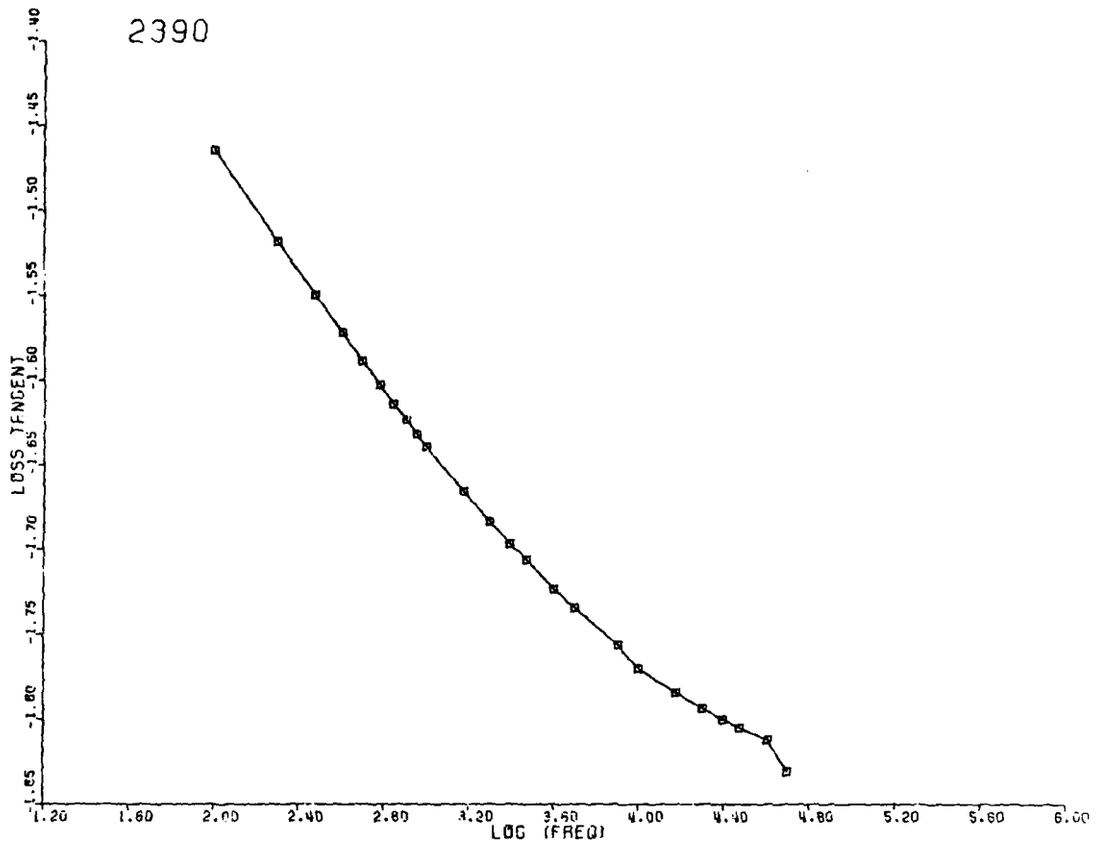

Figure B-10C. Loss tangent of sample 2390, garnet granulite from eastern Adirondacks, New York, as a function of frequency.

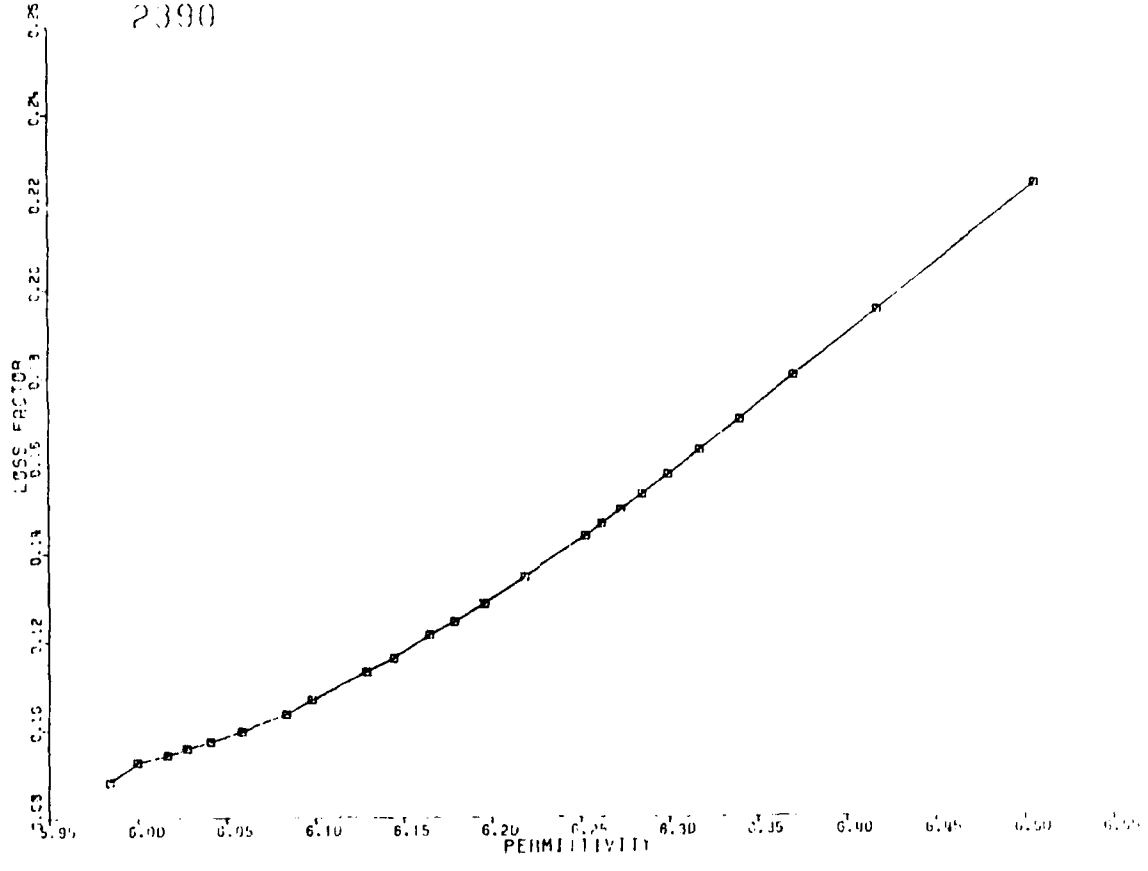

Figure B-10D. Cole-Cole plot, relative loss factor versus relative permittivity, of sample 2390, garnet granulite from eastern Adirondacks, New York.

SAMPLE 2422

FREQUENCY (HERTZ)	RELATIVE DIELECTRIC CONSTANT	CONDUC-TIVITY (MHO/M)	LOSS TANGENT	LOSS FACTOR
100.	6.302	0.1084E-08	0.3132E-01	0.1974E 00
200.	6.226	0.1789E-08	0.2615E-01	0.1628E 00
300.	6.189	0.2386E-08	0.2340E-01	0.1448E 00
400.	6.166	0.2933E-08	0.2165E-01	0.1335E 00
500.	6.148	0.3433E-08	0.2033E-01	0.1250E 00
600.	6.135	0.3900E-08	0.1929E-01	0.1184E 00
700.	6.125	0.4345E-08	0.1845E-01	0.1130E 00
800.	6.116	0.4782E-08	0.1779E-01	0.1088E 00
900.	6.109	0.5190E-08	0.1719E-01	0.1050E 00
1000.	6.102	0.5597E-08	0.1670E-01	0.1019E 00
1500.	6.080	0.7479E-08	0.1493E-01	0.9077E-01
2000.	6.065	0.9229E-08	0.1385E-01	0.8401E-01
2500.	6.055	0.1089E-07	0.1310E-01	0.7932E-01
3000.	6.047	0.1246E-07	0.1250E-01	0.7561E-01
4000.	6.035	0.1554E-07	0.1172E-01	0.7075E-01
5000.	6.027	0.1852E-07	0.1119E-01	0.6743E-01
8000.	6.009	0.2708E-07	0.1026E-01	0.6163E-01
10000.	6.002	0.3241E-07	0.9832E-02	0.5901E-01
15000.	5.988	0.4614E-07	0.9354E-02	0.5601E-01
20000.	5.978	0.5987E-07	0.9116E-02	0.5450E-01
25000.	5.970	0.7322E-07	0.8931E-02	0.5332E-01
30000.	5.964	0.8682E-07	0.8835E-02	0.5269E-01
40000.	5.954	0.1132E-06	0.8652E-02	0.5151E-01
50000.	5.944	0.1345E-06	0.8242E-02	0.4899E-01
80000.	5.922	0.1967E-06	0.7559E-02	0.4477E-01

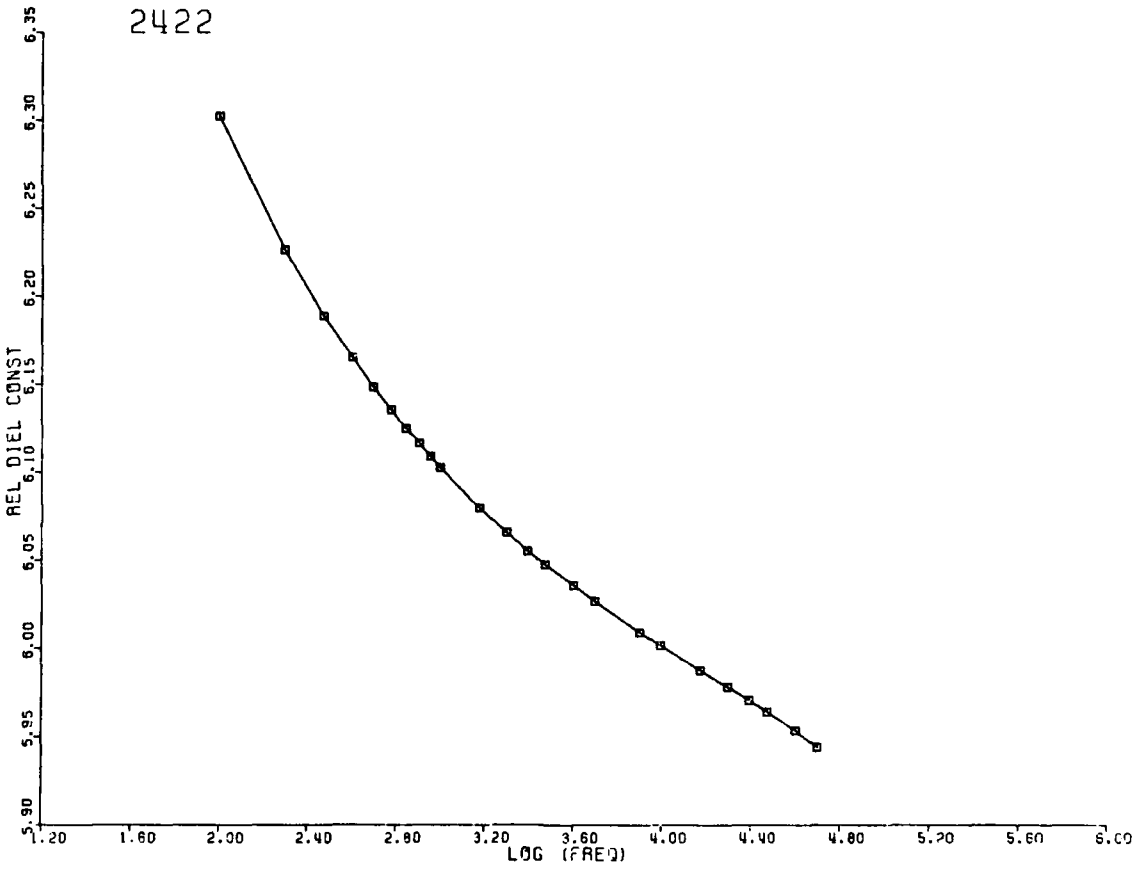

Figure B-11A. Relative permittivity (ε') of sample 2422, phyllite from central Maine, as a function of frequency.

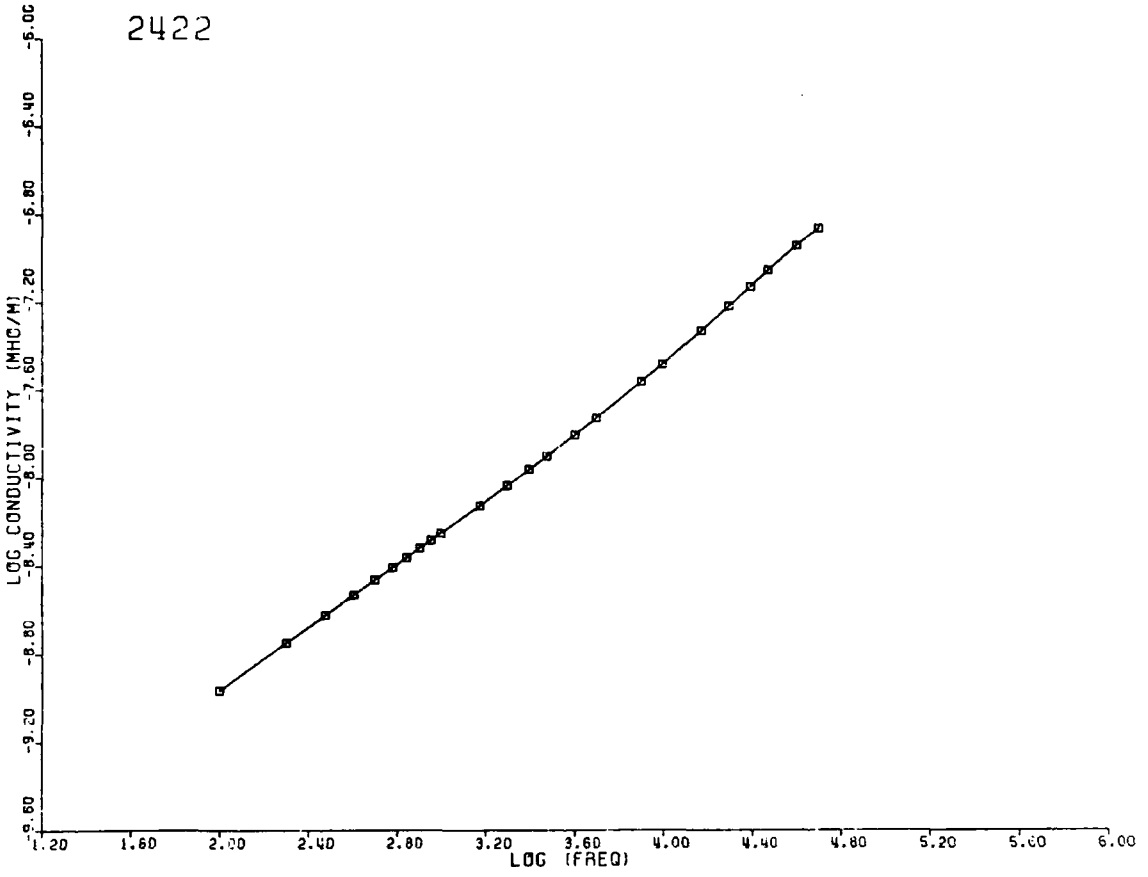

Figure B-11B. Dielectric conductivity ($\sigma = \omega\varepsilon''$) of sample 2422, phyllite from central Maine, as a function of frequency.

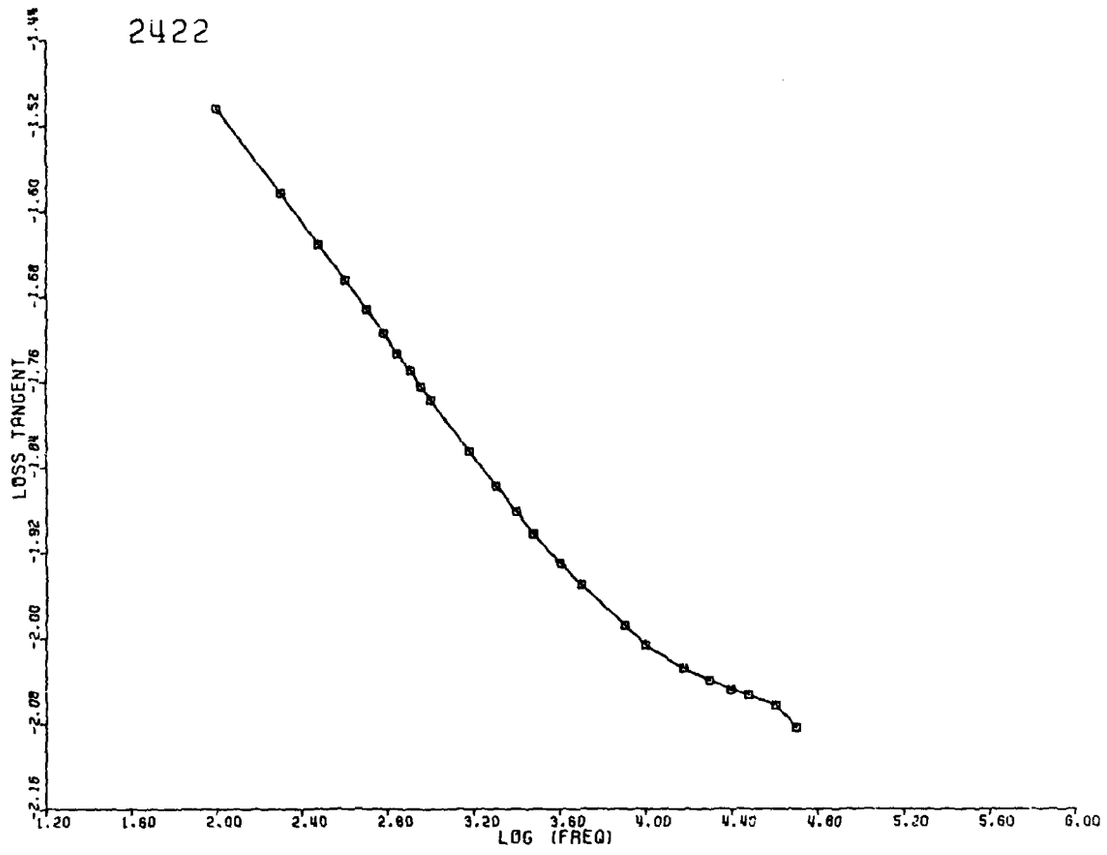

Figure B-11C. Loss tangent of sample 2422, phyllite from central Maine, as a function of frequency.

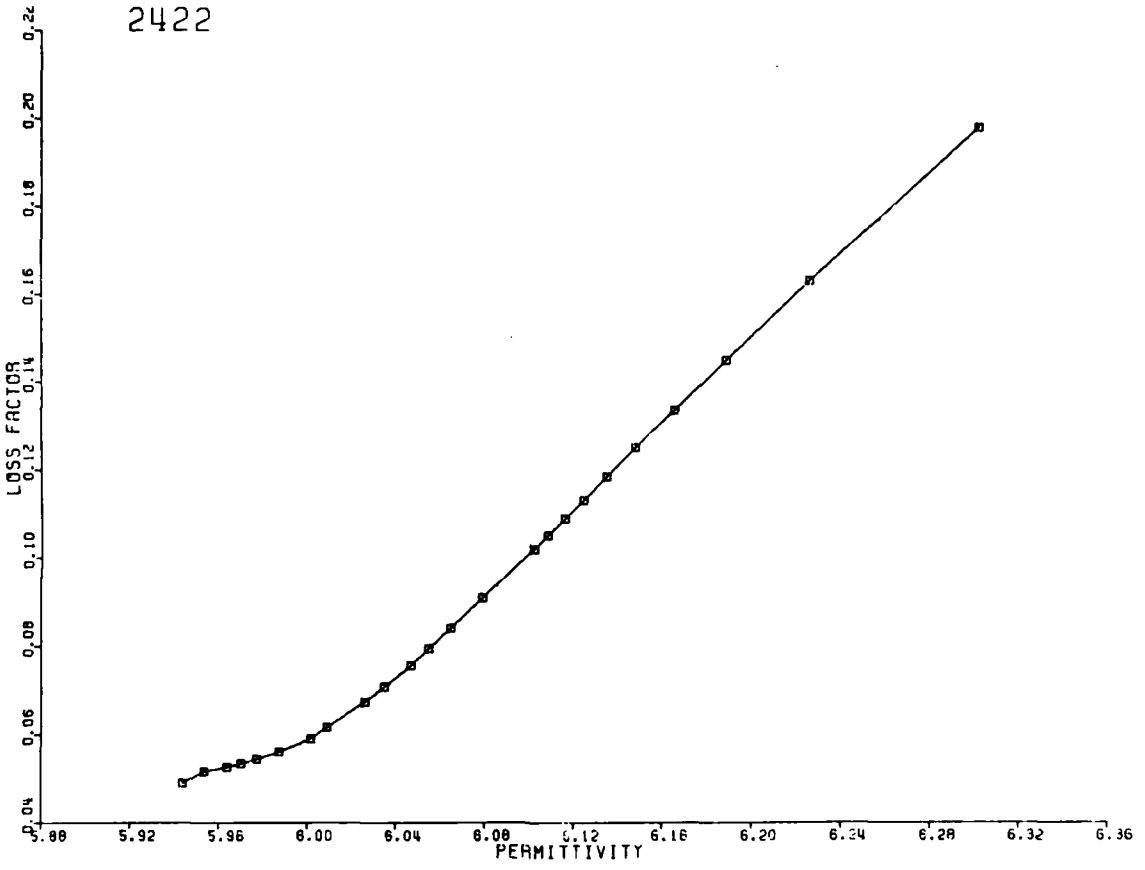

Figure B-11D. Cole-Cole plot, relative loss factor versus relative permittivity, of sample 2422, phyllite from central Maine.

SAMPLE 2425

FREQUENCY (HERTZ)	RELATIVE DIELECTRIC CONSTANT	CONDUC-TIVITY (MHO/M)	LOSS TANGENT	LOSS FACTOR
100.	6.189	0.9074E-09	0.2675E-01	0.1655E 00
200.	6.115	0.1854E-08	0.2766E-01	0.1691E 00
300.	6.071	0.2822E-08	0.2826E-01	0.1716E 00
400.	6.039	0.3787E-08	0.2860E-01	0.1727E 00
500.	6.013	0.4754E-08	0.2884E-01	0.1734E 00
600.	5.993	0.5725E-08	0.2904E-01	0.1740E 00
700.	5.975	0.6676E-08	0.2912E-01	0.1740E 00
800.	5.960	0.7629E-08	0.2919E-01	0.1740E 00
900.	5.946	0.8580E-08	0.2925E-01	0.1739E 00
1000.	5.934	0.9526E-08	0.2928E-01	0.1738E 00
1500.	5.887	0.1416E-07	0.2926E-01	0.1722E 00
2000.	5.854	0.1864E-07	0.2903E-01	0.1700E 00
2500.	5.829	0.2301E-07	0.2881E-01	0.1679E 00
3000.	5.810	0.2715E-07	0.2842E-01	0.1651E 00
4000.	5.778	0.3523E-07	0.2781E-01	0.1607E 00
5000.	5.755	0.4303E-07	0.2728E-01	0.1570E 00
8000.	5.708	0.6466E-07	0.2583E-01	0.1474E 00
10000.	5.688	0.7750E-07	0.2485E-01	0.1414E 00
15000.	5.651	0.1086E-06	0.2338E-01	0.1321E 00
20000.	5.627	0.1367E-06	0.2216E-01	0.1247E 00
25000.	5.609	0.1628E-06	0.2118E-01	0.1188E 00
30000.	5.595	0.1878E-06	0.2040E-01	0.1142E 00
40000.	5.575	0.2332E-06	0.1908E-01	0.1064E 00
50000.	5.559	0.2639E-06	0.1732E-01	0.9626E-01
80000.	5.529	0.3549E-06	0.1464E-01	0.8093E-01

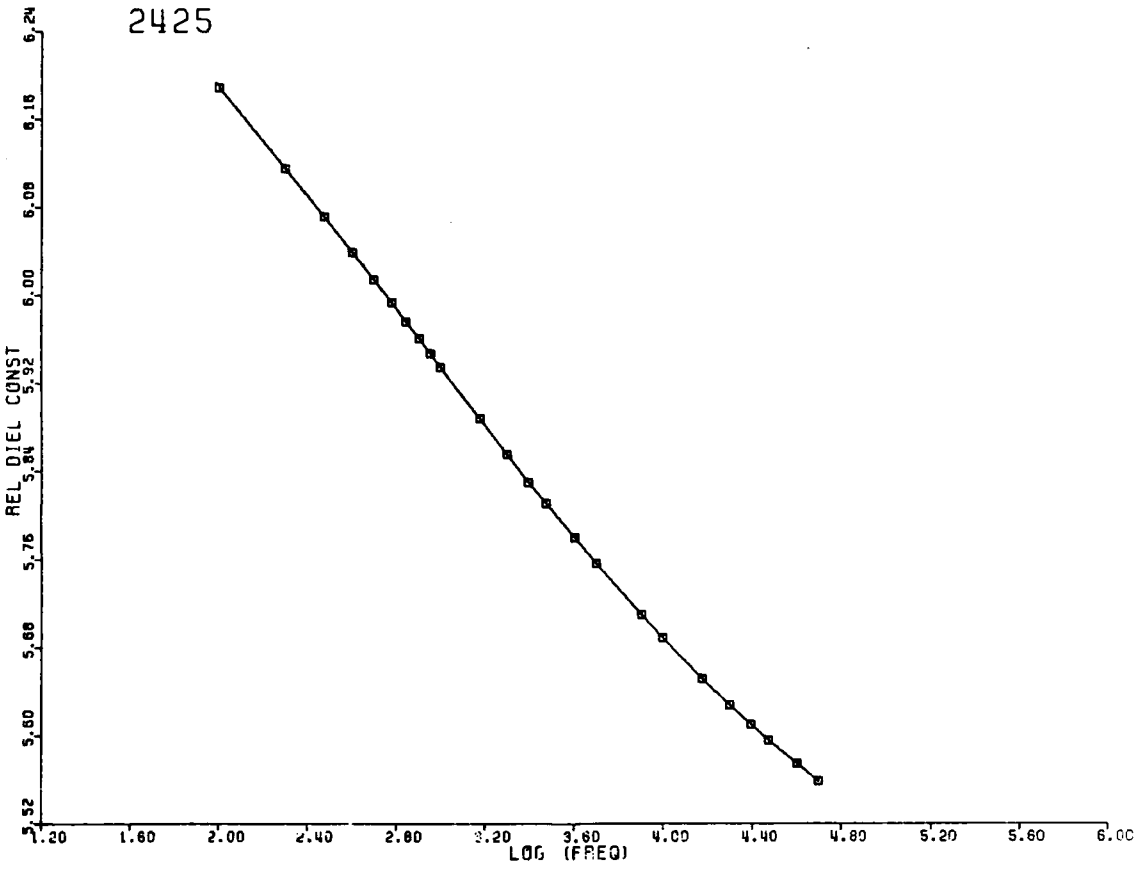

Figure B-12A. Relative permittivity (ε') of sample 2425, metagranite from central Maine, as a function of frequency.

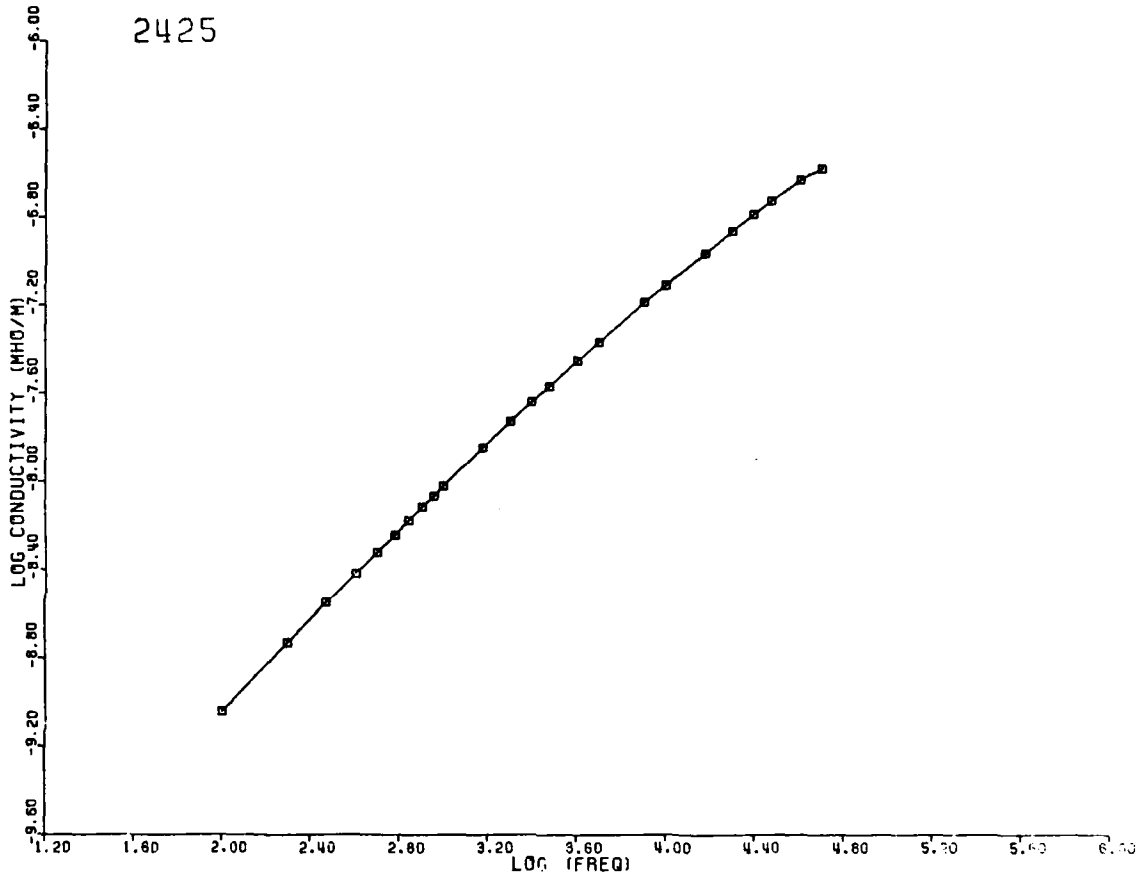

Figure B-12B. Dielectric conductivity ($\sigma = \omega\varepsilon''$) of sample 2425, metagranite from central Maine, as a function of frequency.

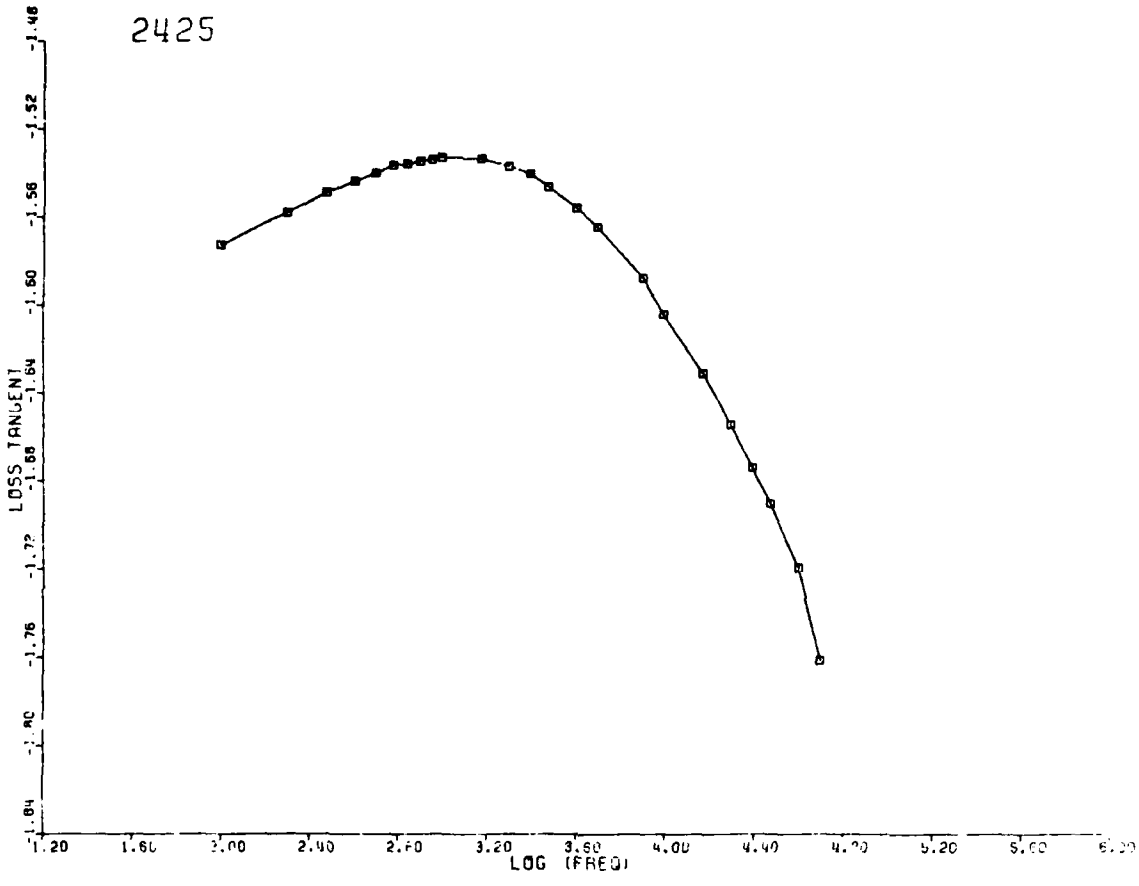

Figure B-12C. Loss tangent of sample 2425, metagranite from central Maine, as a function of frequency.

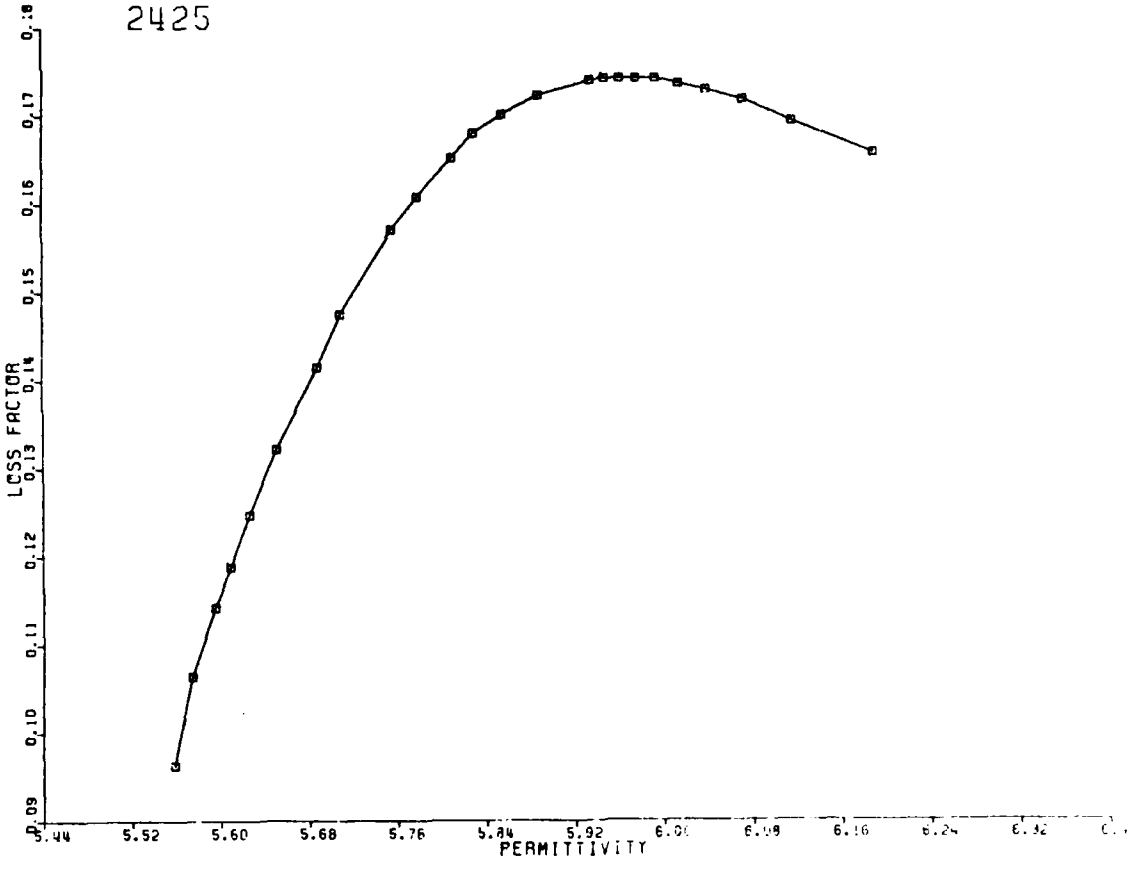

Figure B-12D. Cole-Cole plot, relative loss factor versus relative permittivity, of sample 2425, metagranite from central Maine.

SAMPLE 2426-1

FREQUENCY (HERTZ)	RELATIVE DIELECTRIC CONSTANT	CONDUC-TIVITY (MHO/M)	LOSS TANGENT	LOSS FACTOR
100.	4.992	0.2225E-09	0.8058E-02	0.4022E-01
200.	4.976	0.4449E-09	0.8084E-02	0.4022E-01
300.	4.966	0.6829E-09	0.8288E-02	0.4116E-01
400.	4.959	0.9416E-09	0.8583E-02	0.4256E-01
500.	4.954	0.1211E-08	0.8838E-02	0.4378E-01
600.	4.949	0.1490E-08	0.9073E-02	0.4490E-01
700.	4.944	0.1785E-08	0.9325E-02	0.4610E-01
800.	4.941	0.2084E-08	0.9535E-02	0.4711E-01
900.	4.937	0.2395E-08	0.9745E-02	0.4811E-01
1000.	4.934	0.2711E-08	0.9934E-02	0.4902E-01
1500.	4.921	0.4367E-08	0.1070E-01	0.5263E-01
2000.	4.911	0.6105E-08	0.1124E-01	0.5519E-01
2500.	4.903	0.7890E-08	0.1164E-01	0.5706E-01
3000.	4.896	0.9701E-08	0.1194E-01	0.5846E-01
4000.	4.885	0.1342E-07	0.1241E-01	0.6064E-01
5000.	4.875	0.1714E-07	0.1271E-01	0.6198E-01
10000.	4.846	0.3507E-07	0.1308E-01	0.6340E-01
15000.	4.828	0.5225E-07	0.1305E-01	0.6298E-01
20000.	4.815	0.6855E-07	0.1287E-01	0.6197E-01
25000.	4.806	0.8407E-07	0.1265E-01	0.6080E-01
30000.	4.798	0.9881E-07	0.1241E-01	0.5955E-01
40000.	4.787	0.1269E-06	0.1198E-01	0.5734E-01
50000.	4.778	0.1529E-06	0.1157E-01	0.5528E-01

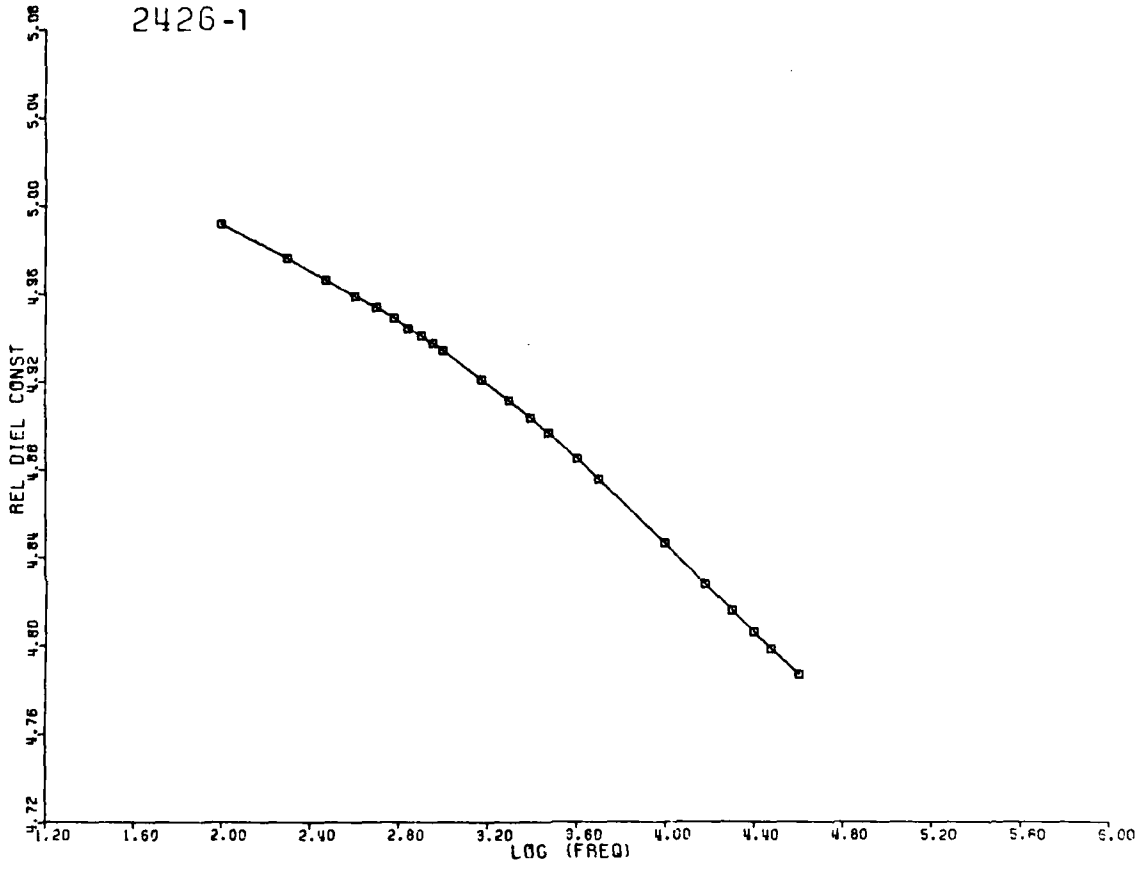

Figure B-13A. Relative permittivity (ε') of sample 2426-1, metaquartzite from Camden, Maine, as a function of frequency.

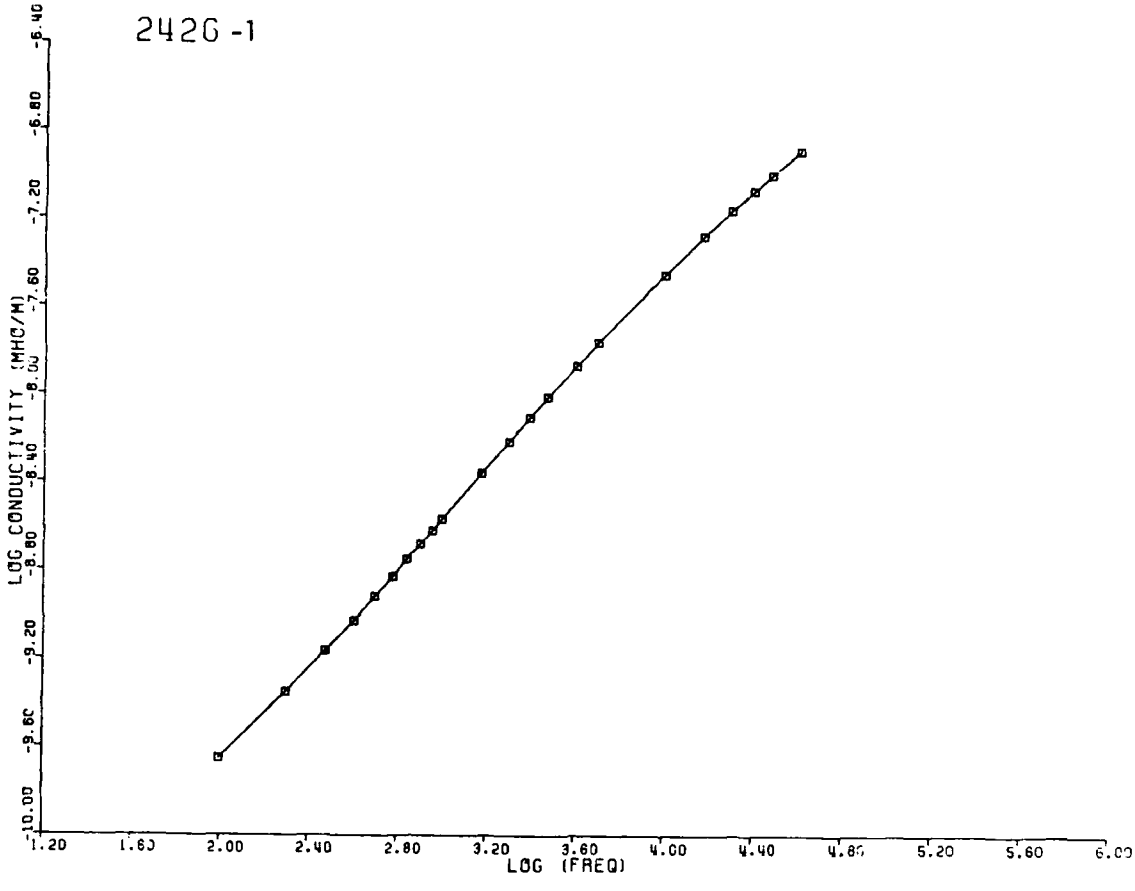

Figure B-13B. Dielectric conductivity ($\sigma = \omega\varepsilon''$) of sample 2426-1, metaquartzite from Camden, Maine, as a function of frequency.

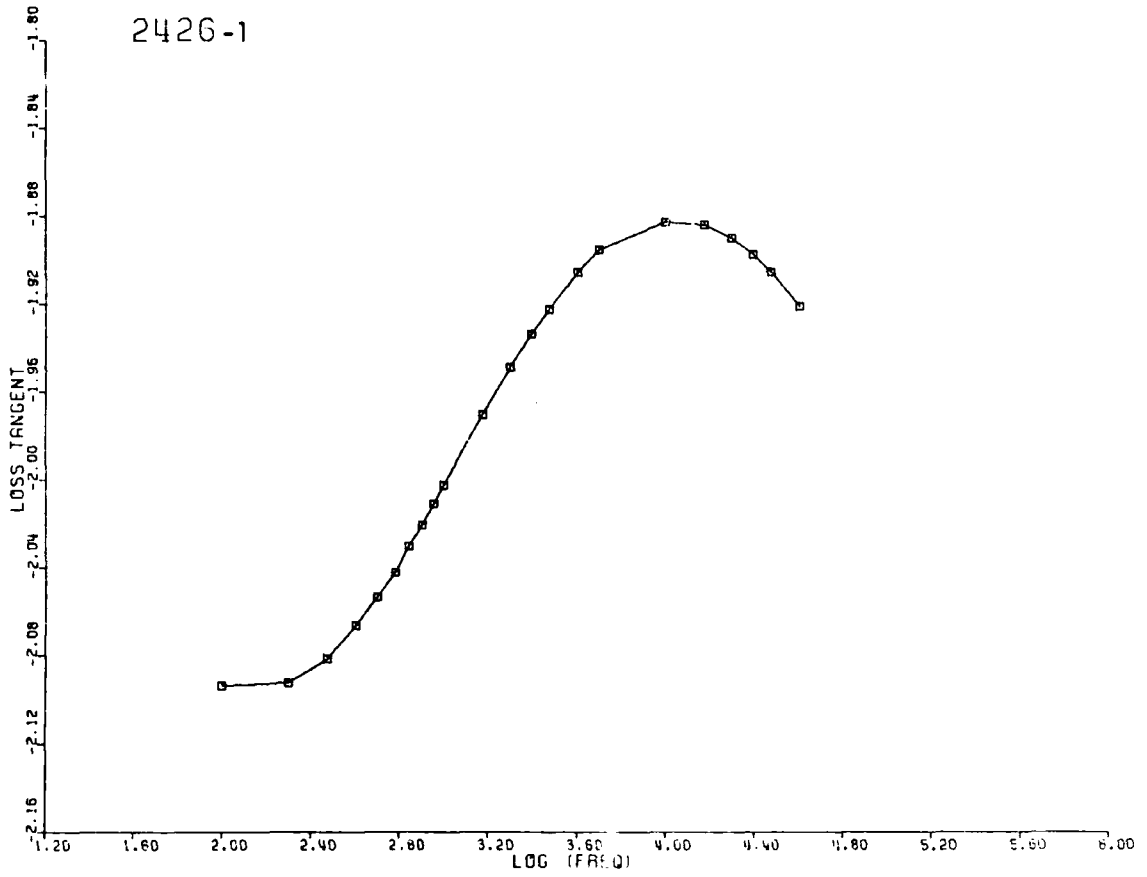

Figure B-13C. Loss tangent of sample 2426-1, metaquartzite from Camden, Maine, as a function of frequency.

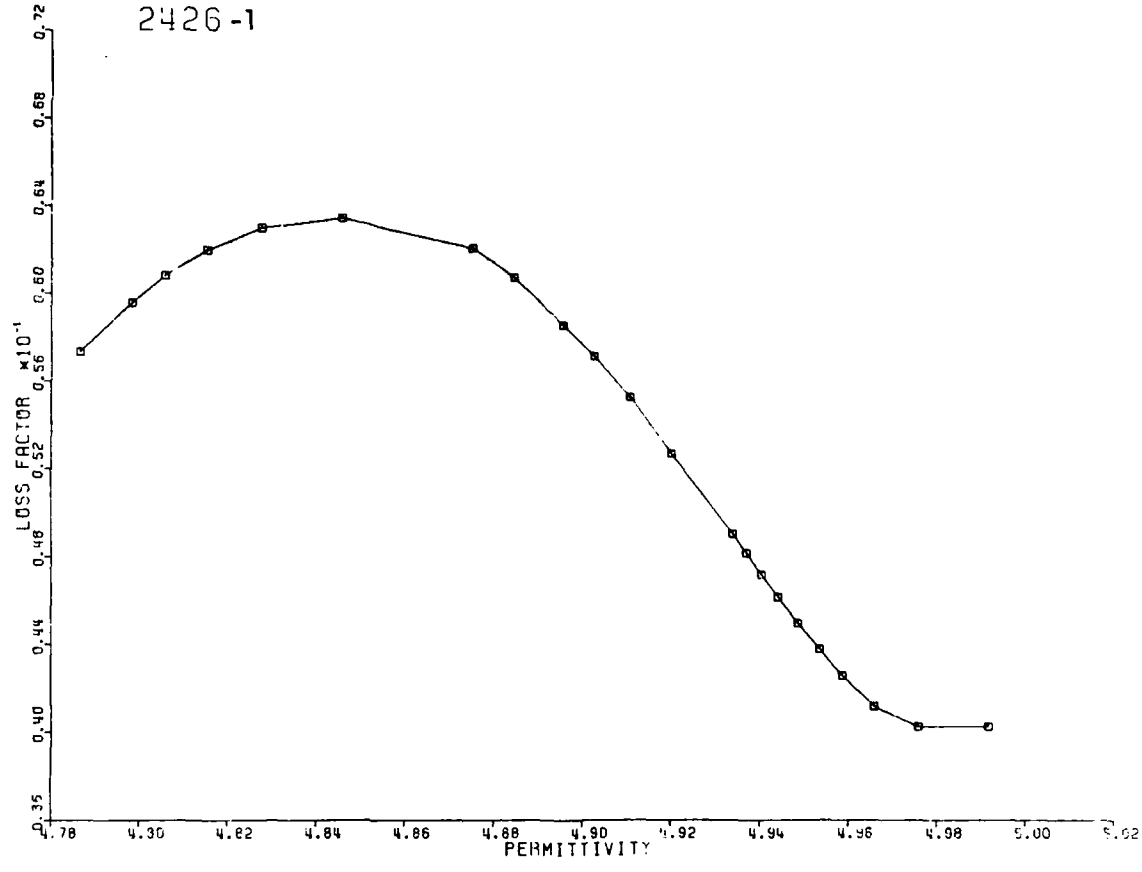

Figure B-13D. Cole-Cole plot, relative loss factor versus relative permittivity, of sample 2426-1, metaquartzite from Camden, Maine.

SAMPLE 2426-2

FREQUENCY (HERTZ)	RELATIVE DIELECTRIC CONSTANT	CONDUC-TIVITY (MHO/M)	LOSS TANGENT	LOSS FACTOR
100.	5.064	0.1899E-09	0.6757E-02	0.3422E-01
200.	5.050	0.3883E-09	0.6929E-02	0.3499E-01
400.	5.035	0.8264E-09	0.7396E-02	0.3724E-01
500.	5.029	0.1058E-08	0.7582E-02	0.3813E-01
600.	5.025	0.1306E-08	0.7806E-02	0.3923E-01
700.	5.021	0.1554E-08	0.7968E-02	0.4001E-01
800.	5.018	0.1802E-08	0.8090E-02	0.4059E-01
900.	5.015	0.2068E-08	0.8256E-02	0.4140E-01
1000.	5.012	0.2329E-08	0.8376E-02	0.4198E-01
1500.	5.001	0.3701E-08	0.8892E-02	0.4447E-01
2000.	4.993	0.5142E-08	0.9281E-02	0.4634E-01
2500.	4.986	0.6603E-08	0.9547E-02	0.4760E-01
3000.	4.980	0.8146E-08	0.9826E-02	0.4894E-01
4000.	4.970	0.1121E-07	0.1016E-01	0.5051E-01
5000.	4.963	0.1433E-07	0.1041E-01	0.5164E-01
10000.	4.939	0.2888E-07	0.1054E-01	0.5205E-01
15000.	4.925	0.4293E-07	0.1047E-01	0.5158E-01
20000.	4.914	0.5677E-07	0.1041E-01	0.5115E-01
25000.	4.906	0.6944E-07	0.1020E-01	0.5006E-01
30000.	4.900	0.8185E-07	0.1003E-01	0.4917E-01
40000.	4.891	0.1047E-06	0.9646E-02	0.4718E-01
50000.	4.885	0.1262E-06	0.9314E-02	0.4549E-01
80000.	4.873	0.1786E-06	0.8256E-02	0.4023E-01

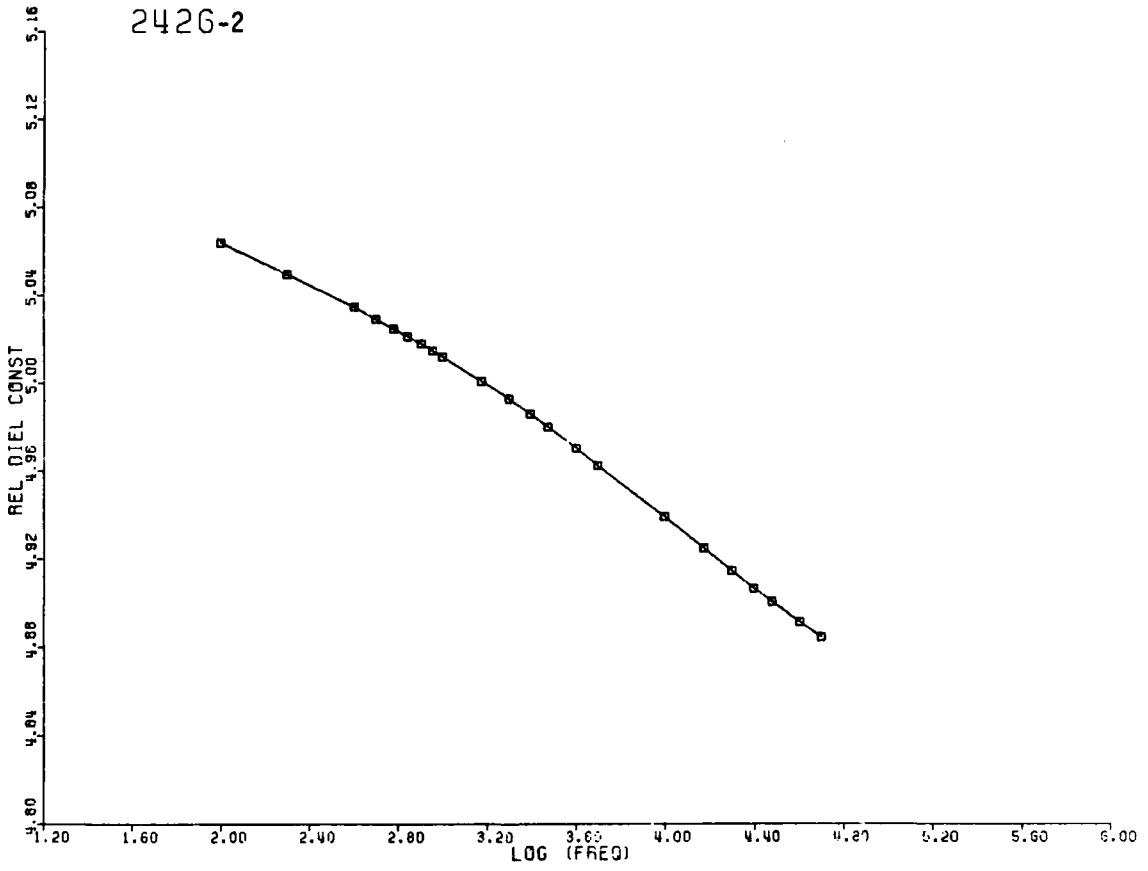

Figure B-14A. Relative permittivity (ε') of sample 2426-2, metaquartzite from Camden, Maine, as a function of frequency.

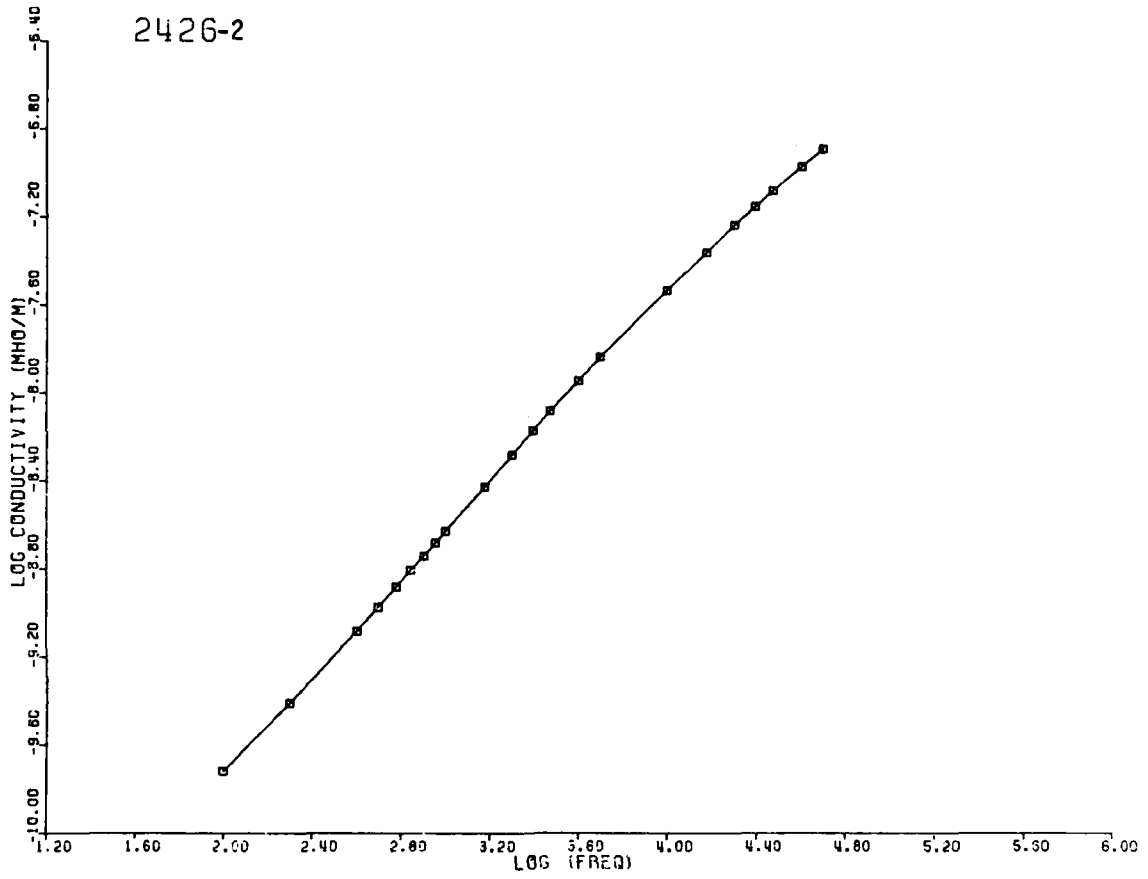

Figure B-14B. Dielectric conductivity ($\sigma = \omega\varepsilon''$) of sample 2426-2, metaquartzite from Camden, Maine, as a function of frequency.

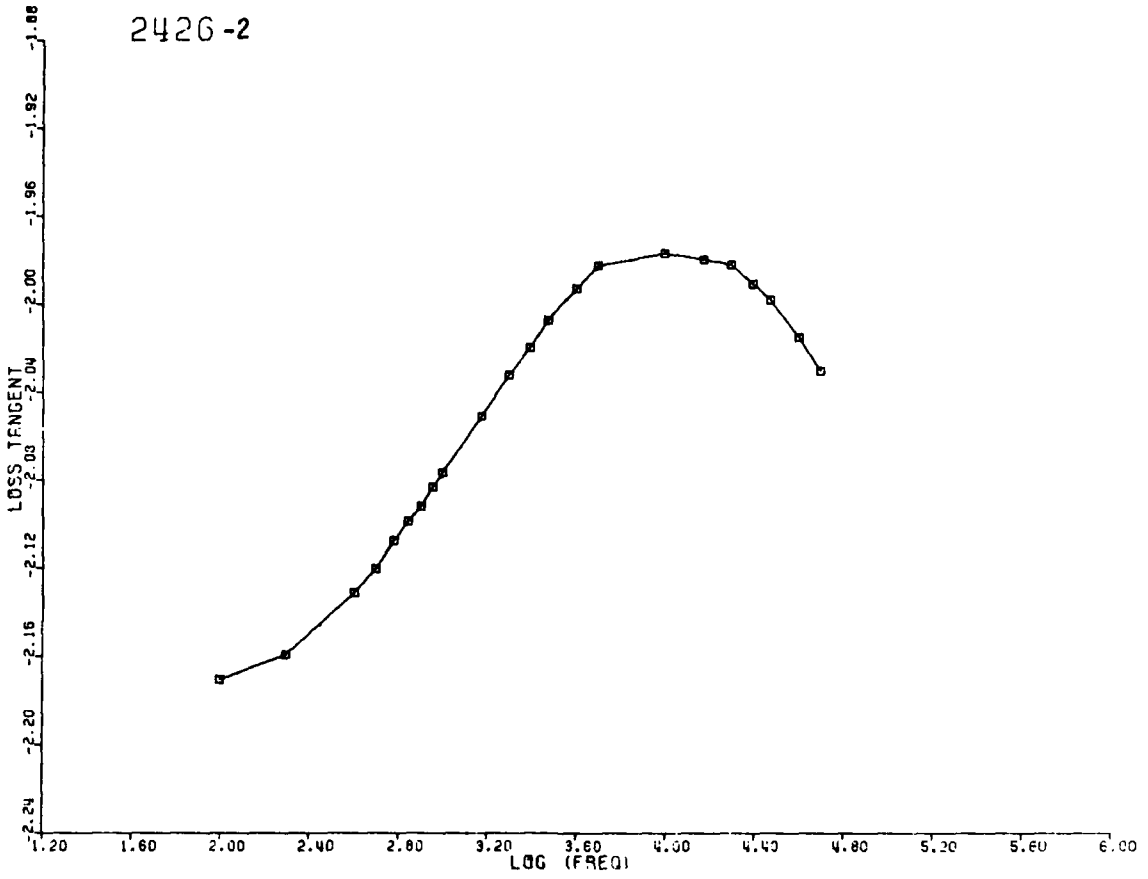

Figure B-14C. Loss tangent of sample 2426-2, metaquartzite from Camden, Maine, as a function of frequency.

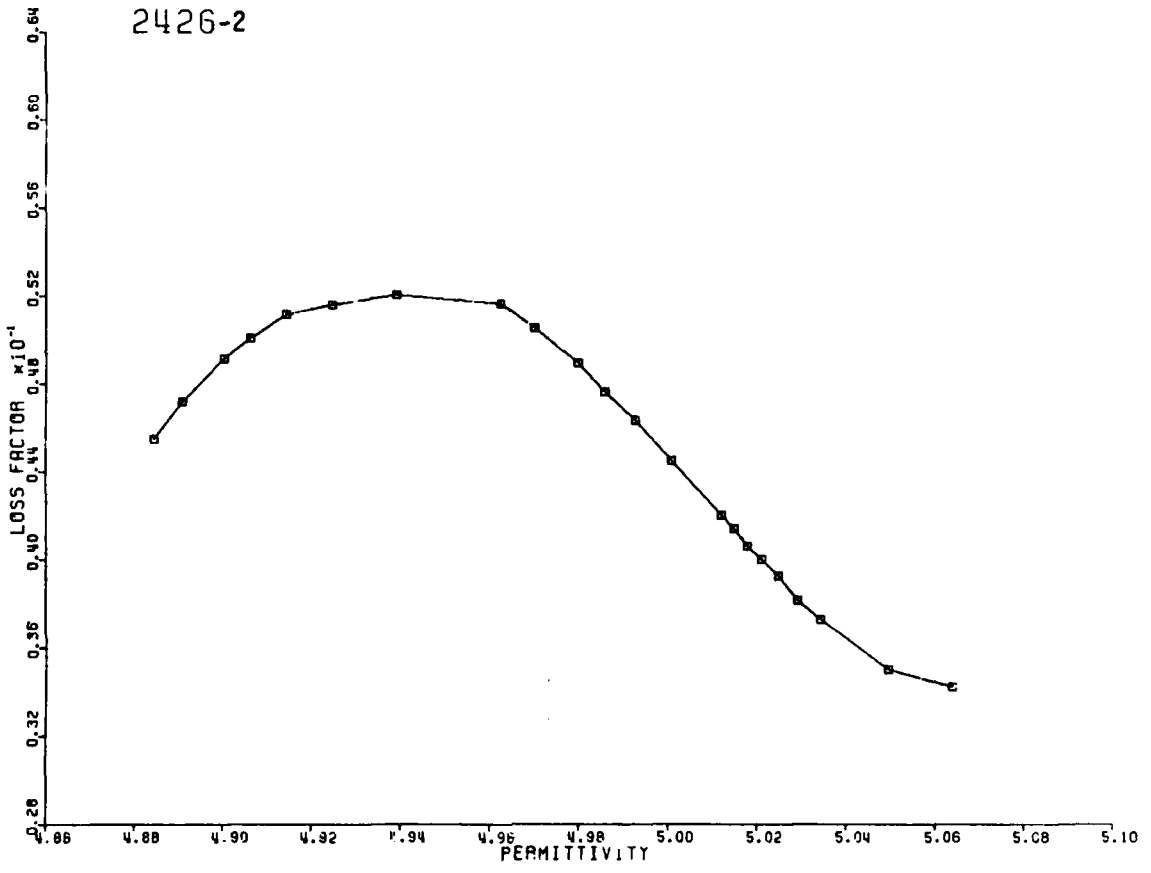

Figure B-14D. Cole-Cole plot, relative loss factor versus relative permittivity, of sample 2426-2, metaquartzite from Camden, Maine.

SAMPLE 2428

FREQUENCY (HERTZ)	RELATIVE DIELECTRIC CONSTANT	CONDUC-TIVITY (MHO/M)	LOSS TANGENT	LOSS FACTOR
100.	6.726	0.4223E-09	0.1134E 00	0.7627E 00
200.	6.462	0.6620E-09	0.9250E-01	0.5978E 00
300.	6.335	0.8673E-09	0.8241E-01	0.5221E 00
400.	6.255	0.1055E-08	0.7614E-01	0.4763E 00
500.	6.198	0.1232E-08	0.7179E-01	0.4449E 00
600.	6.153	0.1401E-08	0.6855E-01	0.4218E 00
700.	6.118	0.1565E-08	0.6601E-01	0.4039E 00
800.	6.088	0.1725E-08	0.6397E-01	0.3894E 00
900.	6.063	0.1881E-08	0.6227E-01	0.3775E 00
1000.	6.041	0.2037E-08	0.6089E-01	0.3678E 00
1500.	5.960	0.2782E-08	0.5620E-01	0.3349E 00
2000.	5.907	0.3500E-08	0.5350E-01	0.3160E 00
2500.	5.867	0.4204E-08	0.5176E-01	0.3037E 00
3000.	5.835	0.4887E-08	0.5042E-01	0.2942E 00
4000.	5.787	0.6239E-08	0.4868E-01	0.2817E 00
5000.	5.750	0.7567E-08	0.4754E-01	0.2733E 00
8000.	5.675	0.1144E-07	0.4549E-01	0.2582E 00
10000.	5.642	0.1384E-07	0.4431E-01	0.2500E 00
15000.	5.577	0.1982E-07	0.4279E-01	0.2386E 00
20000.	5.533	0.2558E-07	0.4175E-01	0.2310E 00
25000.	5.500	0.3109E-07	0.4084E-01	0.2246E 00
30000.	5.473	0.3647E-07	0.4011E-01	0.2196E 00
40000.	5.432	0.4657E-07	0.3870E-01	0.2102E 00
50000.	5.397	0.5590E-07	0.3741E-01	0.2019E 00
80000.	5.337	0.8143E-07	0.3445E-01	0.1838E 00

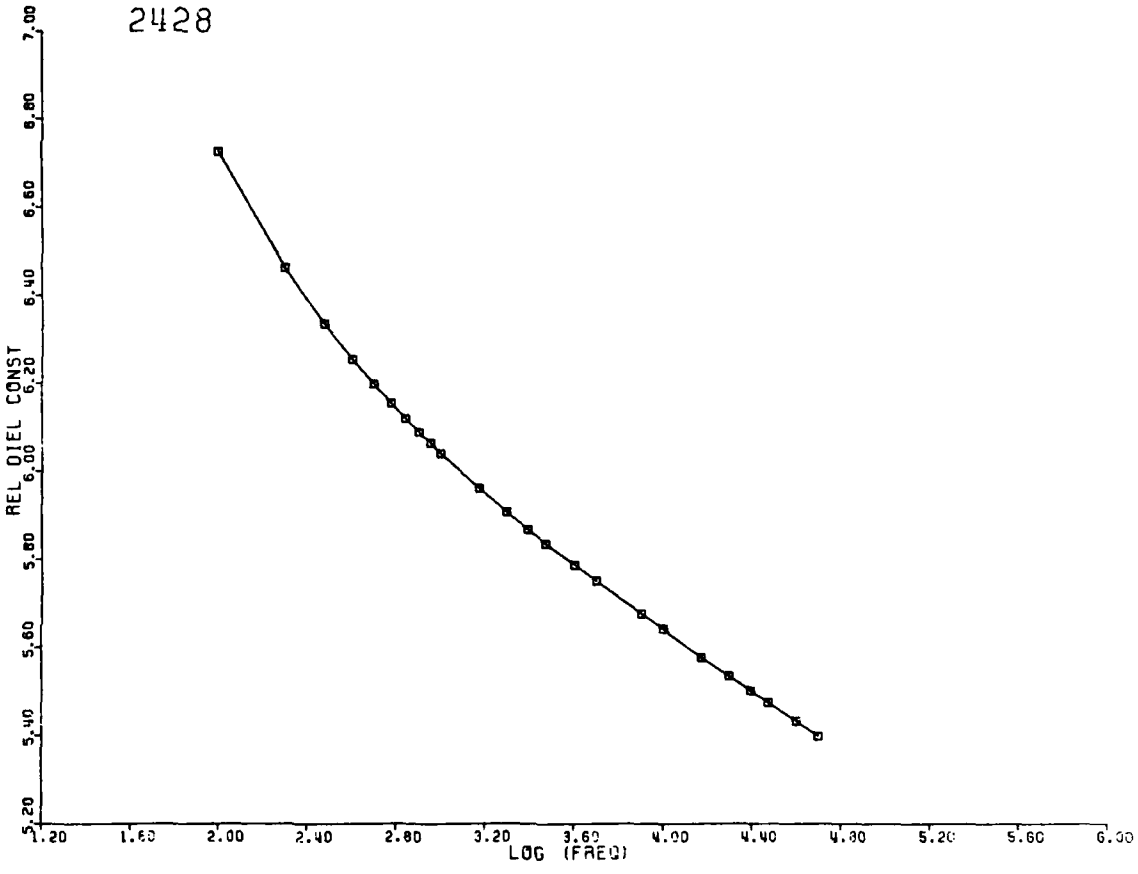

Figure B-15A. Relative permittivity (ε') of sample 2428, metaquartz conglomerate from Camden, Maine, as a function of frequency.

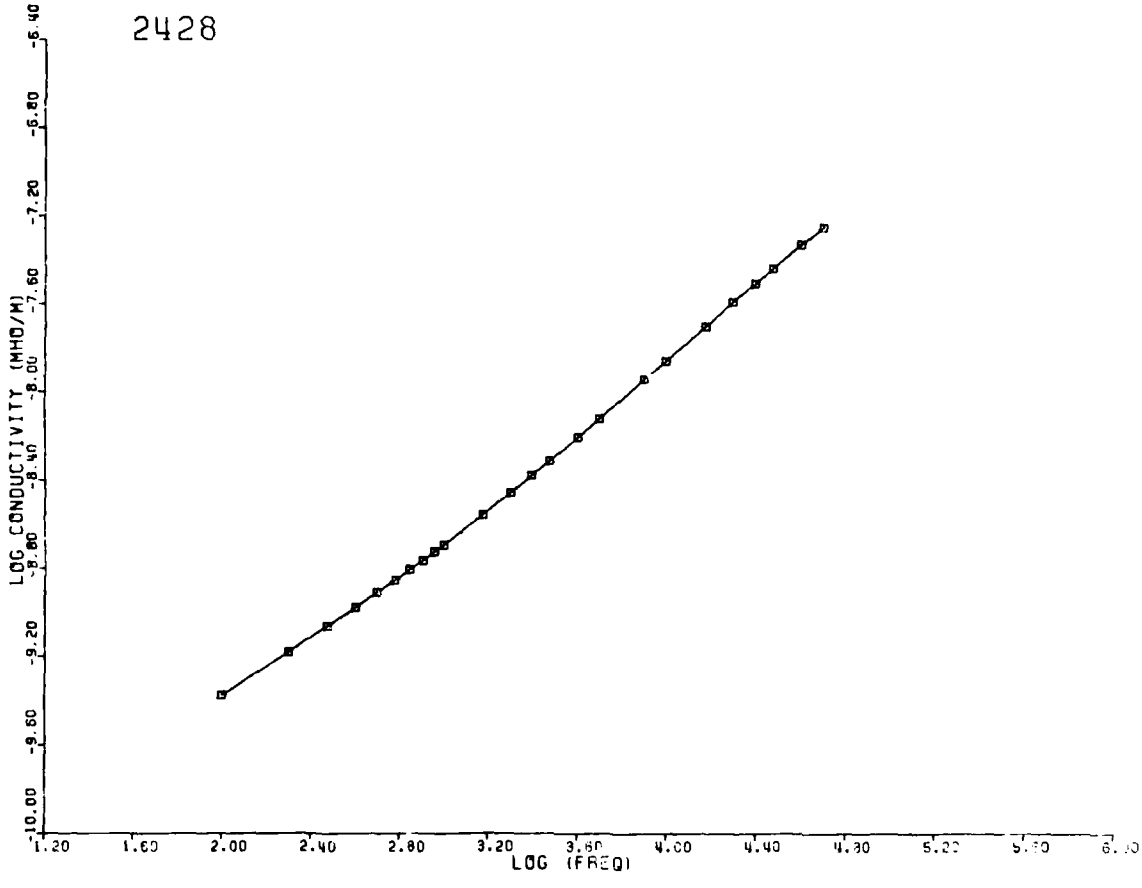

Figure B-15B. Dielectric conductivity ($\sigma = \omega\varepsilon''$) of sample 2428, metaquartz conglomerate from Camden, Maine, as a function of frequency.

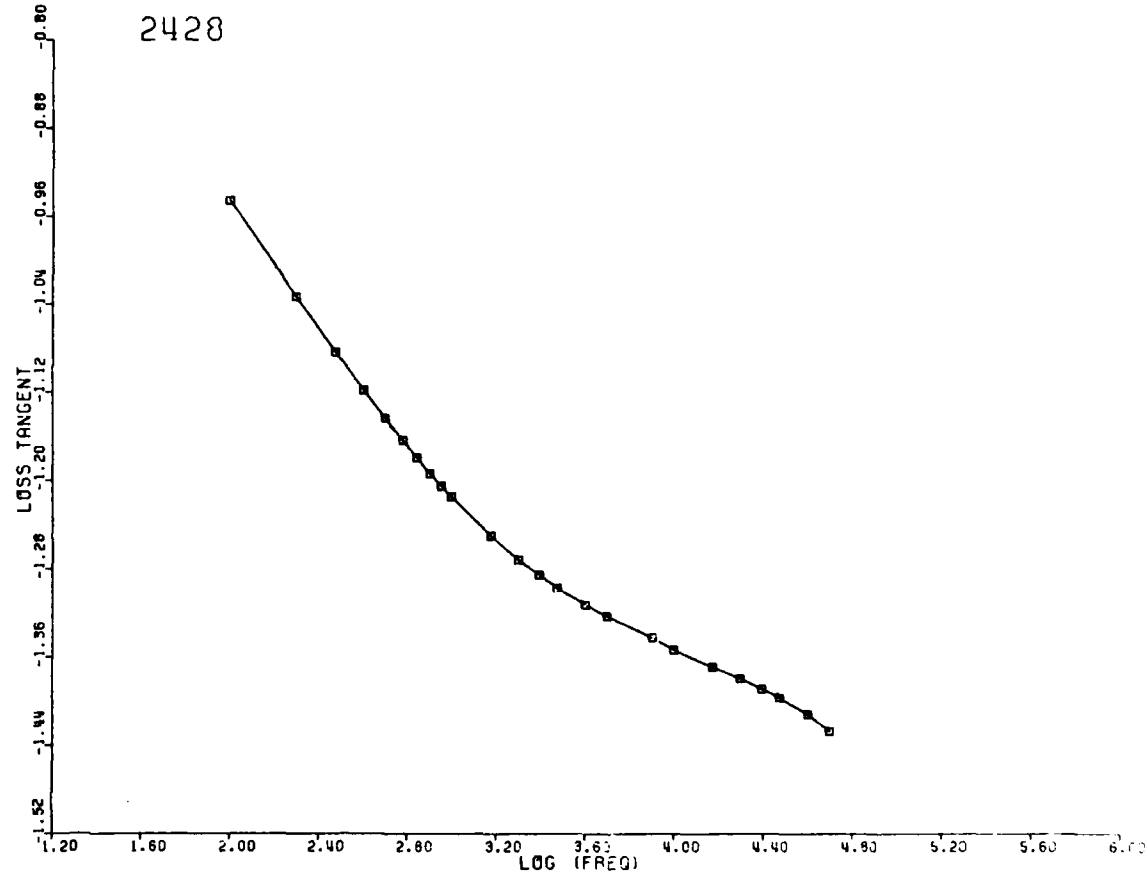

Figure B-15C. Loss tangent of sample 2428, metaquartz conglomerate from Camden, Maine, as a function of frequency.

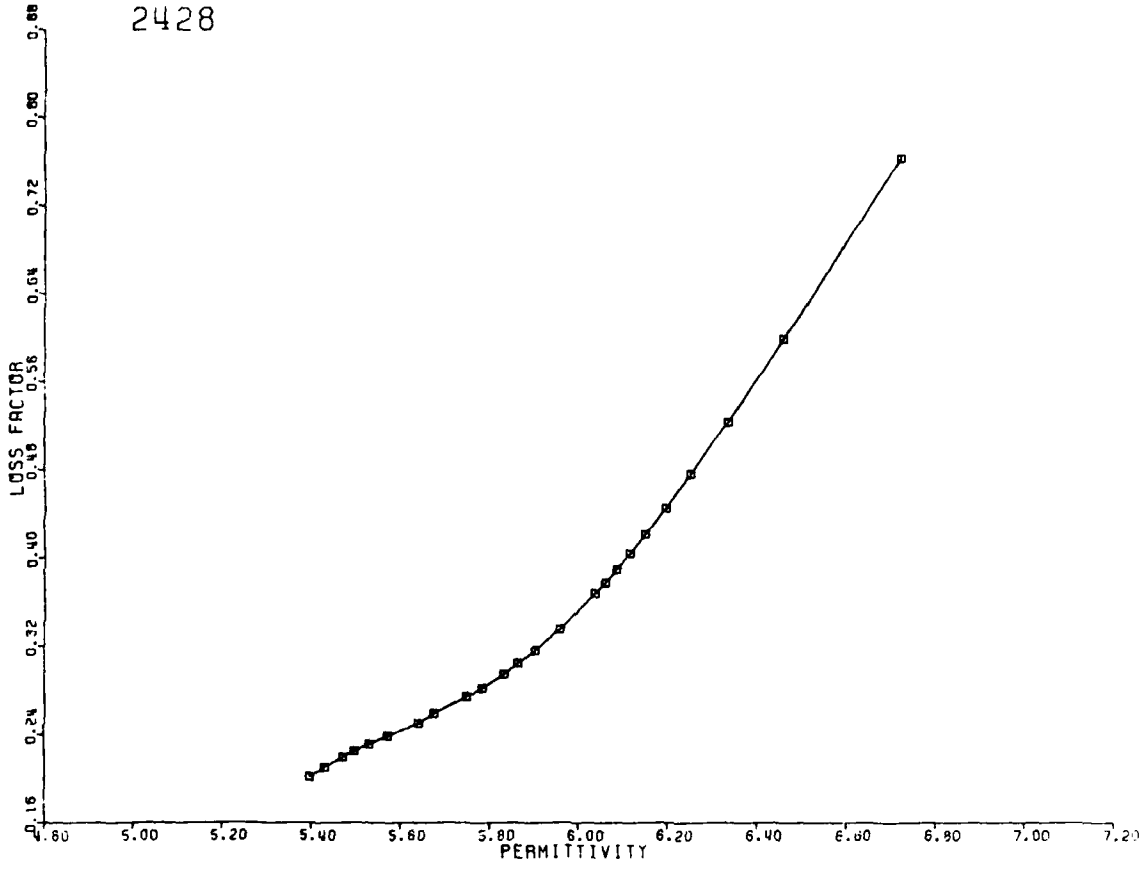

Figure B-15D. Cole-Cole plot, relative loss factor versus relative permittivity, of sample 2428, metaquartz conglomerate from Camden, Maine.

SAMPLE 2432

FREQUENCY (HERTZ)	RELATIVE DIELECTRIC CONSTANT	CONDUCTIVITY (MHO/M)	LOSS TANGENT	LOSS FACTOR
100.	5.026	0.1745E-09	0.6438E-02	0.3236E-01
200.	5.014	0.3088E-09	0.5710E-02	0.2863E-01
300.	5.008	0.4442E-09	0.5483E-02	0.2746E-01
400.	5.004	0.5762E-09	0.5338E-02	0.2671E-01
500.	5.000	0.7116E-09	0.5278E-02	0.2639E-01
600.	4.997	0.8470E-09	0.5239E-02	0.2618E-01
700.	4.995	0.9865E-09	0.5232E-02	0.2613E-01
800.	4.993	0.1126E-08	0.5227E-02	0.2610E-01
900.	4.991	0.1271E-08	0.5247E-02	0.2619E-01
1000.	4.989	0.1416E-08	0.5264E-02	0.2626E-01
1500.	4.983	0.2169E-08	0.5381E-02	0.2681E-01
2000.	4.978	0.2952E-08	0.5499E-02	0.2737E-01
2500.	4.974	0.3753E-08	0.5597E-02	0.2784E-01
3000.	4.971	0.4574E-08	0.5688E-02	0.2827E-01
4000.	4.965	0.6230E-08	0.5817E-02	0.2888E-01
5000.	4.961	0.7913E-08	0.5916E-02	0.2935E-01
8000.	4.952	0.1300E-07	0.6087E-02	0.3014E-01
10000.	4.947	0.1629E-07	0.6108E-02	0.3021E-01
15000.	4.940	0.2283E-07	0.5714E-02	0.2822E-01
20000.	4.934	0.2955E-07	0.5554E-02	0.2740E-01
25000.	4.930	0.3575E-07	0.5378E-02	0.2651E-01
30000.	4.926	0.4155E-07	0.5214E-02	0.2568E-01
40000.	4.921	0.5164E-07	0.4865E-02	0.2394E-01
50000.	4.917	0.5998E-07	0.4524E-02	0.2224E-01
80000.	4.908	0.7526E-07	0.3554E-02	0.1745E-01

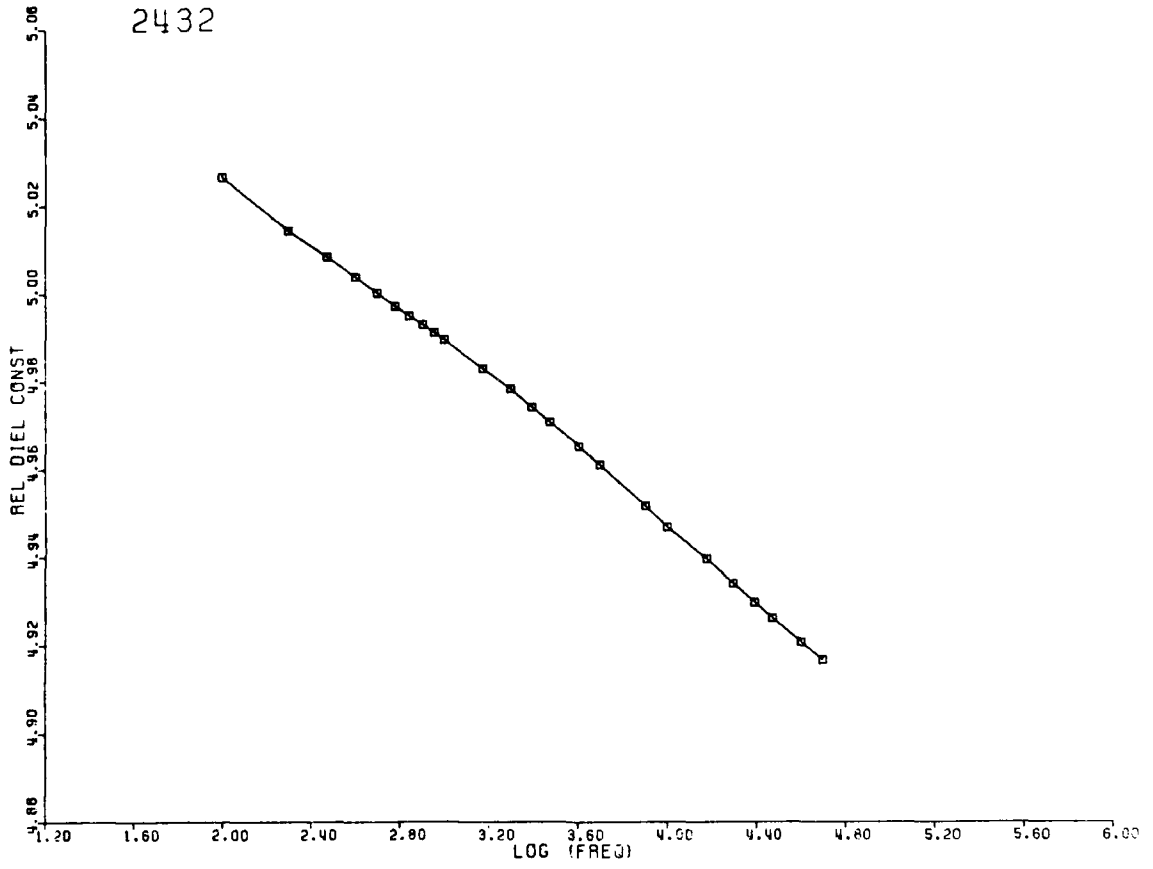

Figure B-16A. Relative permittivity (ε') of sample 2432, metaquartz conglomerate from Camden, Maine, as a function of frequency.

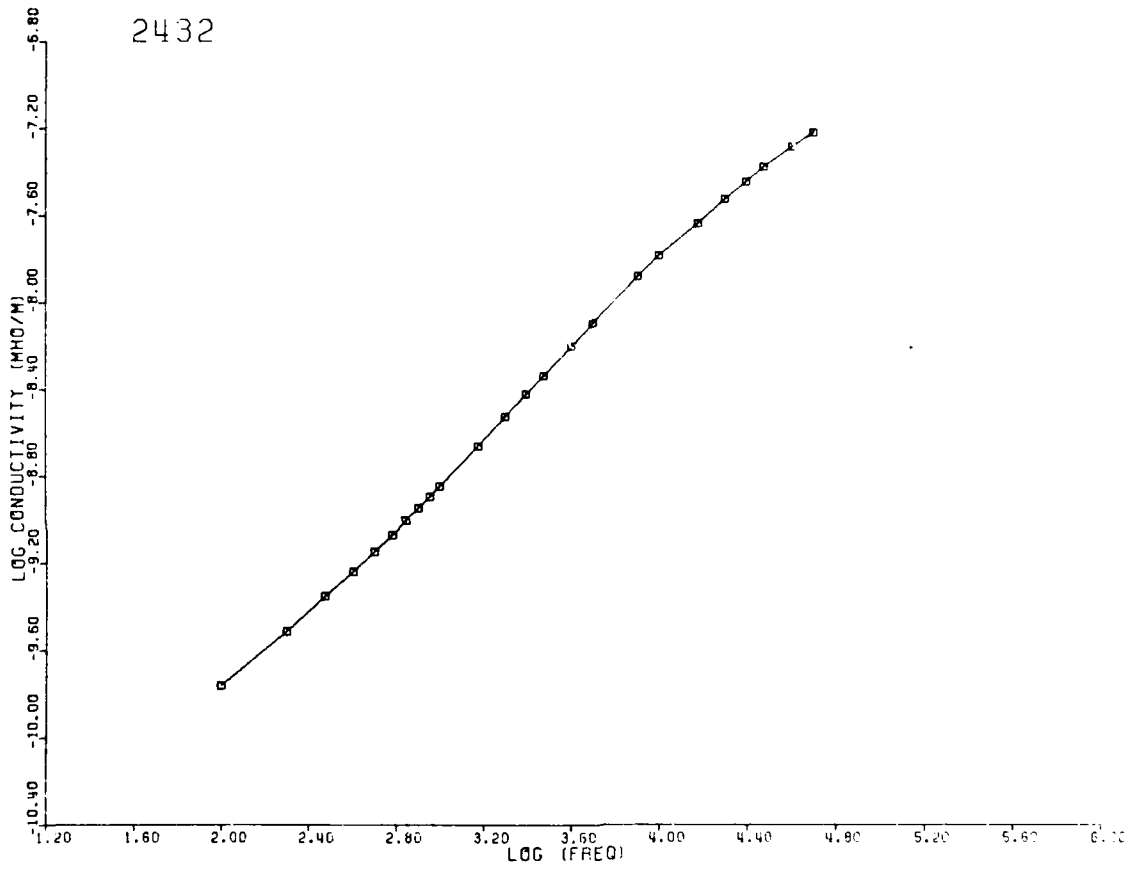

Figure B-16B. Dielectric conductivity ($\sigma = \omega\varepsilon''$) of sample 2432, metaquartz conglomerate from Camden, Maine, as a function of frequency.

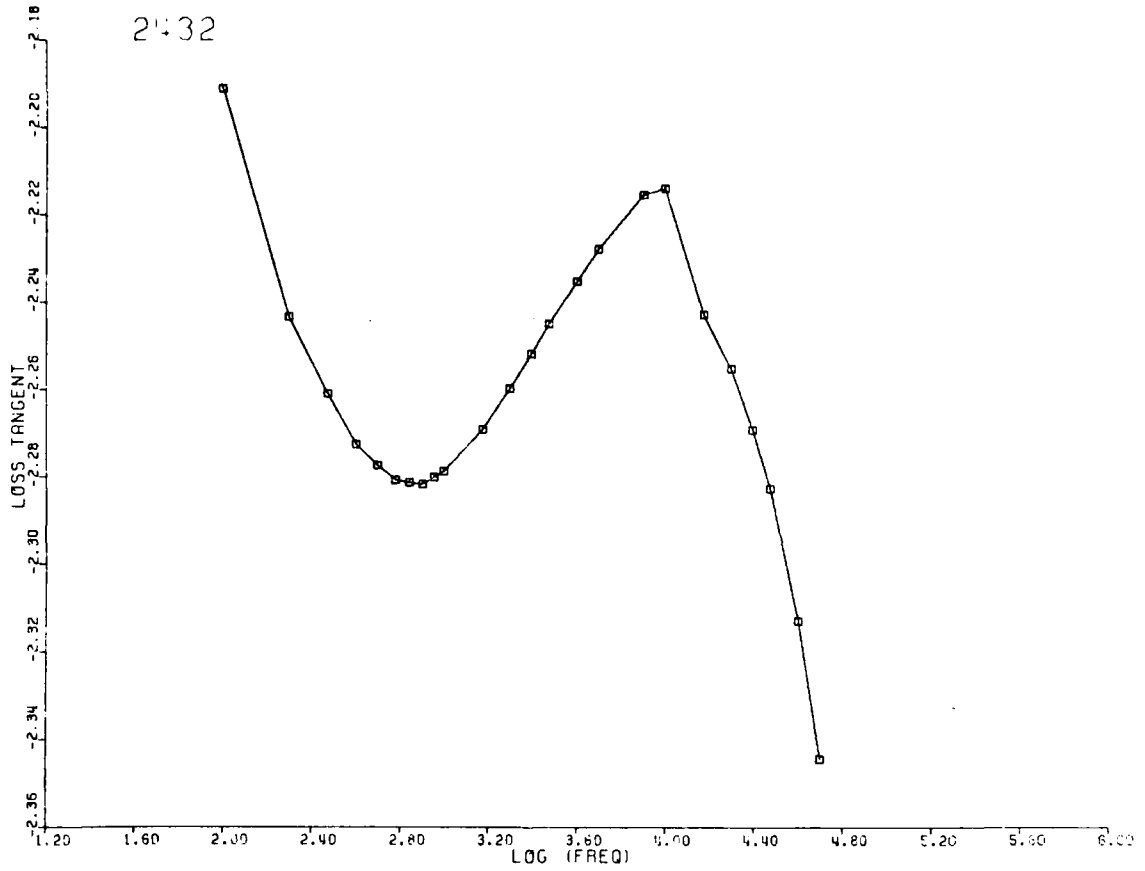

Figure B-16C. Loss tangent of sample 2432, metaquartz conglomerate from Camden, Maine, as a function of frequency.

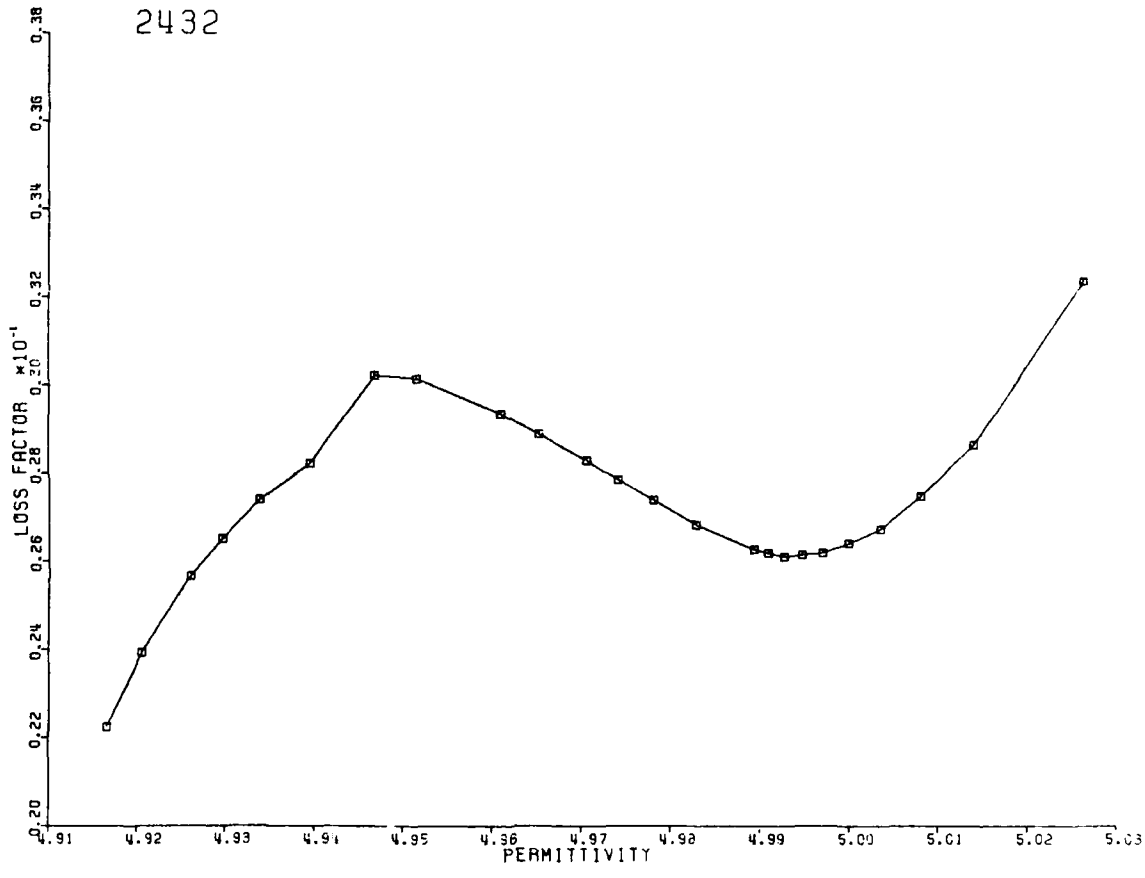

Figure B-16D. Cole-Cole plot, relative loss factor versus relative permittivity, of sample 2432, metaquartz conglomerate from Camden, Maine.

SAMPLE 2434

FREQUENCY (HERTZ)	RELATIVE DIELECTRIC CONSTANT	CONDUC-TIVITY (MHO/M)	LOSS TANGENT	LOSS FACTOR
100.	8.295	0.1991E-07	0.1700E-01	0.1410E 00
200.	8.233	0.4248E-07	0.1827E-01	0.1504E 00
300.	8.194	0.6661E-07	0.1919E-01	0.1573E 00
400.	8.165	0.9172E-07	0.1989E-01	0.1624E 00
500.	8.141	0.1175E-06	0.2045E-01	0.1665E 00
600.	8.121	0.1435E-06	0.2085E-01	0.1693E 00
700.	8.104	0.1697E-06	0.2119E-01	0.1718E 00
800.	8.089	0.1963E-06	0.2148E-01	0.1738E 00
900.	8.075	0.2228E-06	0.2171E-01	0.1753E 00
1000.	8.063	0.2499E-06	0.2195E-01	0.1770E 00
1500.	8.014	0.3848E-06	0.2267E-01	0.1817E 00
2000.	7.979	0.5188E-06	0.2303E-01	0.1837E 00
2500.	7.951	0.6520E-06	0.2323E-01	0.1847E 00
3000.	7.930	0.7810E-06	0.2325E-01	0.1844E 00
4000.	7.894	0.1039E-05	0.2331E-01	0.1840E 00
5000.	7.867	0.1288E-05	0.2319E-01	0.1824E 00
8000.	7.811	0.2004E-05	0.2272E-01	0.1774E 00
10000.	7.786	0.2434E-05	0.2214E-01	0.1724E 00
15000.	7.740	0.3511E-05	0.2142E-01	0.1658E 00
20000.	7.709	0.4514E-05	0.2074E-01	0.1599E 00
25000.	7.685	0.5467E-05	0.2015E-01	0.1549E 00
30000.	7.666	0.6399E-05	0.1971E-01	0.1511E 00
40000.	7.637	0.7955E-05	0.1844E-01	0.1409E 00
50000.	7.616	0.9503E-05	0.1767E-01	0.1346E 00
80000.	7.574	0.1344E-04	0.1571E-01	0.1190E 00

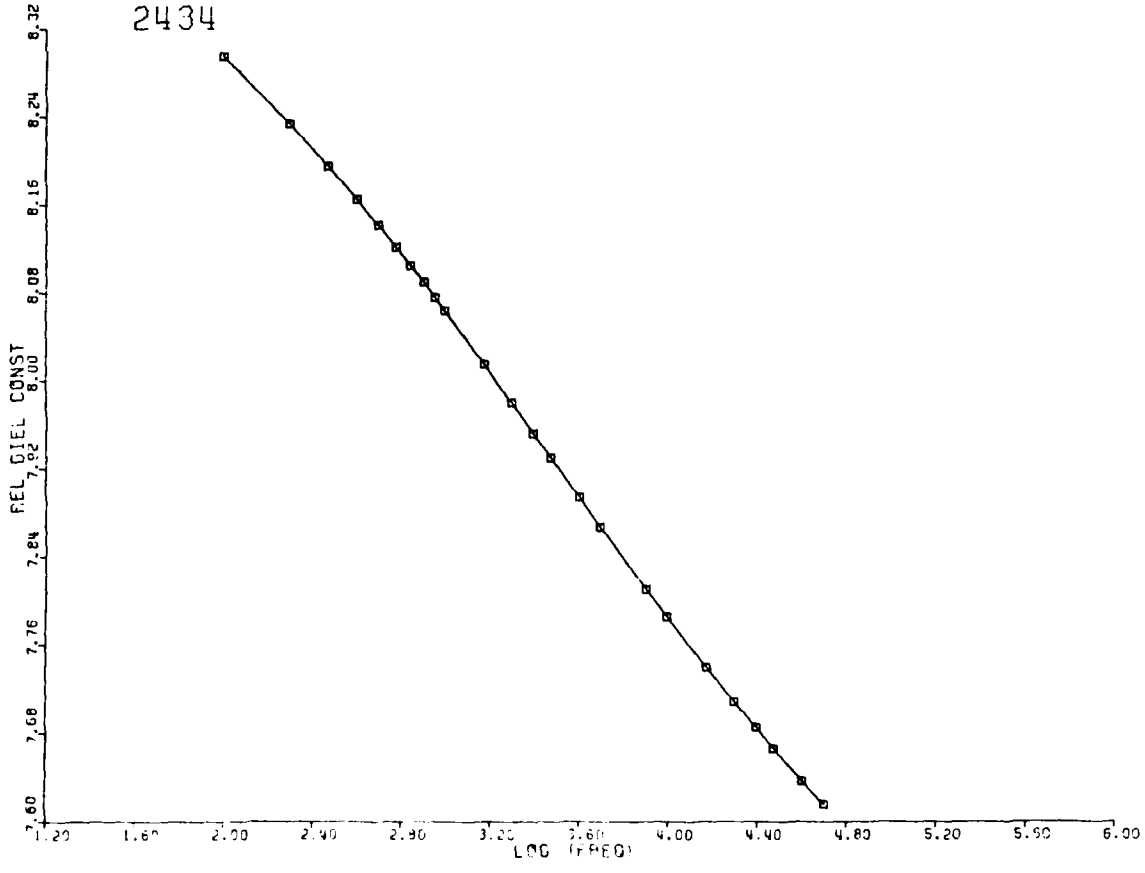

Figure B-17A. Relative permittivity (ε') of sample 2434, calc-silicate from Camden, Maine, as a function of frequency.

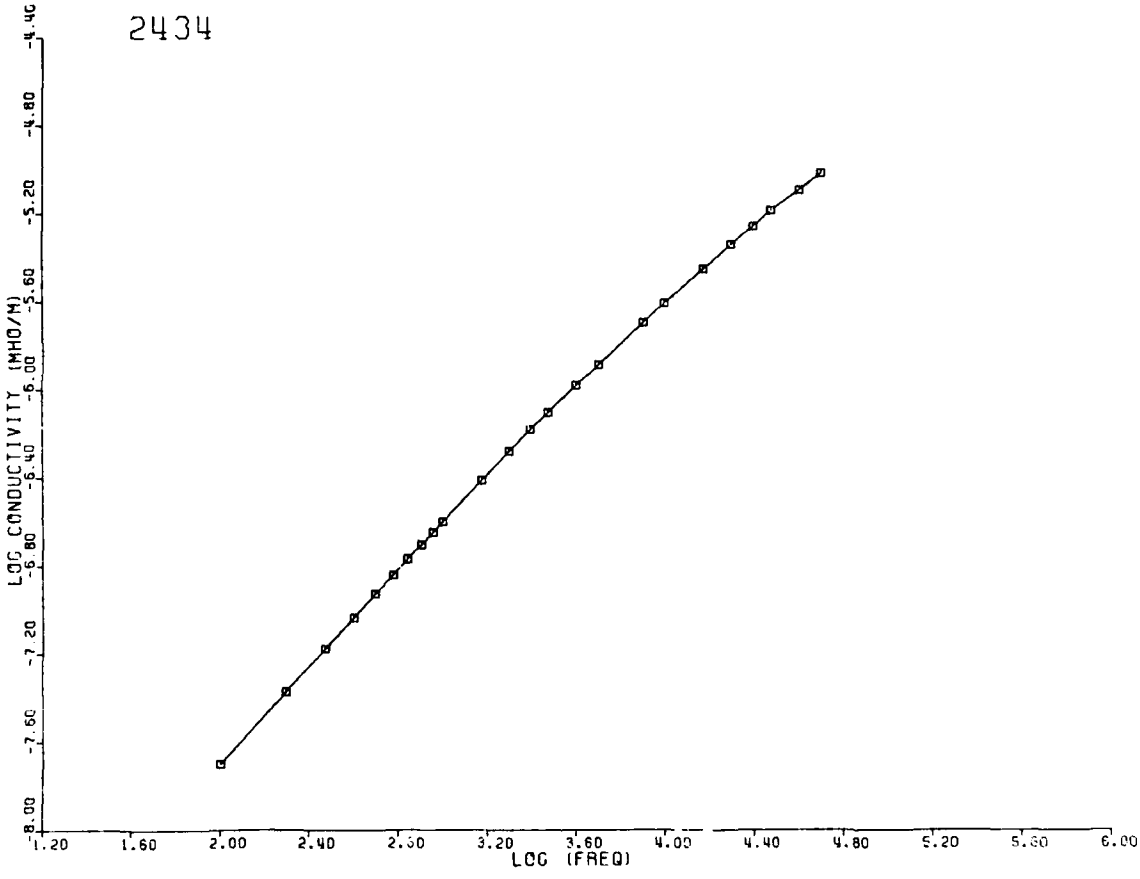

Figure B-17B. Dielectric conductivity ($\sigma = \omega\varepsilon''$) of sample 2434, calc-silicate from Camden, Maine, as a function of frequency.

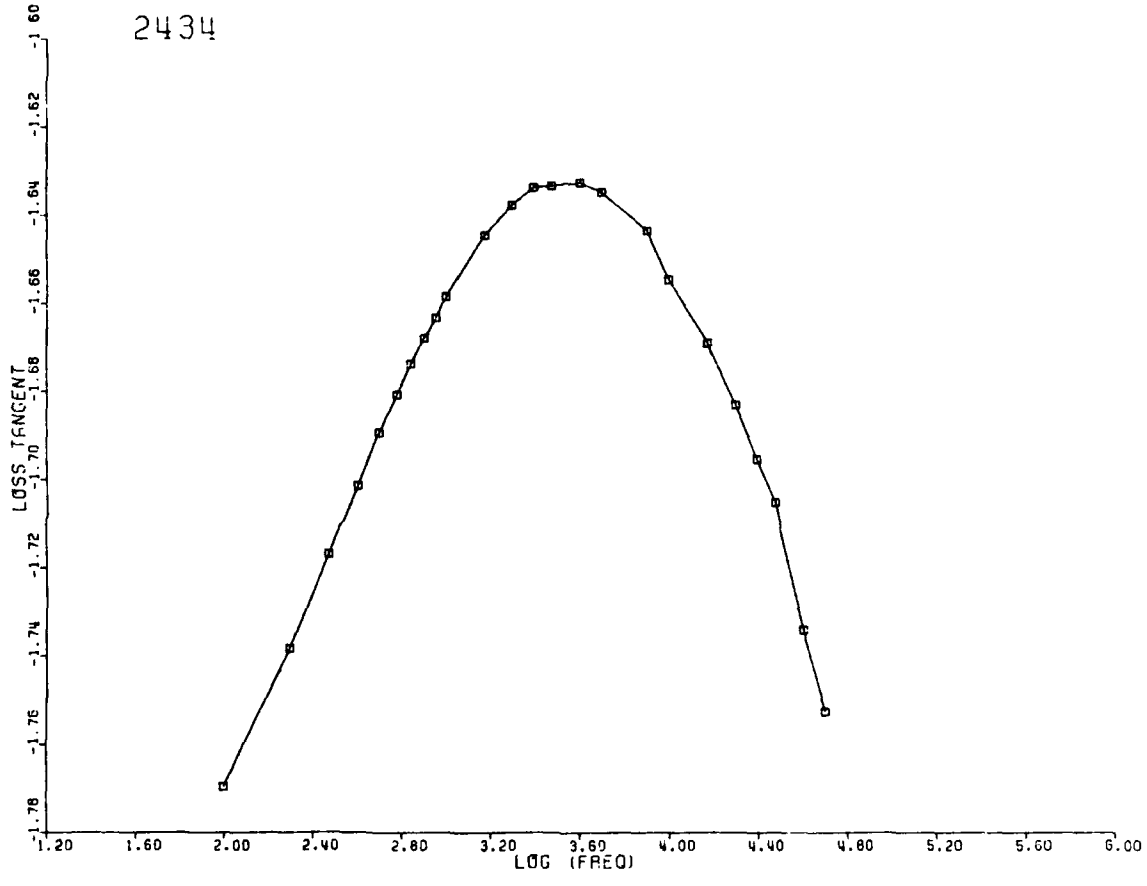

Figure B-17C. Loss tangent of sample 2434, calc-silicate from Camden, Maine, as a function of frequency.

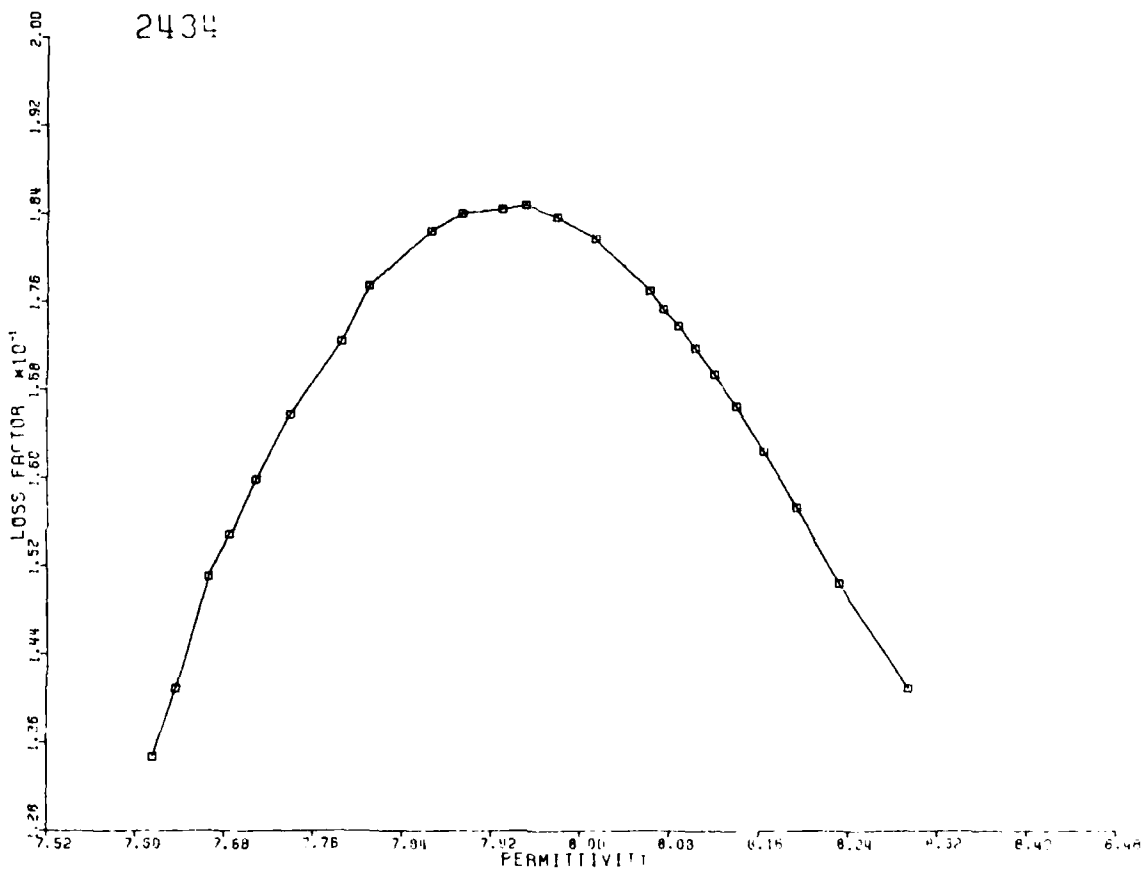

Figure B-17D. Cole-Cole plot, relative loss factor versus relative permittivity, of sample 2434, calc-silicate from Camden, Maine.

SAMPLE 2439A

FREQUENCY (HERTZ)	RELATIVE DIELECTRIC CONSTANT	CONDUC-TIVITY (MHO/M)	LOSS TANGENT	LOSS FACTOR
100.	8.539	0.4880E-08	0.1042E 00	0.8895E 00
200.	8.165	0.9131E-08	0.1019E 00	0.8321E 00
300.	7.957	0.1321E-07	0.1008E 00	0.8023E 00
400.	7.813	0.1719E-07	0.1003E 00	0.7834E 00
500.	7.703	0.2110E-07	0.9985E-01	0.7692E 00
600.	7.615	0.2495E-07	0.9954E-01	0.7580E 00
700.	7.541	0.2873E-07	0.9921E-01	0.7481E 00
800.	7.477	0.3246E-07	0.9893E-01	0.7396E 00
900.	7.421	0.3613E-07	0.9860E-01	0.7317E 00
1000.	7.371	0.3988E-07	0.9862E-01	0.7269E 00
1500.	7.183	0.5757E-07	0.9740E-01	0.6996E 00
2000.	7.054	0.7440E-07	0.9612E-01	0.6780E 00
2500.	6.953	0.9039E-07	0.9477E-01	0.6590E 00
3000.	6.876	0.1059E-06	0.9354E-01	0.6432E 00
4000.	6.756	0.1350E-06	0.9108E-01	0.6154E 00
5000.	6.668	0.1623E-06	0.8872E-01	0.5916E 00
8000.	6.493	0.2352E-06	0.8254E-01	0.5360E 00
10000.	6.419	0.2759E-06	0.7834E-01	0.5029E 00
20000.	6.212	0.4535E-06	0.6653E-01	0.4133E 00
25000.	6.156	0.5263E-06	0.6233E-01	0.3837E 00
30000.	6.113	0.5917E-06	0.5881E-01	0.3595E 00
40000.	6.052	0.7081E-06	0.5352E-01	0.3227E 00
50000.	6.009	0.8102E-06	0.4915E-01	0.2953E 00
80000.	5.934	0.1061E-05	0.4072E-01	0.2416E 00

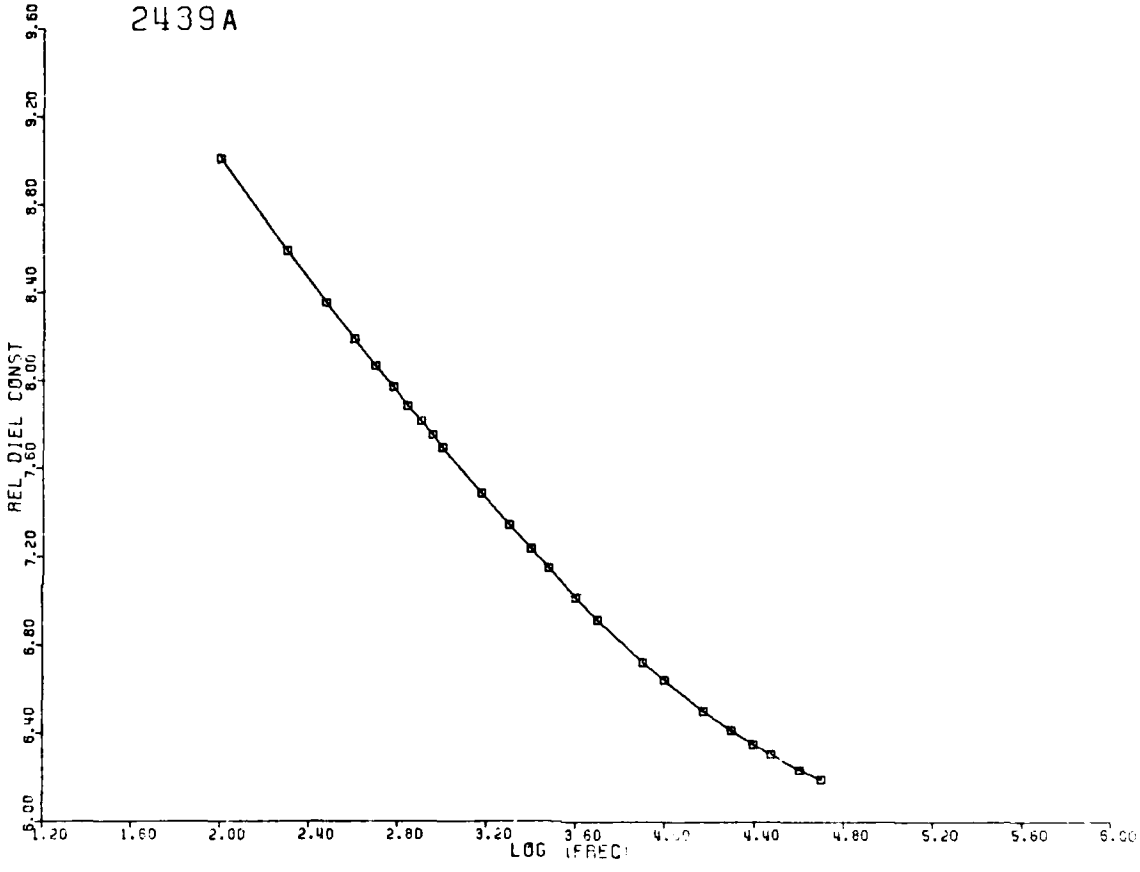

Figure B-18A. Relative permittivity (ε') of sample 2439A, quartzo-feldspathic gneiss from central Maine, as a function of frequency.

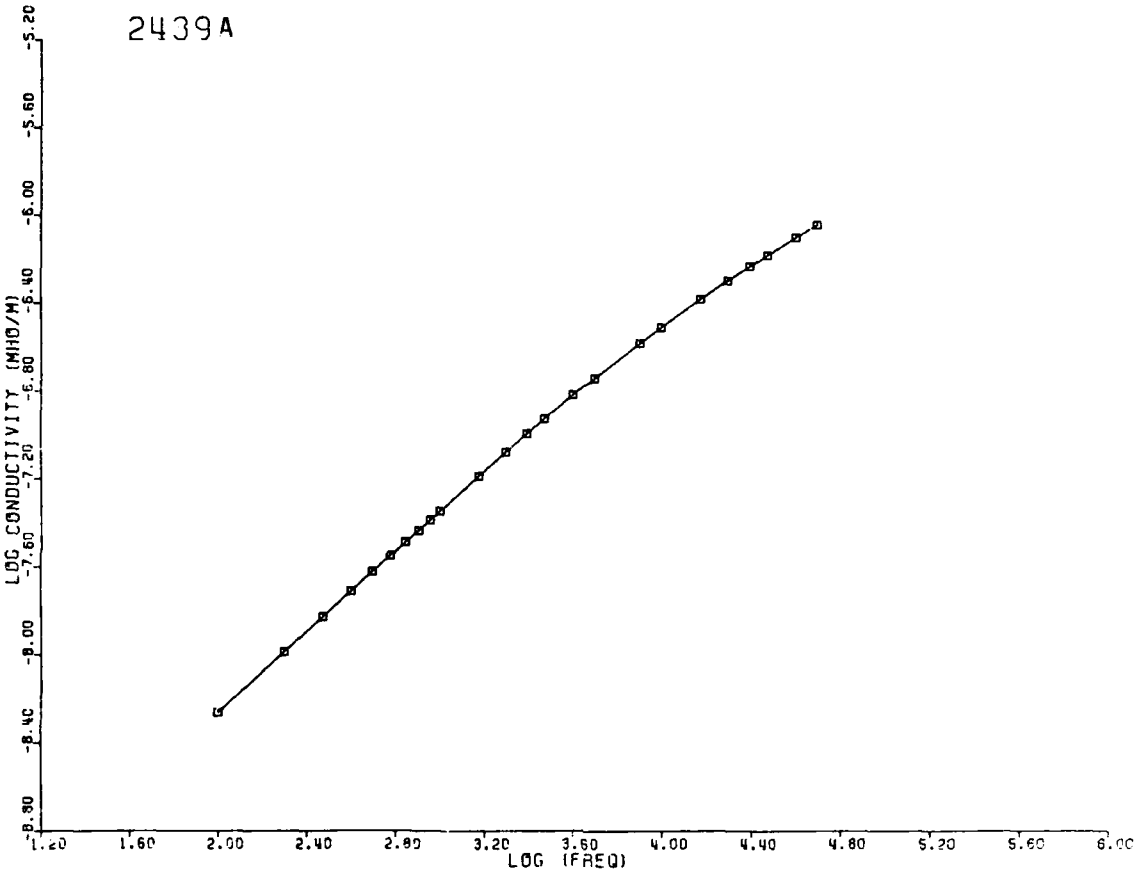

Figure B-18B. Dielectric conductivity ($\sigma = \omega\varepsilon''$) of sample 2439A, quartzo-feldspathic gneiss from central Maine, as a function of frequency.

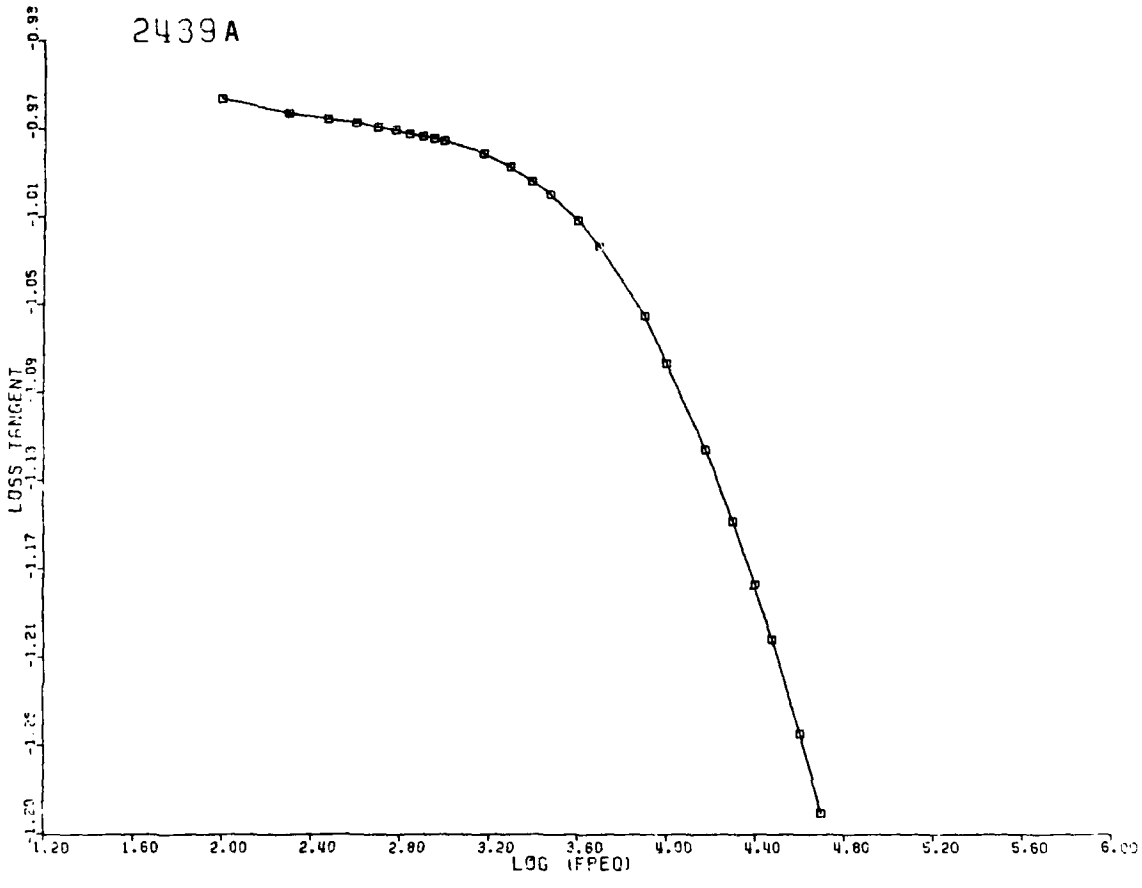

Figure B-18C. Loss tangent of sample 2439A, quartzo-feldspathic gneiss from central Maine, as a function of frequency.

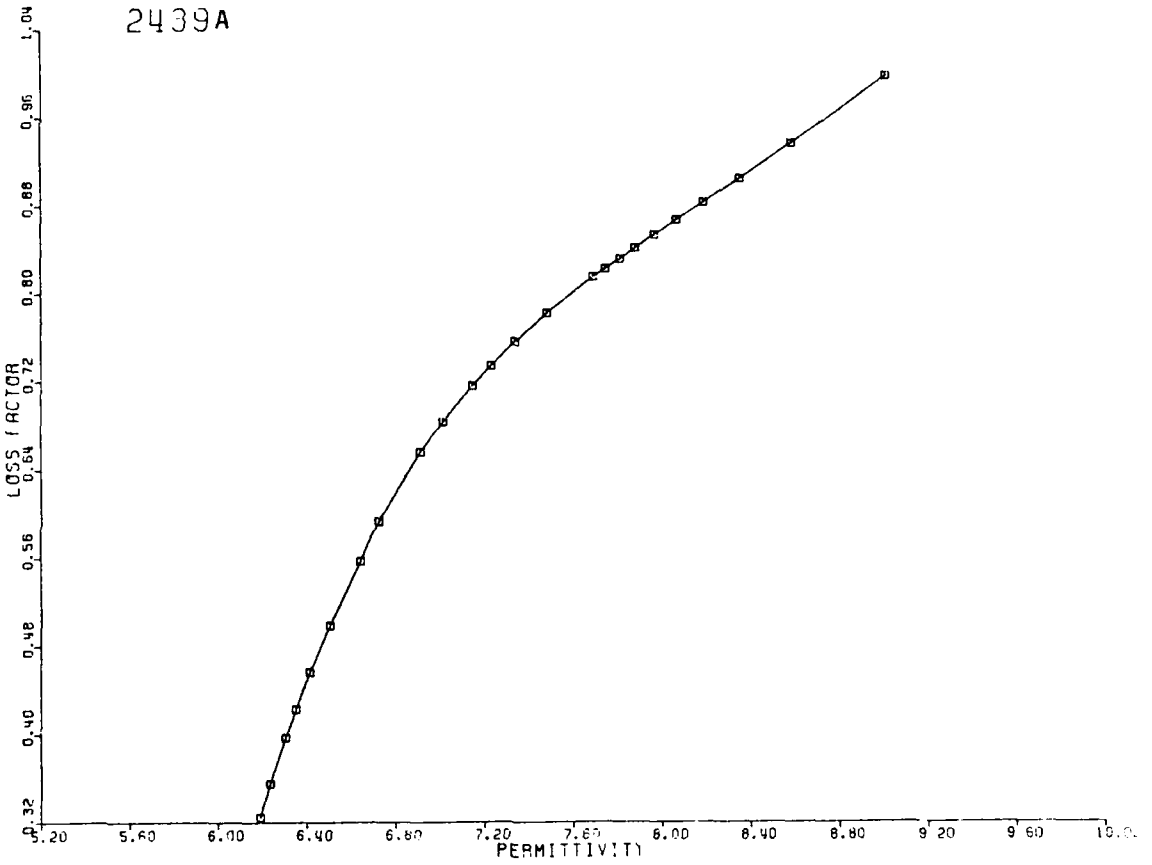

Figure B-18D. Cole-Cole plot, relative loss factor versus relative permittivity, of sample 2439A, quartzo-feldspathic gneiss from central Maine.

SAMPLE 2439B

FREQUENCY (HERTZ)	RELATIVE DIELECTRIC CONSTANT	CONDUC-TIVITY (MHO/M)	LOSS TANGENT	LOSS FACTOR
100.	6.053	0.8521E-09	0.2547E-01	0.1542E 00
200.	5.980	0.1902E-08	0.2878E-01	0.1721E 00
300.	5.932	0.3011E-08	0.3061E-01	0.1816E 00
400.	5.897	0.4147E-08	0.3181E-01	0.1876E 00
500.	5.868	0.5289E-08	0.3262E-01	0.1914E 00
600.	5.845	0.6437E-08	0.3321E-01	0.1941E 00
700.	5.824	0.7573E-08	0.3361E-01	0.1958E 00
800.	5.807	0.8708E-08	0.3392E-01	0.1969E 00
900.	5.791	0.9838E-08	0.3416E-01	0.1978E 00
1000.	5.777	0.1097E-07	0.3438E-01	0.1986E 00
1500.	5.721	0.1650E-07	0.3479E-01	0.1990E 00
2000.	5.682	0.2180E-07	0.3471E-01	0.1972E 00
2500.	5.652	0.2688E-07	0.3442E-01	0.1945E 00
3000.	5.628	0.3180E-07	0.3408E-01	0.1918E 00
4000.	5.592	0.4116E-07	0.3330E-01	0.1862E 00
5000.	5.564	0.5001E-07	0.3252E-01	0.1810E 00
8000.	5.509	0.7400E-07	0.3038E-01	0.1674E 00
10000.	5.486	0.8791E-07	0.2899E-01	0.1591E 00
15000.	5.446	0.1210E-06	0.2681E-01	0.1460E 00
20000.	5.419	0.1507E-06	0.2517E-01	0.1364E 00
25000.	5.400	0.1782E-06	0.2388E-01	0.1290E 00
30000.	5.387	0.2043E-06	0.2288E-01	0.1232E 00
40000.	5.365	0.2524E-06	0.2128E-01	0.1142E 00
50000.	5.350	0.2971E-06	0.2010E-01	0.1075E 00
80000.	5.321	0.4190E-06	0.1781E-01	0.9476E-01

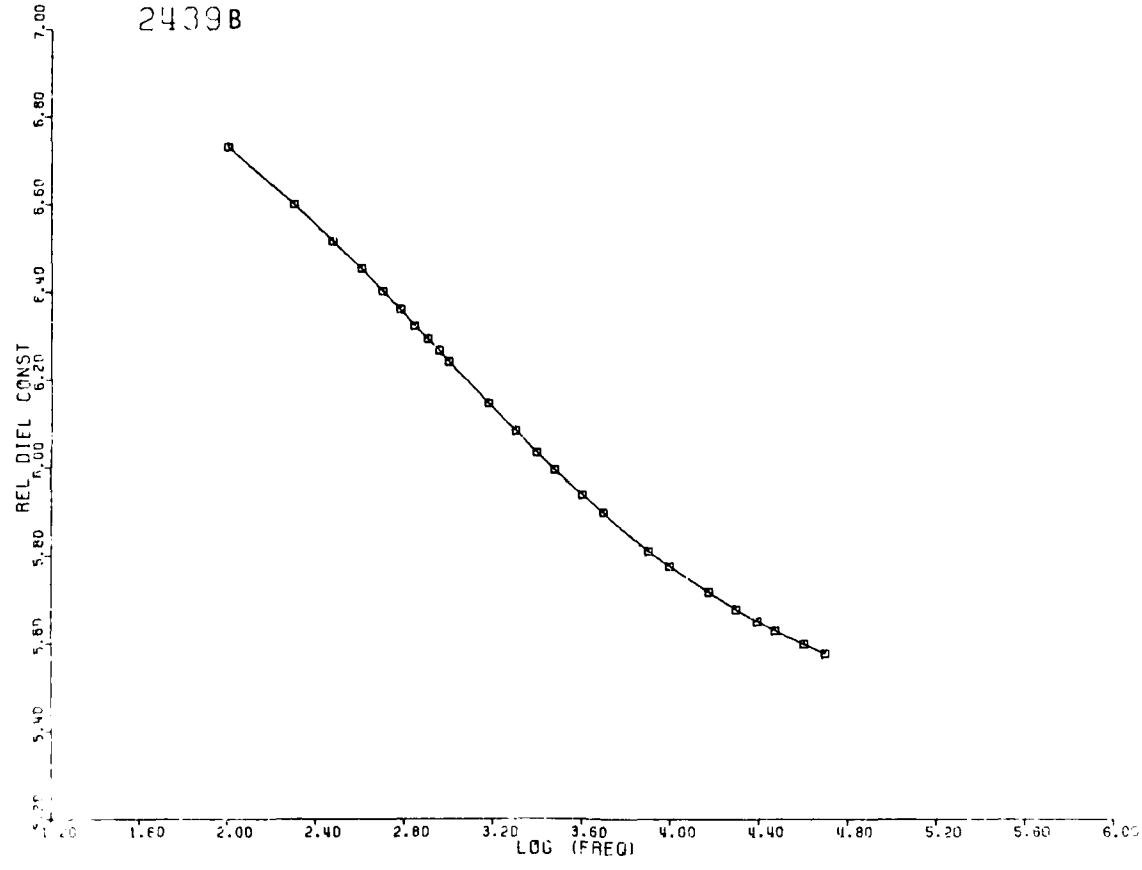

Figure B-19A. Relative permittivity (ε') of sample 2439B, quartzo-feldspathic gneiss from central Maine, as a function of frequency.

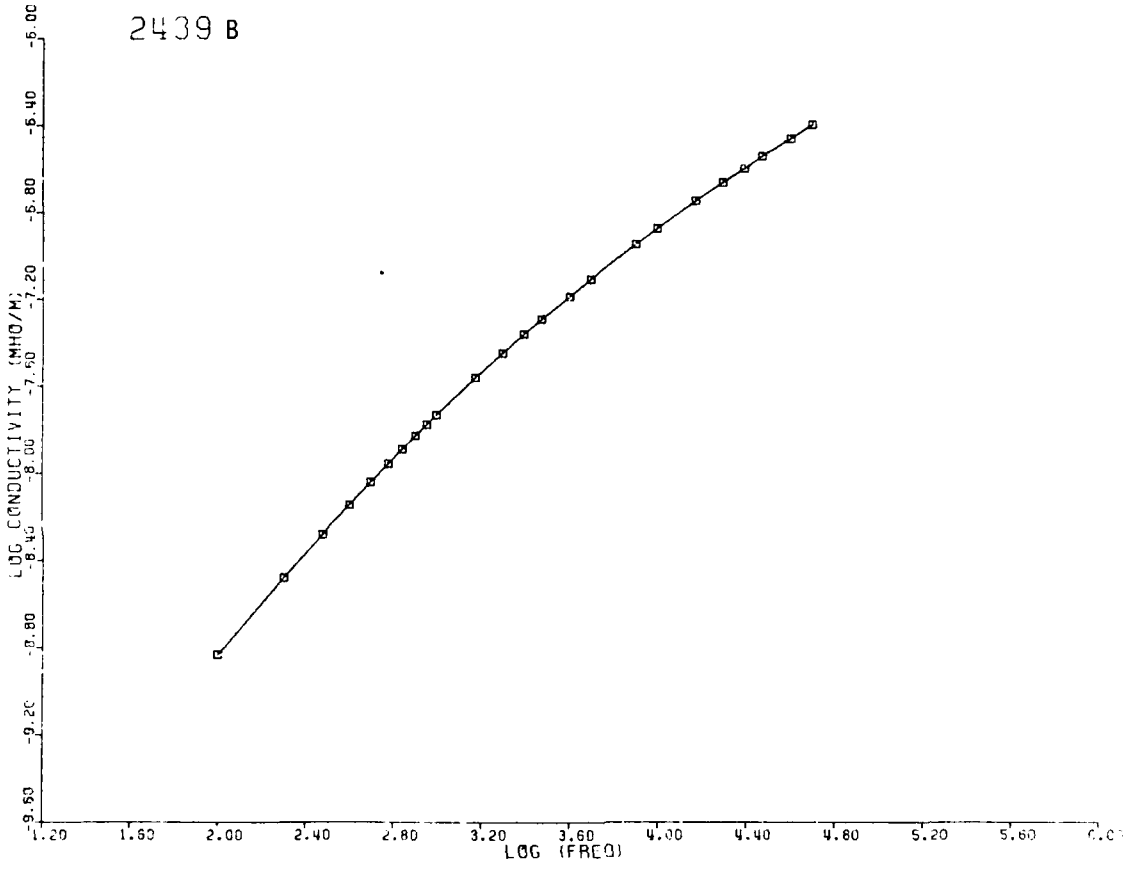

Figure B-19B. Dielectric conductivity ($\sigma = \omega\varepsilon''$) of sample 2439B, quartzofeldspathic gneiss from central Maine, as a function of frequency.

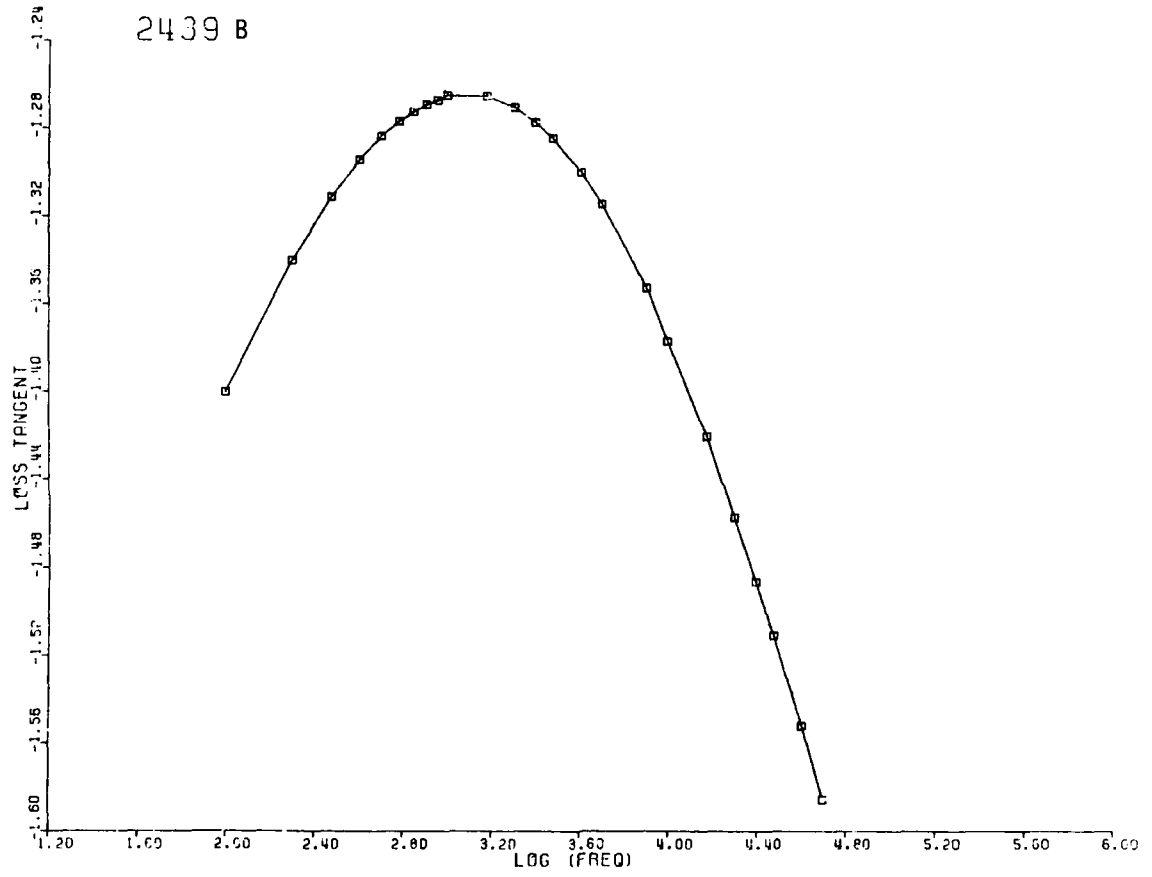

Figure B-19C. Loss tangent of sample 2439B, quartzo-feldspathic gneiss from central Maine, as a function of frequency.

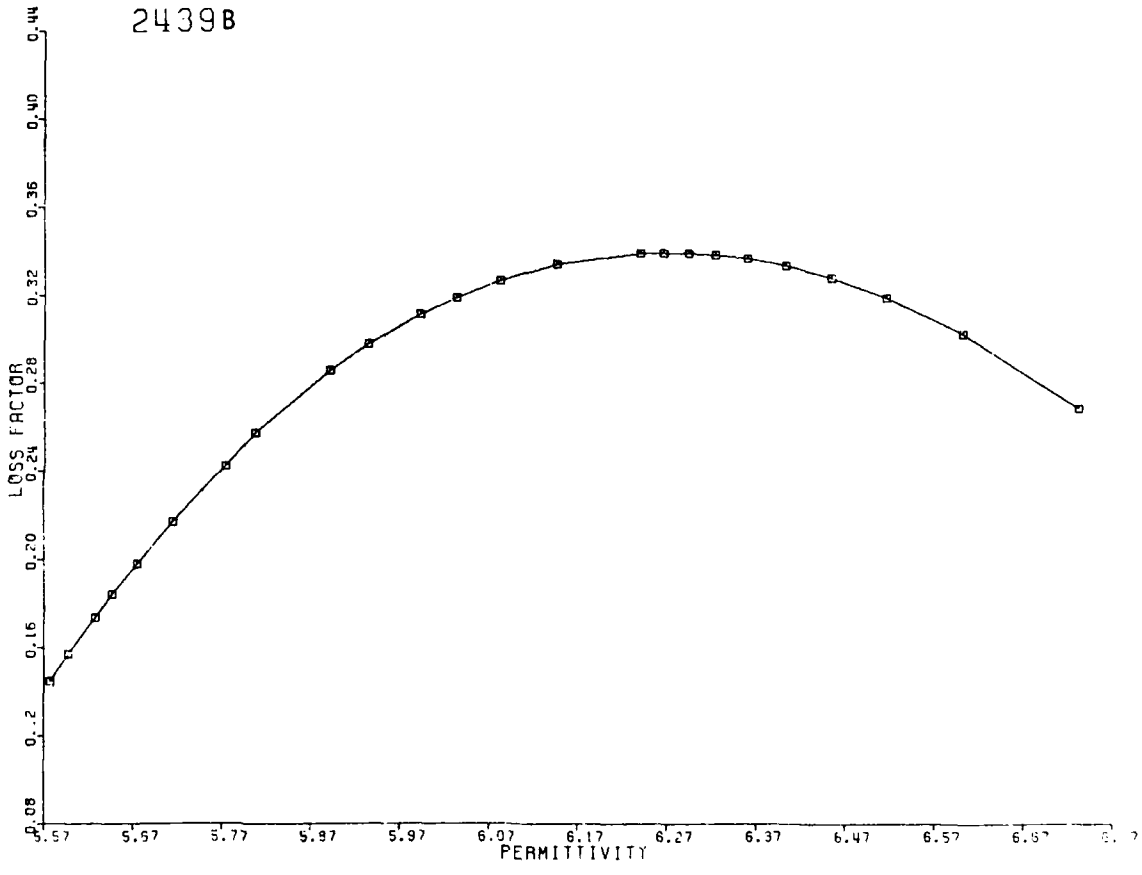

Figure B-19D. Cole-Cole plot, relative loss factor versus relative permittivity, of sample 2439B, quartzo-feldspathic gneiss from central Maine.

SAMPLE 2441

FREQUENCY (HERTZ)	RELATIVE DIELECTRIC CONSTANT	CONDUC-TIVITY (MHO/M)	LOSS TANGENT	LOSS FACTOR
100.	8.169	0.4403E-08	0.9815E-01	0.8018E 00
200.	7.833	0.7955E-08	0.9248E-01	0.7244E 00
300.	7.653	0.1122E-07	0.8898E-01	0.6810E 00
400.	7.533	0.1431E-07	0.8647E-01	0.6513E 00
500.	7.443	0.1727E-07	0.8450E-01	0.6289E 00
600.	7.372	0.2013E-07	0.8290E-01	0.6111E 00
700.	7.315	0.2293E-07	0.8154E-01	0.5965E 00
800.	7.265	0.2564E-07	0.8034E-01	0.5837E 00
900.	7.223	0.2828E-07	0.7924E-01	0.5723E 00
1000.	7.185	0.3093E-07	0.7841E-01	0.5633E 00
1500.	7.046	0.4343E-07	0.7484E-01	0.5273E 00
2000.	6.952	0.5518E-07	0.7227E-01	0.5025E 00
2500.	6.889	0.6631E-07	0.7012E-01	0.4831E 00
3000.	6.829	0.7706E-07	0.6850E-01	0.4678E 00
4000.	6.747	0.9736E-07	0.6570E-01	0.4433E 00
5000.	6.685	0.1166E-06	0.6351E-01	0.4246E 00
8000.	6.566	0.1686E-06	0.5845E-01	0.3838E 00
10000.	6.516	0.1989E-06	0.5560E-01	0.3623E 00
15000.	6.424	0.2686E-06	0.5077E-01	0.3261E 00
20000.	6.366	0.3310E-06	0.4735E-01	0.3014E 00
25000.	6.325	0.3871E-06	0.4459E-01	0.2820E 00
30000.	6.293	0.4393E-06	0.4239E-01	0.2667E 00
40000.	6.248	0.5330E-06	0.3884E-01	0.2427E 00
50000.	6.215	0.6168E-06	0.3615E-01	0.2247E 00
80000.	6.153	0.8237E-06	0.3047E-01	0.1875E 00

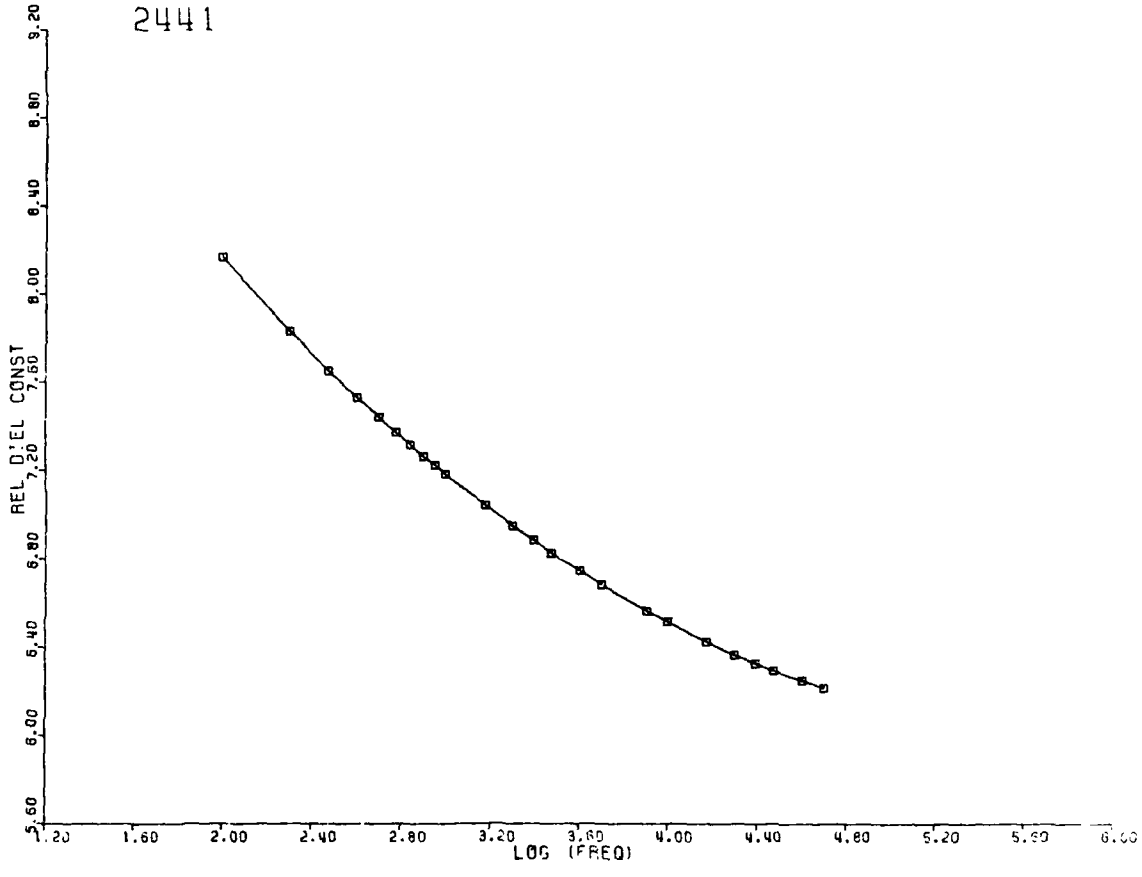

Figure B-20A. Relative permittivity (ε') of sample 2441, schist from central Maine, as a function of frequency.

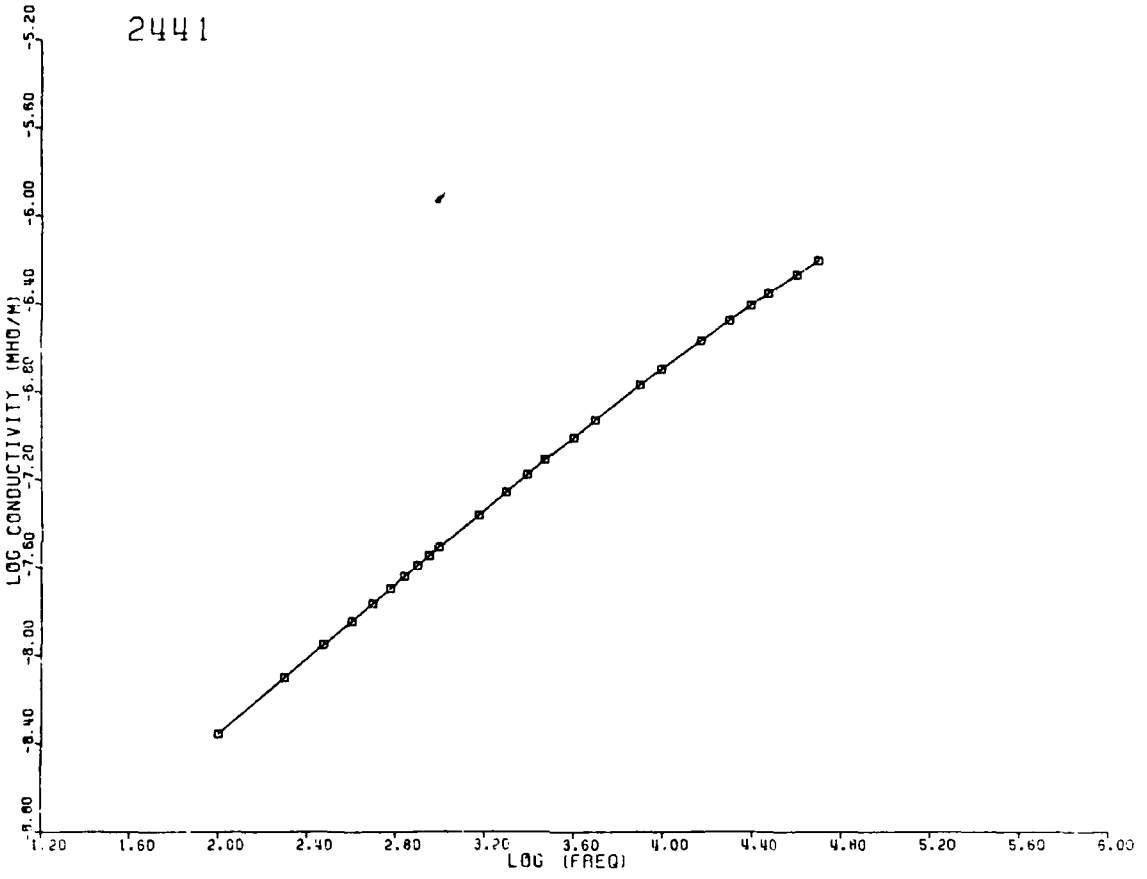

Figure B-20B. Dielectric conductivity ($\sigma = \omega\varepsilon''$) of sample 2441, schist from central Maine, as a function of frequency.

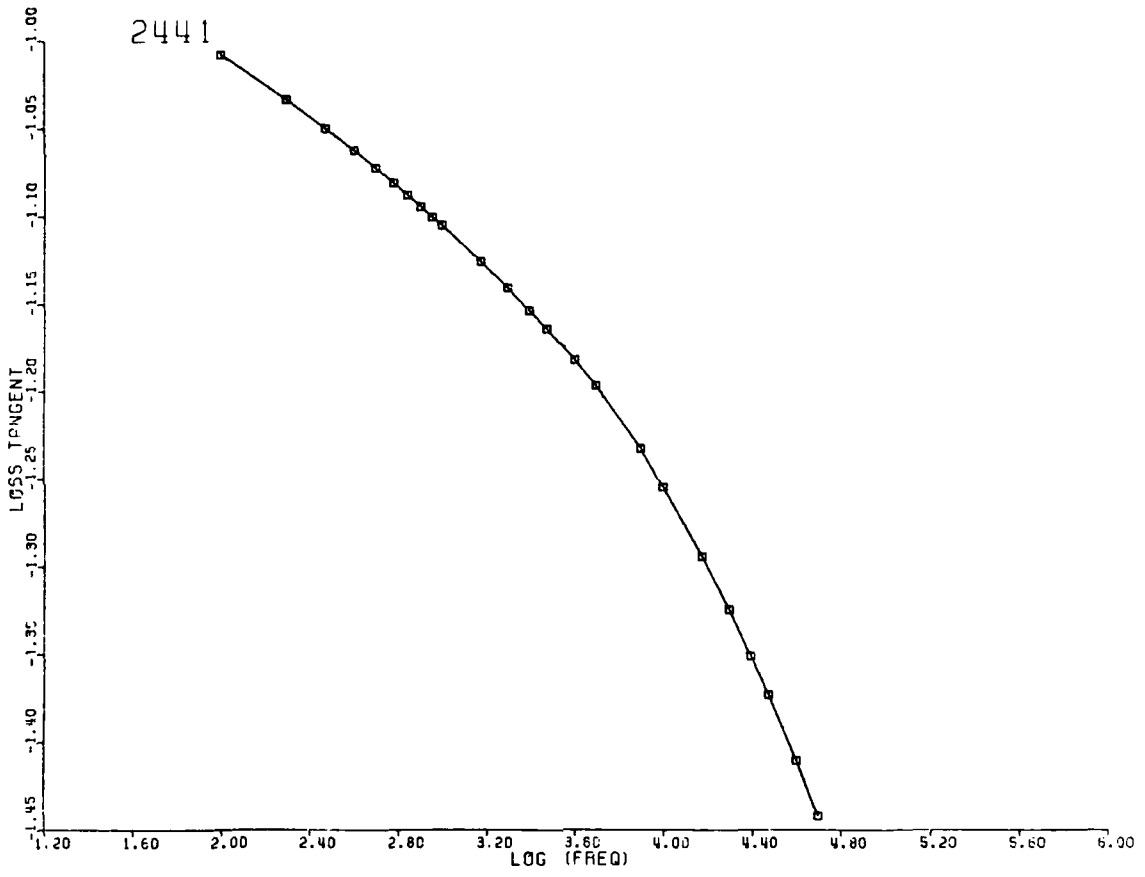

Figure B-20C. Loss tangent of sample 2441, schist from central Maine, as a function of frequency.

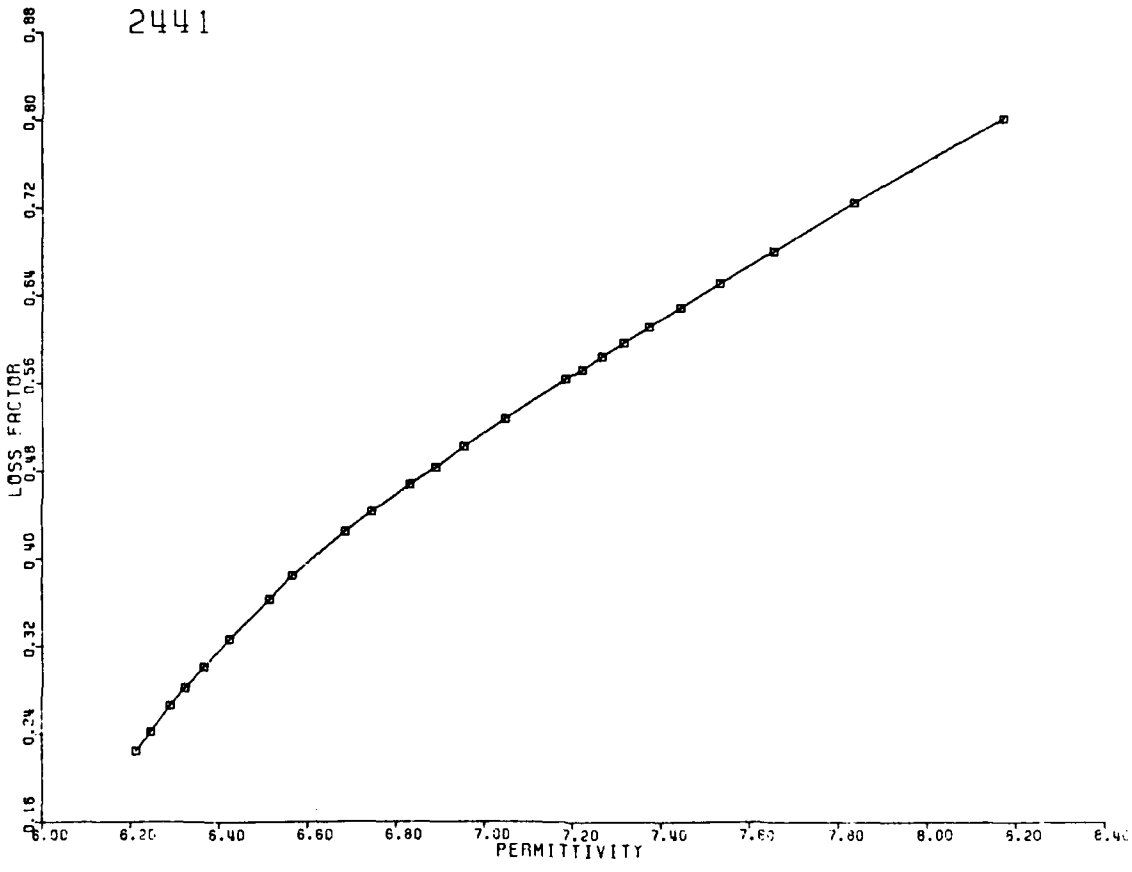

Figure B-20D. Cole-Cole plot, relative loss factor versus relative permittivity, of sample 2441, schist from central Maine.